Distance Learning Operations Course

IC 5.7: Convective Storm Structure and Evolution

Presented by the Warning Decision Training Branch

Version: 0308.2

Table of Contents

Introduction

Instructional Component 5.7 provides instruction on the fundamentals of convective storm structure and evolution. Lesson 1 starts with a look at the fundamental relationships of shear and instability with respect to convective storm type. Lesson 2 offers a short review of some of the environmental parameters used in assessing buoyancy and shear. Lesson 3 details the production and detection of severe weather hazards with respect to weakly sheared storms, supercells, and multicells.

Although this instruction is expansive, it is crucial to understanding important processes in convective storm development and evolution. The knowledge of convective storm processes directly relates to the ability to predict and recognize storm hazards in the warning process. The goal of this instruction is to improve a forecaster's ability to make effective use of radar and other data in recognizing and detecting severe convection.

There are several components to this training including:

- *Capabilities of Kinematic and Thermodynamic Severe Weather Parameters (web site available at wdtb.noaa.gov/resources/IC/svrparams/intro/index.htm)*
- The teletraining session
- Review Exercises
- This Student Guide

This student guide is designed to summarize and review the major topics related to convective storm

structure and evolution. The student guide incorporates new scientific findings related to convective storm structure and evolution. The following are prerequisite objectives for the teletraining portion of IC 5.7:

Prerequisite. Students must know how to determine and interpret thermodynamic and kinematic quantities derived from Skew-T log P soundings according to pure parcel theory.

These quantities include all quantities described in the NWSTC Remote Training Module RTM-230 (Skew T Log P Diagram and Sounding Analysis). RTM-230 is a training module containing basic instruction on upper air sounding analysis. It is available as a printed module from the NWS Training Center (For copies contact Marylin Reed at (816) 880-9594 x 252):

In addition, more detailed sounding parameters are described on the WDTB web site, "***Capabilities of Kinematic and Thermodynamic Severe Weather Parameters***" at:

http://wdtb.noaa.gov/resources/IC/svrparams/svrparams.htm

Objectives

The following are the specific learning objectives for IC 5.7.

Lesson 1

A Review of the Fundamental Relationships of Shear and Instability on Convective Storm Structure and Type.

1. **For a given quantity of buoyancy, determine the influence of shear strength on overall storm structure and evolution.**
2. **For a given hodograph and magnitude of vertical wind shear, identify the influences of variations to the buoyancy profile on overall storm structure and evolution.**
3. **For a given hodograph and magnitude of vertical wind shear, describe the role of midlevel dry air on storm evolution.**
4. **Explain the role of shear depth in controlling the resulting storm structure and evolution.**
5. **Explain the role of hodograph curvature in controlling resulting storm structure and evolution for strongly sheared environments.**

Definitions, Strengths, and Limitations of Parameters Used for Forecasting Severe Weather Type (Objectives are stated in prerequisite) **Lesson 2**

Production and Detection of Severe Weather **Lesson 3**

6. **Identify the typical environment, structure and evolution of weakly sheared cells.**
7. **Describe how to anticipate the motion of ordinary cells.**
8. **Describe the common signatures in ordinary cells that can be used to detect severe winds, large hail, tornadoes and heavy rainfall.**

   a. **Identify the environmental and storm signatures favorable for dry and wet microbursts.**

b. Identify the most likely period of a cell lifetime for non-mesocyclonic tornadoes.

Structure, Morphology and Interpretation of supercells.

9. Identify the typical environment, storm structure, and evolution of supercells.
10. Identify the effects of shear on storm propagation.
11. Describe how to anticipate the motion of supercells.
12. Identify radar reflectivity characteristics of supercells.
13. Identify the criteria for determining the presence of a mesocyclone.
14. Describe the environmental, structural and evolutionary differences that can produce low precipitation, high precipitation and classic supercells.
15. Identify the common signatures in supercells that can be used to detect severe winds, large hail, tornadoes, and heavy rainfall.
    a. Identify three major radar signatures for determining large hail.
    b. Describe the criteria for defining a tornado vortex signature.
    c. Describe two major meteorological contributors that contribute to a flash flooding threat from supercells.
16. Identify multicell storm structures and evolutions including conceptual models, storm (system) motions, environments, and life cycles.

17. **Describe the morphology and the influence of the Rear- Inflow Jet (RIJ) on multicells.**
18. **Identify the characteristics of bow echoes and the mechanisms involved in their formation.**
19. **Recognize multicell storm signatures for monitoring and anticipating: 1) damaging winds, 2) large hail, 3) tornadoes, and 4) heavy (potentially flooding) rain.**

Lesson 1: Fundamental Relationships Between Shear and Instability on Convective Storm Structure and Type.

Objective 1

For a given quantity of buoyancy, determine the influence of shear strength on overall storm structure and evolution.

Based on observations and modeling studies, the organization and longevity of convective storms and storm systems tend to increase with increasing magnitudes of vertical wind shear. For example, ordinary cells tend to occur at the weakest end of the shear spectrum, while supercell environments generally possess some of the strongest values of shear. Figure 1-1, from the COMET CD-ROM, *A Convective Storm Matrix*, illustrates the integrated effects of vertical wind shear on the spectrum of convective storm processes.

Effects of Shear

Generally speaking, the longer the hodograph (length), the more vertical shear (and subsequent horizontal vorticity) will be present in the atmosphere. Increasing vertical shear creates more opportunities for storms to develop midlevel rotation in their updrafts. Another effect of vertical wind shear, due to horizontal pressure gradients induced from vertical shear and a blocking updraft column, is that a convective cloud will become tilted in the direction of the vertical shear vector. This tilting acts to distribute rainfall downshear from the updraft, and has the potential to improve overall storm longevity.

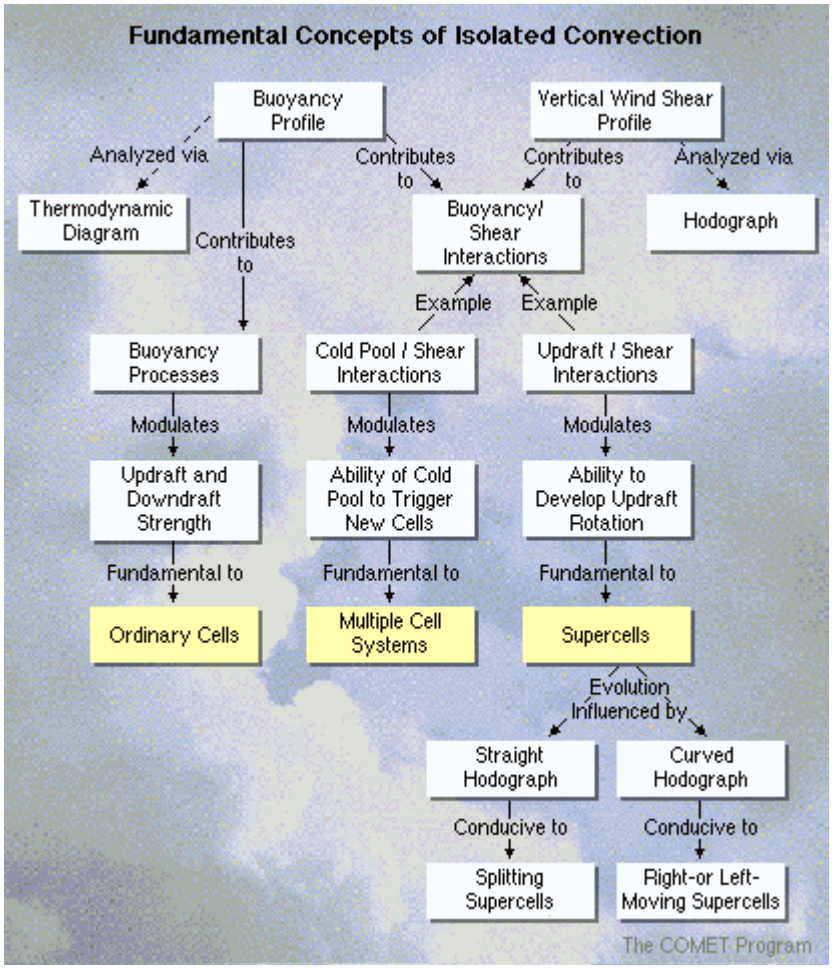

Figure 1-1. A schematic flowchart showing the fundamental concepts of convection. From *A Convective Storm Matrix* (COMET,

Objective 2

For a given hodograph and magnitude of vertical wind shear, identify the influences of variations to the buoyancy profile on overall storm structure and evolution.

Increasing the buoyant energy in a convective storm or system tends to increase the size, depth, and strength of the individual convective cells, and the overall size and strength of the whole convective system. The amount of buoyancy and shear in the environment helps determine storm type. A depiction of the relationship between shear and buoyancy in numerically

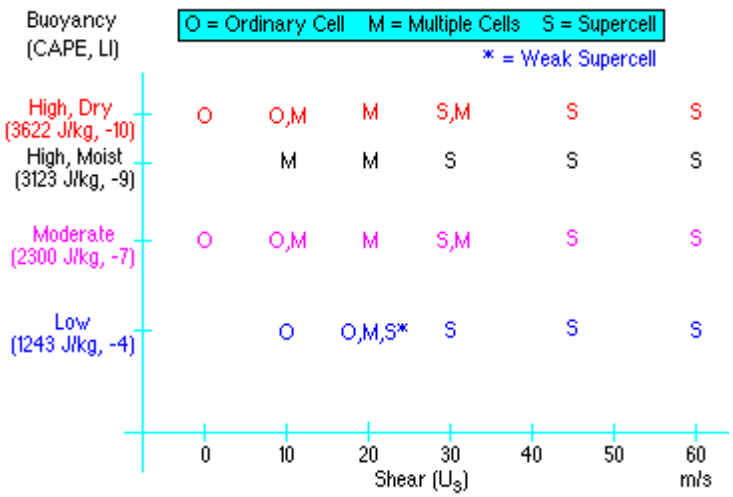

Figure 1-2. Distribution of buoyancy (CAPE, Lifted Index) and shear (hodograph length - U_S) for 3 classes of storms in numerical model simulations from *A Convective Storm Matrix* (COMET, 1995).

simulated storms is shown in Figure 1-2. The general relationship between buoyancy as expressed by Convective Available Potential Energy (CAPE), and Storm-Relative Helicity (SRH), in observations of tornado proximity soundings (Fig. 1-3) are somewhat similar to the numerical modeling results shown in Fig. 1-2. Edwards and Thompson (2000) suggested that increases in CAPE have a stronger influence on tornado likelihood than 0-3 km SRH, with SRH displaying a wider distribution of values for lower CAPE values in non-tornadic events (Fig. 1-3). Johns et al. (1990) indicated a broad range of possible CAPE and SRH (0-2 km) combinations for F2 and greater tornado proximity sounding cases (Fig. 1-4). There are some general relationships that can be gathered from these studies:

- **Increasing shear in a high CAPE environment can increase the probability of supercells.**
- **In low CAPE environments (such as in the cool seasons), stronger shear environ-**

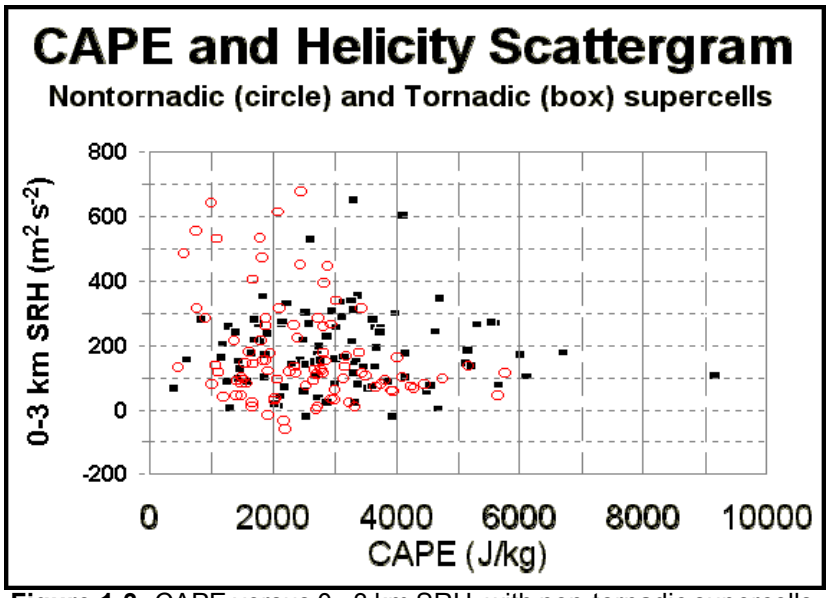

Figure 1-3. CAPE versus 0 - 3 km SRH, with non-tornadic supercells as open circles and tornadic as squares (Edwards and Thompson, 2000)

ments may be sufficient to produce tornadic storms. External forcing mechanisms (such as fronts, upper-level jet streaks, and density boundaries) and the strength of the capping layer (estimated by CIN) also play a large part in modulating convective initiation, storm structure and resultant storm evolution.

Shear and buoyancy (as well as cold pool strength) also play a role in determining squall line and bow echo strength, but their variations and relationships are not as well established as they are for supercells. Objective 16 includes more information on the relationship of shear and buoyancy on squall line and bow echo strength (Multicell thunderstorms include squall lines and bow echoes).

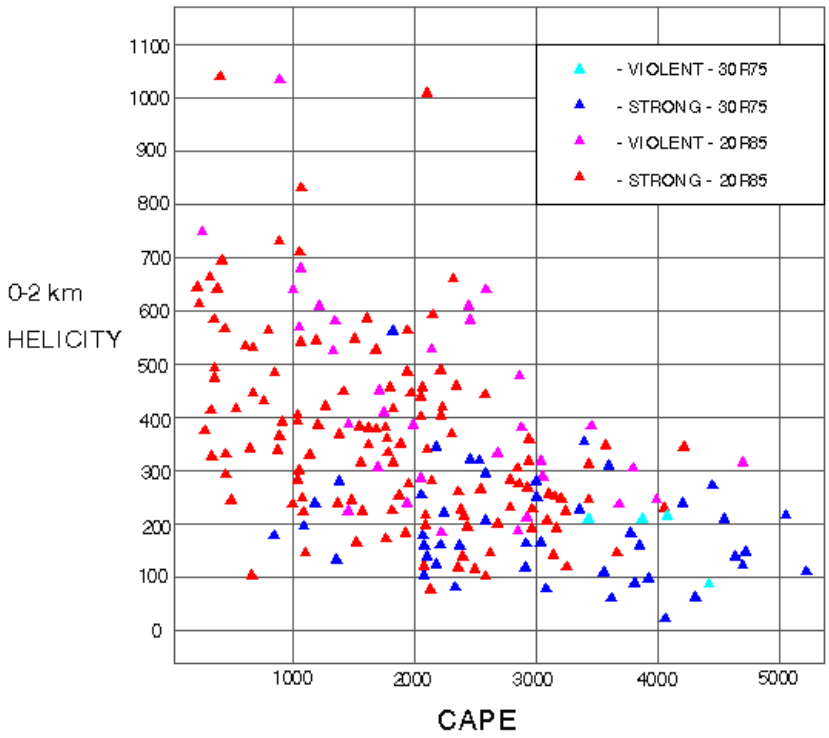

Figure 1-4. CAPE versus 0-2 km SRH for strong and violent tornado cases for two types of storm motion calculations (Johns et al., 1990).

Objective 3

For a given hodograph and magnitude of vertical wind shear, describe the role of midlevel dry air on storm evolution.

Midlevel Dry Air Promotes Stronger Downdrafts

Thunderstorms that form in environments with drier midlevel air (lower wet-bulb potential temperature,Q_w) will tend to produce stronger evaporatively-cooled downdrafts and wind gusts at the surface (Fawbush and Miller, 1954; Browning and Ludlam,1962; Foster, 1958). The Fawbush and Miller (1954) “Type-I” composite sounding for producing tornadoes exhibited dry, capping air in midlevels originating off the hot, dry high Mexican plateau overlaying moist, boundary layer air from the Gulf Coastal region. Early modeling studies of supercell thunderstorms in the 1980s suggested that greater instability, as measured by CAPE, increased storm downdraft strength (Weisman and Klemp 1982, 1984). In

addition, weaker shear, which implied less entrainment, was found to produce stronger downdrafts.

Effect on Storm Evolution Due to Vertical Placement of Dry Midlevel Air

In a three-dimensional modeling simulation, Gilmore and Wicker (1998) found that mid tropospheric dryness helped induce significant differences in low-level supercell storm morphologies and evolutions (Fig. 1-5). For cases with very dry midlevel air (due to smaller vertical wind shear and lower-altitude dry air placements), they found that the resulting low-level outflow moved out faster than the midlevel mesocyclone, which tended to weaken the thunderstorm updraft and the associated mesocyclone. On the other hand, greater midlevel moisture (due to stronger wind shear

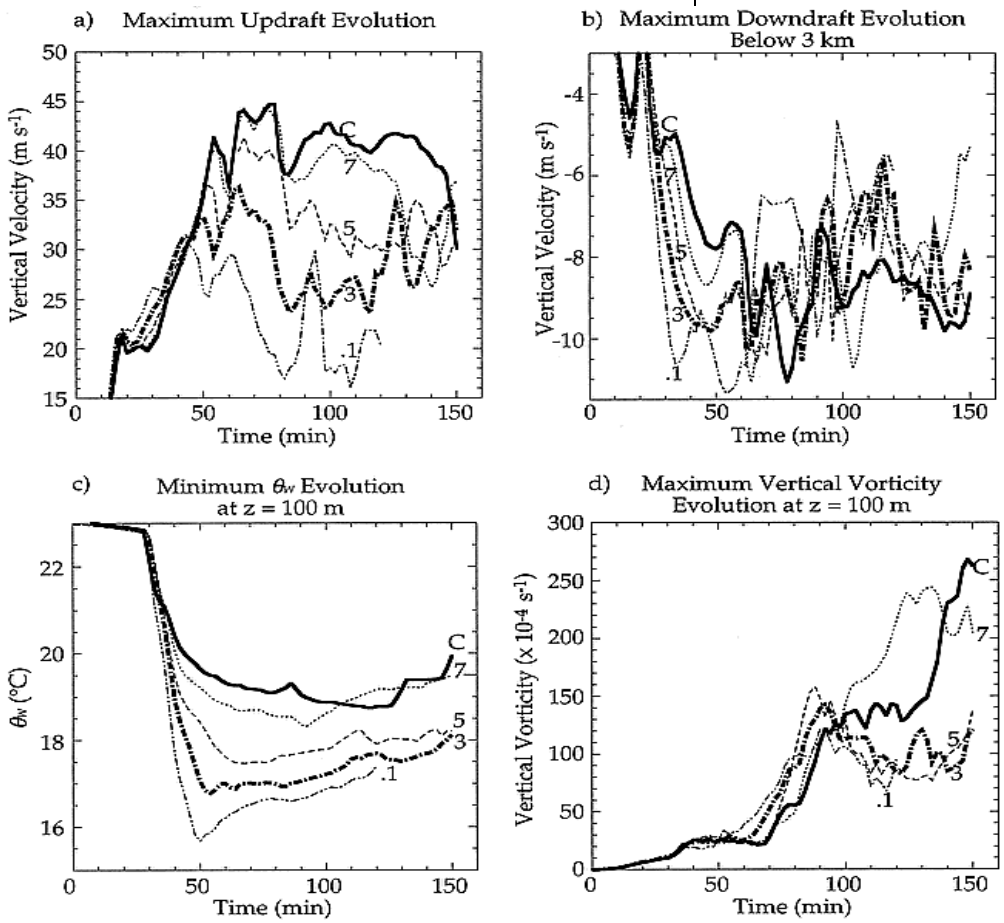

Figure 1-5. Evolutions of a) maximum updraft, b) maximum downdraft below z=3 km, c) minimum Θ_w at z=100 m, and d) maximum vertical vorticity at z=100 m for supercell simulations with driest modified air at z=2.3 km. The value "C" represents the control case while others are represented by their respective water vapor mixing ratios (g/kg) at the height of the driest modified air. Two minute sampling from the model data is plotted. (From Gilmore and Wicker, 1998)

and/or higher altitude dry air placement), induced a delayed (and weaker) surface outflow which enhanced the updraft. Cases with dry air at higher altitudes were less able to bring their minimum Q_w air down to the surface due to a reduced evaporative cooling rate aloft and a longer path where mixing between the downdraft and environment would occur. In the greater midlevel moisture cases, the resulting speed of the low-level storm features maintained alignment of the midlevel mesocyclone and thus, increased storm longevity.

Downdraft Convective Available Potential Energy (DCAPE)

The downdraft potential of the simulated environment from Gilmore and Wicker (1998) was represented by a parameter called DCAPE [Downdraft Convective Potential Convective Energy; Emanuel (1994)]. According to results from Gilmore and Wicker (1998), DCAPE was shown to be a poor indicator of downdraft intensity, or low-level outflow strength, due to parcel theory assumptions. Entrainment of environmental dry air dilutes thunderstorm downdrafts and significantly changes the Q_w of parcels. This dilution increases with greater vertical wind shear or when downdraft parcels with low Q_w descend from higher altitudes. As a result, increases in kinetic energy due to evaporative cooling within the downdraft are much less than predicted.

Dichotomous Effects of Dry Midlevel Air

Numerical cloud model simulations in *A Convective Storms Matrix* showed soundings with similar CAPE and shear but different midlevel relative humidity profiles such that dry midlevel air seemed to weaken the storm system. However, the dry midlevel air did enhance the surface cold pool produced by the rainy air in the downdraft. Thus, in some cases, midlevel dry air, especially when it is associated with steep, midlevel temperature lapse rates, can enhance the strength of multicellular

systems like squall lines and bow echoes. **The reason for this dichotomous effect is that midlevel dry air can be entrained into both convective updrafts and downdrafts, decreasing potential updraft buoyancy, but increasing potential downdraft negative buoyancy.**

Rules of Thumb for Mean Relative Humidity (RH)

Based on operational severe storm forecasting rules, mean Relative Humidity (RH), as indicated from raobs and model soundings as the average RH in the column from near the surface (~1000 mb) to midlevels (~500 mb), is usually greater than 40-45% in severe thunderstorm environments. This empirical rule is a result of synoptic environments supportive of severe weather containing a dry midlevel layer overlying a moist boundary layer. If the environment indicates more saturation through a deep layer (70% mean RH), then, all other factors being equal, storms are more likely to produce heavy rain as opposed to organized severe weather. Thus, as is the case with most other thermodynamic parameters, storm or system evolution is not simply related to a single parameter such as midlevel dry air.

Inverse Relationship Between DCAPE and Mean Winds in Estimating Cold Pool Strength

A recent study (Evans and Doswell, 2001) of derecho environments using proximity soundings suggested that there is an inverse relationship with DCAPE and mean wind (0-6 km). DCAPE was used as an estimate of the potential cold pool strength. When the mean wind and large scale forcing were weak, the potential for strong downdrafts and resulting cold pools played a dominant role in creating strong surface winds. On the other hand, when the mean wind and synoptic forcing were strong, severe surface winds occurred with relatively weak downdrafts and cold pools. Thus, midlevel dry air might not be as

important when stronger environmental winds (and shear) are present.

Objective 4

Explain the role of shear depth in controlling the resulting storm structure and evolution.

While the magnitude of vertical shear is known to be vitally important for supercell potential, the depth, shape, and location of strongest shear in the total shear profile also strongly affects convective storm behavior. In particular, f**rom observations of both significant (F2 or greater) tornadic supercells and long-lasting multicell (derecho) systems, ambient shear was strongest in the lowest 1 to 2 kilometers above the ground** (Evans and Doswell, 2002). Shear that extends through a deep layer (8 to 9 km AGL) influences the resulting flow pattern in the storm system by varying the distribution of hydrometers and precipitation. **Shallow shear in supercells may produce a stronger and colder Rear-Flank Downdraft (RFD) which might inhibit low-level tornadogenesis (Brooks et al., 1994)**. **Shear depth, when combined with storm (or system) motion, determines to a large extent the resulting organizational mode of most storm types.** For example, in an environment with relatively uniform thermodynamic characteristics, **the shear will be deeper for significant tornadoes on average than for other storms (and storm types)**. Moreover, when deep shear is weaker, it is the speed of the storm (or storm system in the case of multicells) which determines the intensity and longevity of the storm (or system). The resulting **rear-to-front flow** progressively increases in the mid and upper levels for discrete supercells. In contrast, deep system-relative flow **(front-to-rear flow)** from the surface through mid and upper lev-

els is critical in the organization and maintenance of multicell systems (such as derechos).

These results are similar to numerical simulations where strong, shallower shear environments were **less** likely to produce long-lived supercells than with environments with strong deeper shear. In terms of convective line systems, the simulations indicated a relationship between shallow shear and resulting cold pool strength. The process led to deeper lifting along the leading edge of convection, and produced longer-lived organized squall lines including bow echoes (Figures 1-6 and 1-7). By contrast, weaker, shallow shear environments produced weaker convective systems. The simulation only tells part of the story. Environmental instability and system relative flow must also be considered.

More discussion on the influences of shear depth and magnitude on storm structure and evolution is presented in Lesson 3.

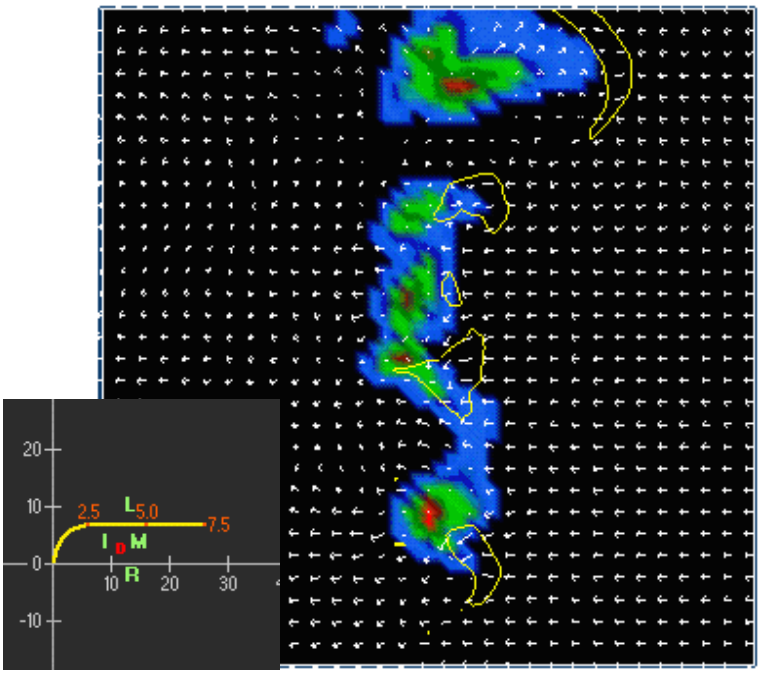

Figure 1-6. Planview map at 4 km above surface of a model simulation of convection three hours after initiation using the hodograph with 30 m/s of shear over 7.5 km. Colored regions represent vertical velocity while thin yellow isohyets are vertical vorticity. The white vectors are system-relative winds. From the *Convective Storm Matrix* (COMET, 1995).

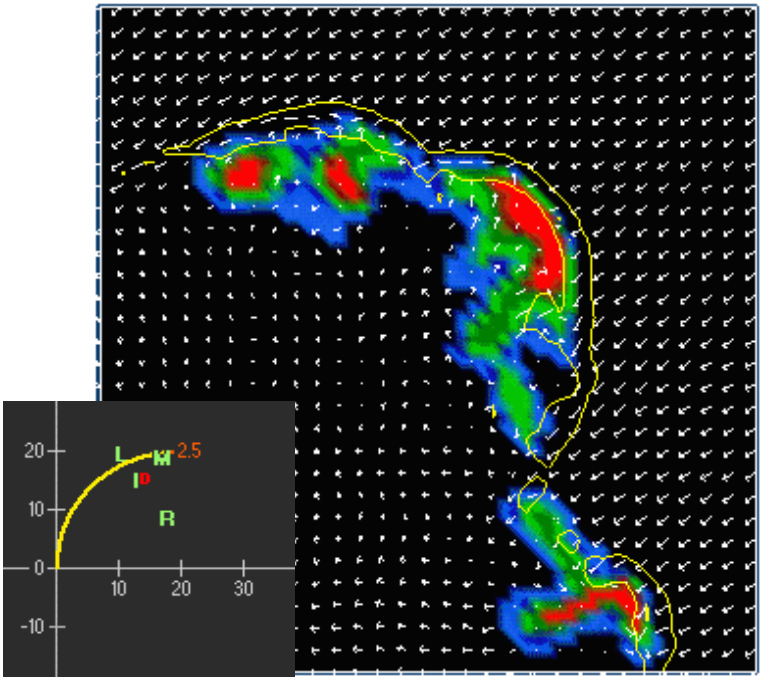

Figure 1-7. As in figure 6 except now there is 30 m/s of shear over 2.5 km. From *The Convective Storm Matrix* (COMET, 1995).

Objective 5

Explain the role of hodograph curvature in controlling resulting storm structure and evolution for strongly sheared environments.

Both straight and curved hodographs produce equally strong supercells given enough shear. However, straight hodographs allow both the right (cyclonic) and left (anticyclonic) moving supercells to be equally strong. Clockwise (counterclockwise) turning hodographs favor the right-moving (left-moving) supercell and weakens the left-moving (right-moving) member. As an example, note the mirror image cyclonic and anticyclonic supercells in Figure 1-8 in an environment characterized by unidirectional shear (straight hodograph example). Conversely, applying the curved hodograph with the same shear magnitude, the cyclonic supercell dominates and the anticyclonic supercell is almost

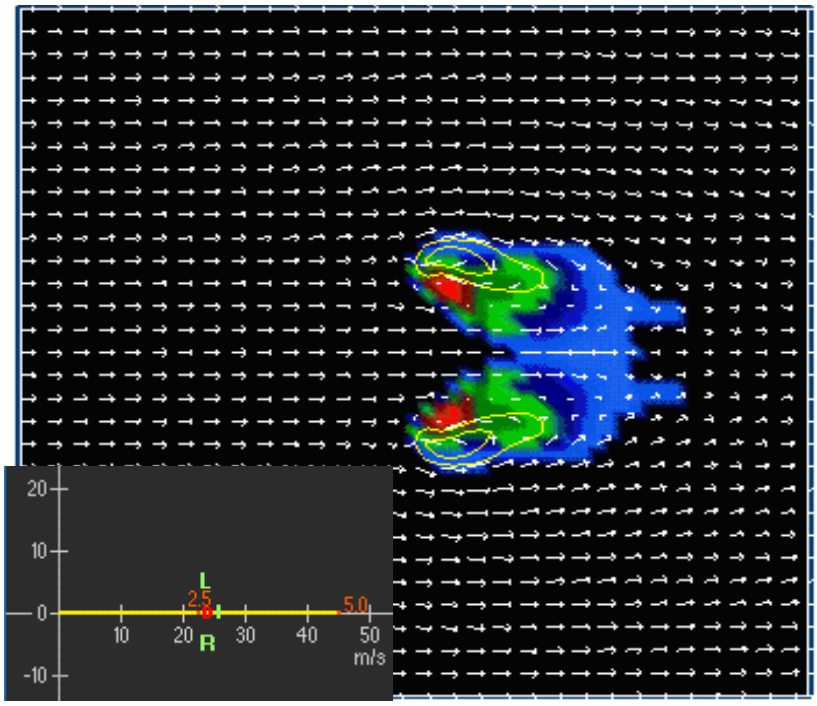

Figure 1-8. Model simulation of updraft strength (shaded colors) and vorticity (yellow contours) at 4.6 km above surface and 1.5 hours after initiation for the straight hodograph shown in the inset. The hodograph has 46 m/s of shear over five kilometers. From *The Convective Storm Matrix* (COMET, 1995).

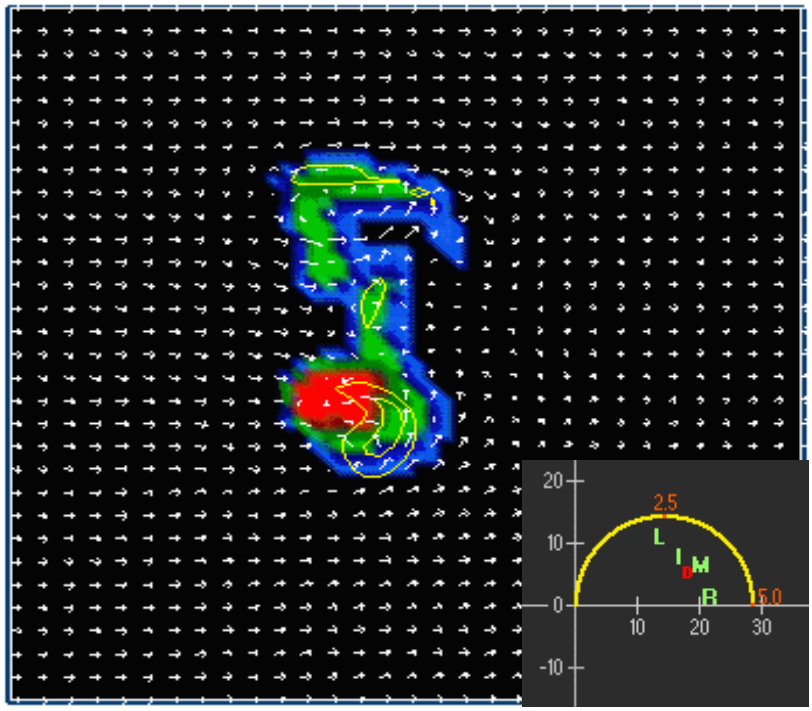

Figure 1-9. Similar to Figure 1-8, except for a curved hodograph with similar shear. From *The Convective Storm Matrix* (COMET, 1995).

gone (Fig. 1-9). Review *A Convective Storm Matrix* (COMET, 1995) to explore other examples of straight and curved hodographs with varying shear magnitudes.

Another way to analyze the differences between straight and curved hodographs is from a streamwise vorticity perspective (Davies-Jones, 1984). An updraft moving with the mean wind in a unidirectional shear environment (straight hodograph) tilts only crosswise vorticity. To create a rotating updraft, it is necessary to tilt streamwise vorticity. The updraft must move off the hodograph before being able to tilt streamwise vorticity. An updraft moving with the mean wind in a clockwise-turning curved hodograph is able to tilt streamwise vorticity without even having to move away from the mean wind.

Lesson 2: Definitions, Strengths, and Limitations of Environmental Parameters

Buoyancy

Several thermodynamic and kinematic parameters have been developed to assess the vertical distribution of buoyancy for the purpose of evaluating convective severe weather potential. Many thermodynamic stability indices such as Lifted Index (LI) or Showalter Index (SI) can easily be computed via sounding analysis from a Skew-T Log-P Diagram (See RTM-230).

CAPE

The best thermodynamic parameter to assess buoyancy is Convective Available Potential Energy (CAPE). CAPE is a cumulative measure of the positive buoyant energy (in J/kg) a rising parcel of air would have between its Level of Free Convection (LFC) and the Equilibrium Level (EL); See RTM-230 for the mathematical definition and graphical representation of CAPE. Whereas the LI or SI uses a temperature difference between rising parcels and the environment at a single level, CAPE is a vertically integrated quantity. Thus, there is not a one-to-one relationship between CAPE and instability. CAPE depends on instability and the depth of integration.

Model CAPE Discrepancies

There are often big differences between model-derived computations of CAPE values and CAPE values derived from observed sounding data. These differences result from several factors, including:

1. Assimilation and initialization processes used in the models. These processes incorporate more data than raobs (including first guess fields), such that model soundings at initialization are not exact duplicates of actual soundings.

2. The methodology that is used to determine from where the parcel is lifted. The method of lifting the parcel with the most unstable characteristics in the lowest 300 mb (AGL) often produces the most reliable estimates of CAPE in all situations (SPC, private communication).

Importance of CAPE Density, 0-3 km CAPE

CAPE is very sensitive to both the magnitude of buoyancy and the depth of the integration. Modeling work examining mini-supercells by Wicker and Cantrell (1996) found that the coupling of low-level shear and small values of low-level CAPE (i.e., CAPE located in the lowest 1-3 km) appeared to be more important for the development of rotational characteristics within these storms than were larger values of CAPE through a deeper layer. Some of the mini-supercell CAPE values were as low as 600 J/kg in simulations which produced significant low-level accelerations and vertical velocities. Other research such as McCaul and Weisman (1996) and Johns and Doswell (1992) have also noted that a large fraction of supercell cases nationwide arise in situations where CAPE values are less than 1500 J/kg (likely mini-supercells or low-topped events). Grant (1995) found that the average CAPE as deduced from proximity soundings in elevated severe thunderstorms was approximately 700 J/kg. Blanchard (1998) suggested that it is possible for environments to have similar CAPE values but different degrees of instability. The vertical distribution of CAPE, whether the CAPE area is “tall and thin” or “short and wide”, should be considered when assessing the convective potential of a sounding. Normalized CAPE (NCAPE), introduced by Blanchard (1998), may provide forecasters with a better indication of instability in environments in which the depth of free convection is shallow (low-topped mini-super-

cells or tornadoes associated with landfalling tropical storms).

Convective Inhibition (CIN)

To effectively evaluate the effects of buoyancy in forecasting severe weather type, one must also assess Convective Inhibition (CIN). CIN is a measure of the “negative area” on a sounding between the surface and the LFC. CIN is a measure (in J/kg) of the capping-intensity of the atmosphere and assesses the ability of the vertical temperature profile to suppress surface-based convection. In most cases, when an air parcel moves upward away from the earth's surface, it will be cooler than the surrounding environment until it moves above the Level of Free Convection (LFC). This negative buoyancy implies that surface-based convection must be forced upward beyond the LFC before an updraft will be sustained. CIN measures the negative buoyancy working against this rising parcel. In situations of elevated convection, the forcing mechanism acts to lift parcels above the stable capping layer and thus, does not necessarily have to overcome all the negative buoyancy. In those cases, a strong cap (large CIN) might be favorable for sustaining the convection given sustained synoptic or mesoscale forcing and sufficient instability existing above the stable surface layer.

Lifting Condensation Level

The Lifting Condensation Level (LCL) is the height at which a parcel becomes saturated when lifted dry adiabatically (See RTM-230). It is related to the amount of low-level relative humidity which would affect cooling through evaporation of rain in the downdraft portion of a storm. The higher the LCL is in the storm environment, the drier the boundary layer will be. Rasmussen and Blanchard (1998) showed that LCLs in tornadic supercell (TOR) soundings were significantly lower than that for non-tornadic supercells (SUP) and in non-

supercell storms (ORD). Half of their TOR soundings had LCLs below 800 m, while half of their SUP soundings had LCLs above 1200 m. Substantial variations undoubtedly occur on small time and space scales with LCLs, so sampling with network soundings may not be representative. Actual LCL heights near tornadic supercells may be considerably lower than those documented in research.

Shear

Several parameters are used to estimate vertical shear, which, along with buoyant energy, strongly influences what type of convective storm may develop. Forecasters typically analyze hodographs (both hodograph curvature and overall length) in the lower troposphere to assess vertical wind shear (See RTM-230 and the Background Section of the *Convective Storm Matrix* Web module developed by COMET for a good explanation of hodographs). Vertical wind shear, as you recall from Objective 1, is the most important factor for storm organization. Surface-to-6 km (AGL) shear has been used extensively in research and operations for evaluating environments that support supercell storm processes. Hodograph length, which measures the total magnitude and depth of vertical wind shear, is easily calculated by adding up the wind vectors along the hodograph through a certain layer. This total value (in m/s) can be used to estimate if the dynamics of internal storm rotation in supercells are likely if thunderstorms develop. Typically, the lower bound threshold of hodograph length for supercells (as derived from observed and model soundings on the synoptic scale) is around 20 m/s (from SPC communication).

Minimum Shear for Supercells

In numerical modeling simulations (Weisman, 1992, 1993) environments that had hodograph lengths greater than 20 m/s (with CAPE values of at least 2000 J/kg) over the lowest 2-3 km AGL were often associated with very long-lived, multiple storm systems. However, in analyzing proximity soundings along the path of mature derechos, Evans and Doswell (2001) found much lower values of 0-2 km shear were common, with three-fourths of the cases containing shear magnitudes less than 16 m/s, and values ranging from near 3 to 30 m/s. These shear values were found in cases typically associated with 0-6 km shear vector magnitudes less than 20 m/s, weak forcing, and high values of CAPE.

Shear in Tornadic and Non-tornadic Supercells

From analyzing over 6000 proximity soundings, Rasmussen and Blanchard (1998) established a baseline climatology of several severe storm kinematic parameters, such as Boundary-Layer-(BL)-to-6 km shear vector, mean shear, Storm-Relative Helicity, and storm-relative upper-tropospheric wind speed. All of these parameters showed some value in differentiating between supercell and non-supercell environments. However, BL-to-6 km shear had no utility for distinguishing between supercells which produced significant tornadoes and those which only produced large hail. On the other hand, Storm-Relative Helicity (SRH) and boundary mean shear, which was computed as the length of the hodograph divided by the depth of the layer measured (4 km in their studies), were better able to distinguish between supercells that produced significant tornadoes and those that only produced large hail. In the study of kinematic parameters, SRH showed the best discrimination ability between storm type categories (Fig. 2-1), suggesting that the streamwise component of hori-

zontal vorticity is the component that dominates in the production of rotating updrafts in supercells.

Storm-Relative Helicity (SRH)

SRH is proportional to both streamwise vorticity and storm-relative winds and takes into account storm motion. The equation for SRH, as defined by Davies-Jones et al. (1990), is

$$SRH = \int_0^h (V - C) \bullet \omega dz \ , \qquad (2\text{-}1)$$

where V is the horizontal velocity (ground-relative vector wind), C is the storm motion, and **w** is the horizontal vorticity vector. The integration is over the inflow layer of the storm from 0 km (the ground) to some depth h (typically 1 to 3 km).

Correlations in SRH and Tornado Intensity

Johns et al. (1990) and Davies-Jones et al. (1990), using observed storm motions in calculations of SRH, indicated correlations between increasing SRH values and tornado intensity. The observed 0-2 km mean SRH magnitude for strong (F2/F3 tornadoes) was about 360 m^2s^{-2}, while the mean SRH for their violent (F4/F5) category tornadoes was about 450 m^2s^{-2}.

Can You Predict Maximum Tornado Intensity From SRH?

Kerr and Darkow (1996) examined SRH values for 184 tornado proximity soundings. The table below (Table 2-1) shows the mean SRH values for the corresponding F-scale intensities. Their study contained no F5 tornado proximity soundings. The mean SRH for the entire data set was 142 m^2s^{-2}.

F-scale	F0	F1	F2	F3	F4
Helicity value m^2s^{-2}	66	140	196	226	249

Table 2-1: SRH vs. F-scale (from Kerr and Darkow, 1996)

They concluded that by examining regions where CAPE values were positive and 0-3 km SRH values were greater than 100 m^2s^{-2}, one could generally identify areas where supercell thunderstorms were possible if convection developed.

SRH is a Better Supercell Forecasting Tool

These types of studies suggest that SRH may have some predictive value as a tornado forecast tool. However, later studies have shown that it is a much better tool for estimating supercell potential as opposed to tornado potential. Two problems for using SRH as a forecast tool are that an estimate of storm motion is required and the depth for computing SRH is critical. Deviant right motion is often observed, but the speed of storms vary considerably depending on external factors. This is why

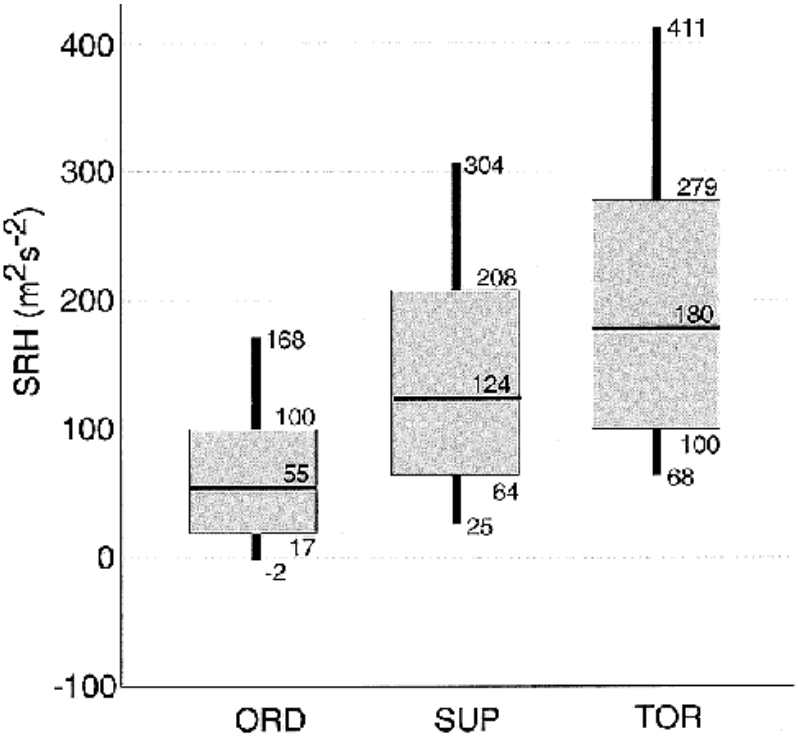

Figure 2-1. Box and whiskers graph of Storm-Relative Helicity (0-3 km) for soundings associated with supercells with significant tornadoes (TOR; right), supercells without significant tornadoes (SUP; middle), and non-supercell thunderstorms (ORD; left). Gray boxes denote the 25th to 75th percentiles, with the heavy horizontal bar at the median value. Thin vertical lines (whiskers) extend to the 10th and 90th percentiles (Rasmussen and Blanchard, 1998).

using hodograph length as a shear parameter can be an advantage over SRH in providing an estimate of rotation potential before storms develop.

Depth of SRH to be Used

In the past, the depth chosen for calculating SRH was usually 3 km. Recent and ongoing studies (e.g., Rasmussen, 2001) have found that the near ground (0-1 km AGL) layer may have critical implications to tornado potential in supercells (Fig. 2-2) and actually have better discrimination ability than 0-3 km SRH.

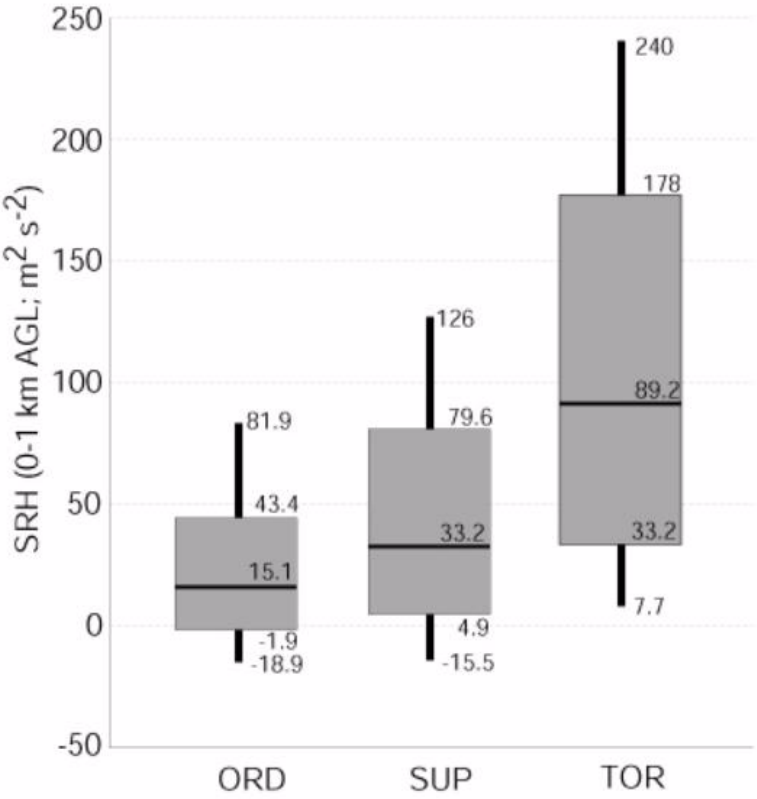

Figure 2-2. Similar to Figure 2-1 except for 0-1 km AGL SRH for soundings associated with supercells with significant tornadoes. (From Rasmussen, personal communication)

Thus, it is important to conclude from all of these studies that large SRH values (at any level) do not imply that a particular sounding will be associated with a significant tornado. In the Rasmussen and Blanchard (1998) study, almost 25% of their non-supercell soundings (600 soundings) had SRH

values between 100 and 168 m^2s^{-2}. That amount is more than the total number of soundings in both of the supercell categories. Since forecast storm motion is used in the computations of SRH, it is important to re-analyze your local estimates of SRH once observed storm motions are known.

Midlevel Flow in Tornadic and Non-tornadic Storms

The role of midlevel shear has also been investigated in the prediction of storm type. Specifically, the character of the midlevel storm-relative flow has been shown to influence the production of low-level mesocyclones and the potential for storms to produce significant tornadoes (Thompson, 1998). Thompson found that supercells were more likely to produce tornadoes when the midlevel (estimated at 500 mb) storm-relative winds were greater than 8-10 m/s.

Shear and Buoyancy Combinations

BRN

Mean shear, as well as SRH, becomes a much stronger predictor of supercells and tornadoes when paired with CAPE. The Bulk Richardson Number (BRN) has been used as a supercell predictor ever since it was investigated using numerical simulations (Weisman and Klemp, 1982).

BRN is a rough measure of the buoyancy to shear ratio.

$$BRN = CAPE / ½ (U^2), \qquad (2\text{-}2)$$

where CAPE is Convective Available Potential Energy and U is the bulk shear, determined by subtracting the density-weighted mean wind vector in the lowest half-kilometer layer from the den-

sity-weighted mean wind vector in the lowest six-kilometer layer.

BRN vs. BRN Shear

Weisman and Klemp (1982, 1984) determined that environments with BRN < 50 favored the development of supercells, while BRN > 35 favored multicells. The overlap area (35 < BRN < 50) suggested that both supercells and multicells were possible at the same time. Operational viability of this parameter is questionable because of the wide range of CAPE values typically observed in environments which produce tornadoes. For very large values of CAPE (> 4000 J/kg), the BRN is dominated by the CAPE such that BRN is large regardless of the values in the denominator (known as BRN shear; Stensrud et al., 1997).

Other BRN Limitations

Moreover, Rasmussen and Blanchard (1998) found that even though 75% of their (SUP) supercell soundings had BRN values < 17, over 50% of the ORD (ordinary thunderstorm) soundings had those values as well. In addition, another limitation is that BRN does not account for detailed aspects of the wind profile, particularly low-level curvature. Johns et al. (1990) examined the mean shear and buoyancy values for 242 strong-to-violent mesocyclone-induced tornadoes. From proximity soundings, their study showed 15% of the tornado events had CAPE values less than or equal to 1000 J/kg, with 47% of the events having BRN values less than 8. One explanation that was offered for the low BRN values is that in low-buoyancy environments, shear-induced pressure forces, related at least in part to the low-level curvature shear, can be the dominant factor in controlling updraft strength. Therefore, it appears likely that in many situations where the BRN value is a very low value and supercells do occur, that the low-level

curvature shear plays a crucial role in helping to sustain the rotating updrafts.

BRN Shear Values for Non-tornadic and Tornadic Supercells

The denominator of BRN (½ (U^2)) was shown by Stensrud et al. (1997) to be a surrogate for storm-relative midlevel flow, citing the advantage that BRN shear is independent of storm motion. Utilizing MM4 mesoscale model output in their study of selected severe weather cases, they found that BRN shear values of 40-100 m^2/s^2 indicated a significant possibility of tornadic supercell storms, whereas values less than 40 m^2/s^2 were associated with storms dominated by outflow (e.g., bow echoes).

Energy Helicity Index (EHI)

The Energy-Helicity Index (EHI; Hart and Korotky, 1991; Davies 1993) is defined as

$$EHI = (CAPE)\,(SRH) / 1.6 \times 10^5 \qquad (2\text{-}3)$$

This index is used operationally for supercell and tornado forecasting, with values > 1.0 indicating a potential for supercells, and values > 2.0 indicating a high probability of supercells. As with BRN, EHI has some value in discriminating between supercells that produce tornadoes and those that do not (Fig. 2-3). The main forecasting application of using EHI is that the likelihood of significant tornadoes increases with increasing EHI.

Vorticity Generation Parameter (VGP)

The Vorticity Generation Parameter (VGP) is derived from an examination of the parameter space investigated in Rasmussen and Wilhemson (1983) and the physical concept of tilting of horizontal vorticity (to vertical vorticity). The equation used by Rasmussen and Blanchard (1998) is

$$VGP = [S(CAPE)^{1/2}], \qquad (2\text{-}4)$$

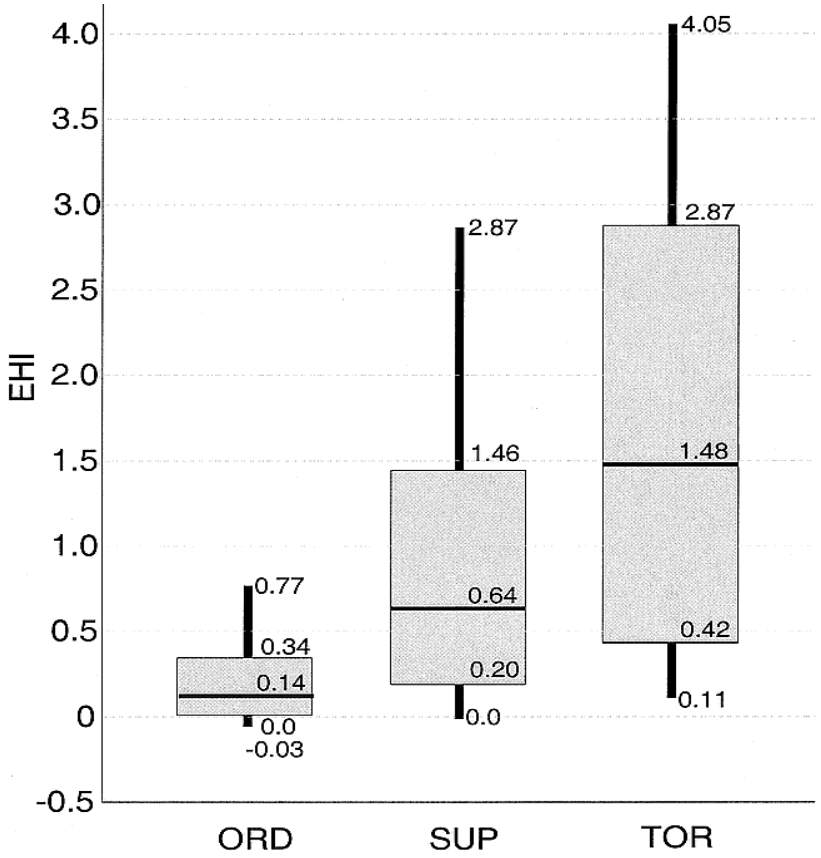

Figure 2-3. As in Figure 2-1, except for Energy Helicity Index (EHI). From Rasmussen and Blanchard (1998).

where S was the mean shear (hodograph length divided by depth). Mean shear was assumed to be proportional to the horizontal vorticity vector and $CAPE^{1/2}$ proportional to the vertical component of velocity. So VGP was roughly proportional to the rate of tilting of horizontal vorticity to vertical vorticity. Similar to EHI, VGP has been shown to significantly discriminate between supercells and non-supercells, but is not as good as low-level shear (SRH) paired with CAPE at distinguishing between storms with significant tornadoes.

Summary

The combination of CAPE and shear in parameters such as EHI or VGP improves the use of soundings in discriminating between supercells with significant tornadoes, supercells with no tornadoes, and ordinary thunderstorms. Evaluating shear and CAPE together helps to provide ranges

for potential storm evolutions. For forecasting storm type, one must first assess the synoptic-scale environment to analyze regions of low-level moisture, instability and lift. Proximity soundings can tell us a lot about the potential for a specific type of severe weather such as tornadoes, large hail, or damaging wind. However, changes in the mesoscale environment often strongly influence the large scale conditions and dictate the eventual severe weather mode. Often, multiple convective modes exist simultaneously making a priori assessment of a preferred storm type quite difficult.

One must be aware that there is a high false alarm rate for any parameter value derived from any given sounding. The distributions in the parameter spaces discussed in Rasmussen and Blanchard (1998) and Johns et al. (1990) bear this fact out. Limitations in sampling the actual storm environment also contribute to considerable estimations to reality. Combinations of several parameters, indicating not only the updraft-based aspects of the storm but also the downdraft aspects, will likely provide the best forecast of eventual storm type.

Lesson 3: Production and Detection of Severe Weather

Introduction

While the previous section dealt with fundamental concepts of how shear and buoyancy organize convection, this section's primary topics are the recognition and interpretation of severe storm signatures and their influence on producing severe weather. In this section, we provide you with an understanding of how forecasters can recognize the potential for deep convection to produce severe winds, large hail, tornadoes and flash flood producing rainfall.

We choose to organize this section by storm type including:

- weakly sheared cells,
- moderate and strongly sheared cells,
- and multicells.

Individual weakly sheared (i.e. ordinary cells) to strongly sheared cells (i.e. supercells) are discussed first as they comprise the basic structure of individual cells in deep, moist convection. We then discuss the structure and behavior of multicells. In a multicell storm, the cold pool and its relationship to environmental flow are the dominant mechanisms for initiating new convection. In this section, a group of ordinary cells, supercells, or a combination of ordinary and supercells that share a common cold pool and precipitation area are defined as a multicell.

For each storm type, we will discuss evolution, structure and motion of storms, and characteristics of the near storm environments favorable for the occurrence of:

- severe winds,
- large hail,
- tornadoes,
- and flash flood producing rainfall.

Identify the typical environment, structure and evolution of weakly sheared cells.

Objective 6

Typical Environment

All convection is dependent on sufficient instability. **It is the vertical wind shear that modulates how the convection is organized**. By convention, we use the shear in the near-surface-to-6 km Above Ground Level (AGL) to help us determine whether ordinary cells or supercells are more likely. **If the shear in this layer is less than 20 kts (10 m/s), ordinary cells dominate**. There are caveats to picking the right shear layer to determine the most likely cell type. **The vertical extent of the shear layer should represent approximately the lower half of the convective layer.**

Ordinary Cell Evolution

While most convection contains groups of cells, the life cycle of each cell is often similar to that of an isolated ordinary cell. Typically, an ordinary cell undergoes a life cycle that lasts for an average of 30 minutes from first towering cumulus to dissipation (Fig. 3-1). Most of the life cycle of a convective cell occurs before the onset of heavy precipitation at the ground.

The initial towering cumulus causes sharp gradients in the refractive index of the atmosphere along the cloud edges. These gradients scatter just enough of the incident WSR-88D energy back to result in 15-20 dBZ echoes just above the boundary layer. **The first real precipitation echoes develop as the towering cumulus top rises into the subfreezing layer**. **The most intense**

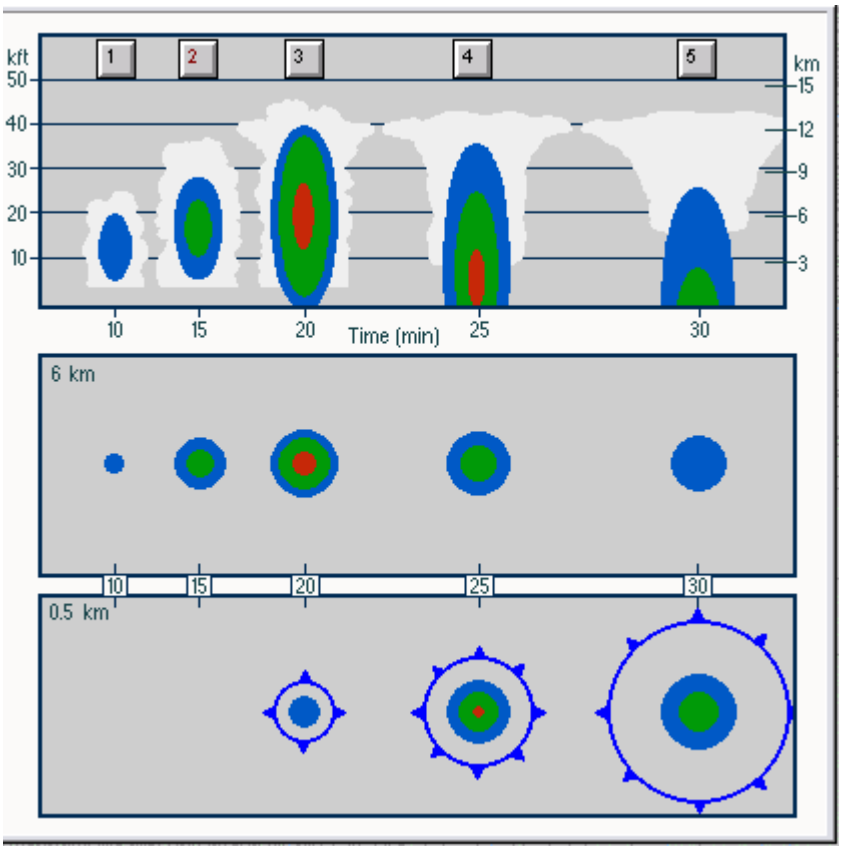

Figure 3-1. A schematic of the life cycle of an ordinary convective cell. (COMET, 1996).

core develops as the updraft passes through the -10^{o} to -20^{o}C layer. Stronger initiating updrafts will produce more intense reflectivities to higher elevations.

A downdraft is likely to initiate as the reflectivities in the precipitation core exceed 45-50 dBZ. The downdraft usually begins between 15 and 20 minutes after cell initiation. As the downdraft commences, environmental air may become entrained into the core. If that air is dry, significant evaporational cooling in the core may significantly contribute to the strength of the downdraft. The base of the descending precipitation core and the downdraft are typically coincident. Therefore, when the core has reached the ground the downdraft begins to spread out into a cold pool. At this time, the updraft remains strong around or preferentially on,

one side of the descending core. **At 25-30 minutes after initiation, the updraft begins to weaken as the outflow stabilizes the low-level environment at its roots**. Without a continuous feed of unstable low-level air in a weakly sheared environment, the updraft dies in the lowest several km above ground leaving an anvil behind.

Objective 7

Describe how to anticipate the motion of ordinary cells.

Weakly Sheared Cell Motion

Single cell storms in the absence of shear move with the flow at any level (which is not surprising since the flow at any one level is about the same as any other level). Adding vertical wind shear complicates predicting single storm motion since an updraft experiences a range of flows depending on the storm's depth and the magnitude of the shear. However, early studies such as the "Thunderstorm Project" found a solid relationship between a mean steering-layer wind and thunderstorm motion (Byers and Braham, 1949). **Most schemes for estimating convective steering-layer flow use the mean 0-6 km AGL wind.**

Since air density increases exponentially toward the ground, a common mean wind calculation is weighted by density giving more influence to the low-level flow. Using the raw 0-6 km mean wind or the 0-6 km density-weighted mean wind provides a relatively accurate method for estimating ordinary thunderstorm motion in most cases. If the averaging utilized a deeper layer, say 0-12 km, then weighting the average by density becomes more important to producing accurate results.

Cautions About Using 0-6 km Mean Winds

There are cautions about using a 0-6 km mean wind for estimating ordinary thunderstorm motion. **Low- (high-) topped thunderstorm motion may**

be influenced better by a shallower (deeper) mean wind. For example, Wilson and Megenhardt (1997) found a reasonable steering layer flow for summertime Florida thunderstorms was the 2-4 km layer. However, for the typically deeper thunderstorms on Tiwi Island (near Darwin, Australia), the same layer mean wind calculation proved less accurate in estimating thunderstorm motion (Wilson et al., 2001).

Weakly sheared cell updraft considerations

The life cycle of a weakly sheared cell just described represents the processes that occur in most if not all observed thunderstorms. However, the timing and the intensity of the updraft vary widely depending on the environment.

Updraft Strength

Given a representative value of CAPE, a maximum theoretical updraft velocity (W_{max}) can be derived ($Wmax = \sqrt{2CAPE}$). **However, this estimate does not take into account precipitation loading or dry air entrainment. Most ordinary cell updrafts reach only about 50% of W_{max} due to these effects**.

Effects of Precipitation Loading

For example, a storm with 3000 J/kg of CAPE over 18 km of depth will have a weaker updraft acceleration than one with the same CAPE over 12 km. **A weaker updraft acceleration increases the chance that precipitation loading will diminish the strength of the updraft before it has a chance to reach the high theoretical speeds**. Stronger updraft accelerations advect cloud condensation nuclei upward so quickly that significant hydrometeor growth does not occur. Therefore, it is important to look at not just the CAPE but also how that CAPE is distributed in the convective layer. CAPE density (or normalized CAPE) is one way to estimate this distribution.

Updraft Strength and Entrainment

Given the same CAPE and CAPE density, not all updrafts will be the same. Some storms remain weak regardless of the environmental CAPE. **Narrow updrafts are likely to entrain dry air to the core limiting updraft strength**. Also, significant midlevel dry air can increase the entrainment efficiency reducing the strength of an updraft even given large values of CAPE.

Given the effects of entrainment, look for these factors when considering the storm with the greatest updraft potential.

- **The widest updrafts allow the updraft core to be protected**. Satellite imagery of the width of the cumulus, or radar imagery of the initial precipitation core width are two ways to estimate which storm will have the least entrainment potential.
- **Secondary updrafts developing near a previous storm may grow in a moister midlevel environment than what the models or raob indicate**. The enhanced moisture is most likely due to outflow induced ascent.
- **A large area of towering cumulus growing in a region of mesoscale ascent (e.g., a boundary) provides a clue that the environment will be more moist than analysis show**.

Objective 8

Describe the common signatures in ordinary cells that can be used to detect severe winds, large hail, tornadoes and heavy rainfall.

- **a. Identify the environmental and storm scale signatures favorable for dry and wet microbursts.**
- **b. Identify the most likely period of a cell lifetime for non-mesocyclonic tornadoes.**

Updraft Location and Strength on Radar

Detecting the location and strength of updrafts is the first step in gauging the potential severity of an ordinary cell. **However, the WSR-88D cannot directly observe updrafts since the radial velocity is mostly horizontal.** Only in situations where the highest few elevation slices pass through the storm updraft can a significant component of radial velocity be considered an updraft. Therefore, other techniques must be used to infer the location of an updraft.

Elevated Core

The most common technique for inferring an updraft location is to observe the location of the upper-level reflectivity core. Hydrometeor growth is strongest as the most intense part of the updraft passes through the -12 to -20^{o}C layer. Therefore, the strongest core in a layer centered just a bit higher should be the location of the strongest updraft.

The intensity and elevation of the elevated core both increase as the updraft intensity increases (Burgess and Lemon, 1990)**.** The maximum height of the 45, 50, 55 dBZ reflectivities in a storm reach higher altitudes for more intense updrafts. **As updraft intensity increases, the likelihood for intense downdrafts and large hail also increases given the same environment**. Table 3-1 shows the likelihood of severe weather associated with the height of the 55 dBZ reflectivity for pulse storms in the Northeast US based on a study by Cerniglia and Snyder (2002). Note that as the 55 dBZ reflectivity reaches higher altitudes, the False Alarm Rate (FAR) decreases for some types of severe reports (wind or hail). Another study (Gerard, 1998) examined 64 storms from either the Jackson, MS CWA or the Cleveland, OH CWA, and found that those storms with 65 dBZ above the 0^{o}C level were severe 96% of the time. They

Height (kft) at or above	POD	FAR	CSI
21	0.625	0	0.625
20	0.734	0.021	0.723
19	0.813	0.088	0.754
18	0.875	0.111	0.789
17	0.906	0.147	0.783
16	0.938	0.189	0.769
15	0.953	.208	0.762

Table 3-1: Probability of Detection (POD), False Alarm Rate (FAR), and Critical Success Index (CSI) for the 55 dBZ echo top thresholds to be associated with severe weather (Cerniglia and Snyder, 2002).

defined a hit for severe storm as having a report of at least 0.75 inch hail or a wind gust exceeding severe limits.l

Storm Top Divergence

Radar base velocity or storm-relative velocity data show a divergent flow pattern at the storm summit once the equilibrium level has been reached and an anvil begins to form. **The center of the divergence indicates the updraft summit location. The intensity of the divergence is positively correlated to the intensity of the updraft** (Witt and Nelson, 1990). Storm top divergence is shallow and can easily be missed by radar because of limited vertical sampling. However, the maximum inbounds and outbounds can be quite strong, exceeding 50 kts in both directions in the stronger storms. As an example, Figure 3-2 shows a radar beam sampling a young storm top. Note that the

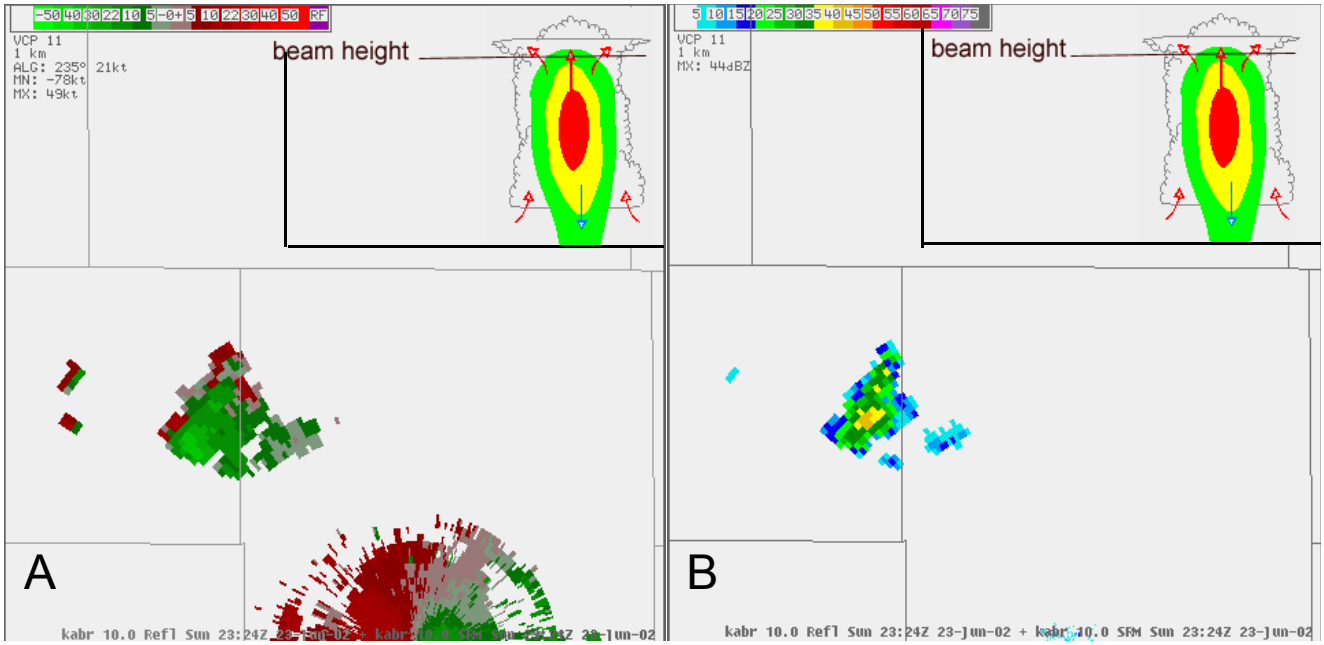

Figure 3-2. Radar beam sampling the top of a young storm showing storm top divergence in A, at the same place as the reflectivity core in B. The insets show the relative location of the beam in a storm cross-section schematic.

divergence axis and the reflectivity core coincide. This storm top divergence is about 45 kts.

Low-level Convergence

During the initial stages of a pulse thunderstorm, there may be a weak radial convergence feature within the lowest two kilometers of the ground as air flows in to feed the updraft. **Low-level convergence can only be detected close to the radar and the maximum radial velocities typically are very small (< 15 kts) for pulse storms.** Remember that if convergence is detected above cloud base, it is likely a reflection of a downdraft and not an updraft.

Radar Base Data Detection of Updraft Location and Intensity

The best way to measure the altitude of elevated reflectivities is with the all-tilts scan in AWIPS. Four-panel displays can be used to track the location of the elevated core. However, it is not the preferred way to monitor all the available elevation slices to track the tendencies of reflectivity heights. **Be sure to pick the slice that cuts**

through the anvil and be careful not to place too much value in the trends of storm top divergence since these are shallow phenomena.

Derived Product Data Detection of Updraft Location and Intensity

Derived products can also be used to track updraft intensity and location. **LRM medium and high products show reflectivity cores at high enough altitudes to imply that they are updrafts.** The LRM medium product in the warmest soundings should be high enough for dendrite and graupel formation within the updraft. High reflectivities (>55 dBZ) in the LRM high product are a strong indication of updrafts associated with severe storms. Figure 3-3 shows that a new updraft is creating an elevated reflectivity core in the Layer Maximum Reflectivity (24-33 kft) product whereas the 3.4^{o} slice cuts through the updraft at 6500 ft ARL; too low for significant hydrometeor growth. However, looking at base reflectivity well above 3.4^{o} elevation angles would also reveal the elevated core.

The Hail Detection Algorithm (HDA), uses the height of intense reflectivities above the freezing level, and therefore, **the POSH product is useful to determine updraft intensity**. **Be careful in that the HDA also depends on a good representation of vertical thermal structure** as input into the ORPG HCI (Witt et al., 1998).

Downdraft Strength

Downdraft Nomenclature

The downdrafts discussed in this section are typically on the same scale as the individual ordinary cell updraft. Downbursts and microbursts are outflows of an ordinary cell downdraft. **The only difference is that downbursts are considered**

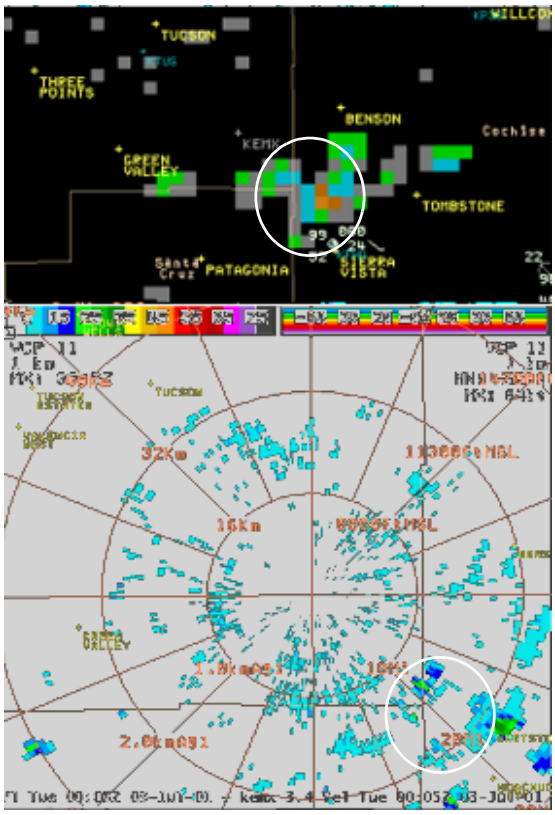

Figure 3-3. Layer Mean Reflectivity from 24 to 33 kft ARL (top) shows higher reflectivities than the 3.4^{o} slice on the bottom over the same storm marked by the circle.

outflows larger than 4 km in diameter while microbursts refer to outflows less than 4 km in diameter. In this section, downbursts, microbursts and downdrafts refer to the same process of downdraft and subsequent outflow from ordinary cells.

Whereas updrafts have a relatively definable source level, downdrafts have an uncertain starting level. In addition, evaporative cooling from precipitation never completely counteracts the adiabatic warming in a downdraft. Therefore, downdrafts almost never follow the moist adiabat. Updrafts follow the moist adiabat much more often if they are big enough to prevent entrainment from reaching their cores. This makes an assessment of downdraft strength potential more difficult than that of updrafts (Wakimoto, 2002). Nevertheless,

there are two main forcing mechanisms that influence downdraft strength in pulse storms.

Evaporational Cooling

This process attempts to cool the downdraft to the wet bulb temperature through evaporation of precipitation or cloud droplets. The drier the air or the more entrainment, the greater the negative buoyancy of the downdraft, and therefore, the more likely a severe downburst. Dry air may help evaporational cooling in two ways:

- **Lateral dry air entrainment**. Dry air is drawn into the sides of a thunderstorm updraft above the LCL and interacts with the precipitation. The amount of cooling is positively correlated to the eqivalent potential temperature (theta-E) of the dry air. A lower theta-E in midlevels corresponds to greater potential negative buoyancy. **Theta-E differences (>25-30^{o} K) between the surface and a midlevel layer somewhere 3-6 km Above Ground Level (AGL) containing the level of minimum theta-E, indicate a significant potential for severe downdrafts** (Atkins and Wakimoto, 1991). This kind of entrainment is mostly accompanied by convection containing high reflectivities of greater than 35 dBZ.
- **Subcloud evaporational cooling**. As precipitation begins to cascade into air below cloud base, evaporational cooling occurs. The final downdraft speed depends on the available precipitation for evaporation and the distance from cloud to ground. Increasing the LCL height implies an increasingly dry boundary layer assuming the convection is surface-based. When LCLs reach over 4 km AGL with dry adiabatic subcloud lapse rates, even storms with light precipitation can produce intense downdrafts (Wakimoto, 1985). **Subcloud evaporational cooling is typically the sole forcing mechanisms for low reflectiv-**

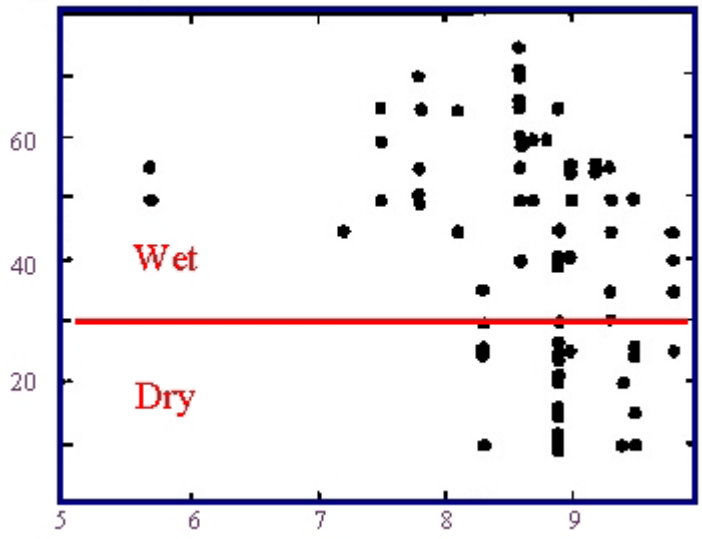

Figure 3-4. Observed microbursts as a function of environmental lapse rates. This figure is adapted from Srivastava (1985).

ity (<35 dBZ) dry microburst producing storms (Wakimoto, 1985).

DCAPE

The parameter DCAPE accumulates all potential negative buoyancy below its starting level. If the starting level is from the midlevels, then DCAPE can quantitatively assess the combined potential negative buoyancy from lateral dry air entrainment and subcloud evaporational cooling.

Precipitation Loading

As lapse rates decrease, downdrafts have an increasingly difficult time of maintaining their descent based on negative buoyancy effects alone. Heavy precipitation can force the descent of a downdraft even if it loses negative buoyancy. This becomes important once reflectivities exceed 45 dBZ (Srivastava, 1985). **Observed microbursts compared with reflectivity and lapse rates show that high reflectivities (>45 dBZ) are needed as the lapse rates drop below 8 K/km (Fig. 3-4 on page 44)**. Observations indicate that many downdrafts are associated with the descending precipitation core of a mature pulse storm.

Latent Heat of Fusion

Melting and evaporation or sublimation of frozen precipitation adds even more to the negative buoyancy of a downdraft than pure evaporation alone (Wakimoto 1985).

Objective 8a

Identify the environmental and storm signatures favorable for dry and wet microbursts.

Downdraft Types

Based on numerous observations, there is a spectrum of pulse storm downdrafts dependent on the amount of embedded precipitation. **At the dry end of the spectrum, dry microbursts are associated with less than .01" of precipitation reaching the ground.** Dry microbursts typically originate from storms with less than 35 dBZ of reflectivity. On the other end of the spectrum, **wet microbursts are loaded with heavy precipitation and originate from high reflectivity (>35 dBZ) storms.** There are dynamic differences between the two ends of the spectrum that require different techniques to detect or infer their presence.

Dry Microbursts

Dry microbursts are forced by evaporating precipitation below the LCL. These events are most common in the arid or semi-arid regions where LCLs are at least 3 km AGL (Wakimoto, 1985)**.** Favorable dry microburst environments often have 500 J/kg of CAPE or less with moist midlevels above the LCL (See Fig. 3-5.). Consequently, there is typically such a weak convective updraft that precipitation loading and/or lateral entrainment are not major concerns. **Dry microbursts are especially favored by situations where the LCL is below freezing and the precipitation cascading below the LCL consists of numerous snowflakes maximizing the total surface area exposed to dry air.**

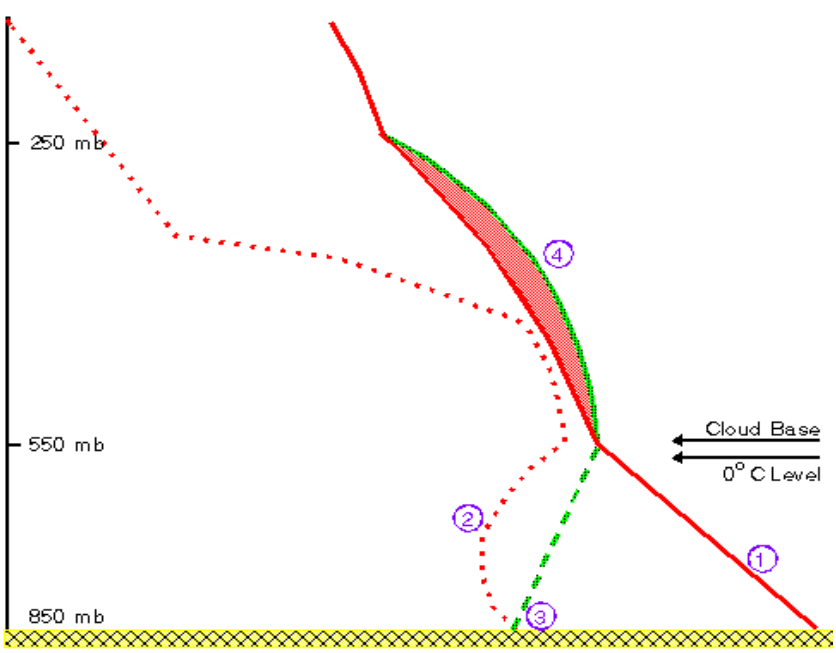

Figure 3-5. A schematic of a typical dry microburst sounding. The labels are as follows: 1) a deep nearly dry adiabatic lapse rate from the LCL to the surface, 2) low RH below cloud base, 3) a well mixed moisture profile with some variations, and 4) a weak CAPE typically < 500 j/kg. Note that the LCL is subfreezing.

There are clues in the radar and environmental data that a dry microburst is imminent. Given an environment depicted in Figure 3-5, a typical dry microburst producing storm shows an elevated but weak reflectivity structure as shown in a cross-section in Figure 3-6. Note the development of a 30-35 dBZ core 15-24 kft above the surface. This core of frozen precipitation is descending and sublimating just below the LCL. A velocity cross-section in Figure 3-7 shows weak convergence forming near and just below cloud base indicating the downdraft is initiating. Radial convergence is weak (15 kts), typical for most dry microbursts, and often is not visible due to radar sampling limitations. Note that 5 minutes later, the reflectivity core is descending through the melting layer, and the reflectivities are overestimated because of the bright band effect due to melting (see Fig. 3-8). **Monitoring the descent of the reflectivity core**

helps provide some lead time of a dry microburst.

Wet Microbursts

Wet microbursts are forced mostly by midlevel entrainment and precipitation loading. These events are common anywhere there is significant CAPE (>1000 J/kg), steep lapse rates, or

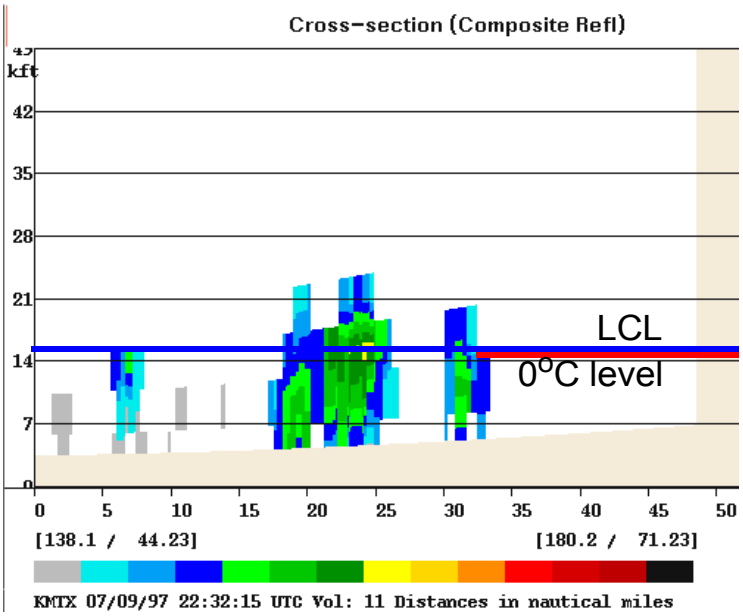

Figure 3-6. . A reflectivity cross-section through a dry microburst-producing storm taken from the KMTX WSR-88D on 2232 UTC, 09 July 1997.

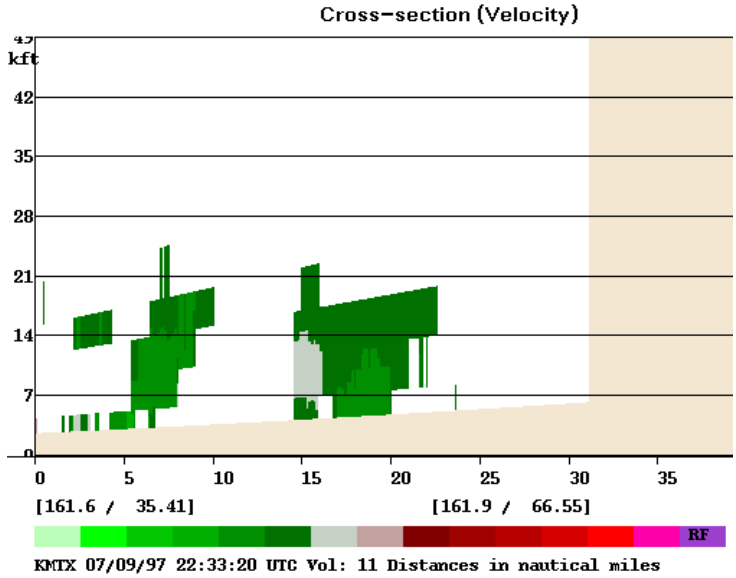

Figure 3-7. Velocity cross-section through a dry microburst-producing storm taken from the KMTX WSR-88D 09 July 1997 - 2232 UTC

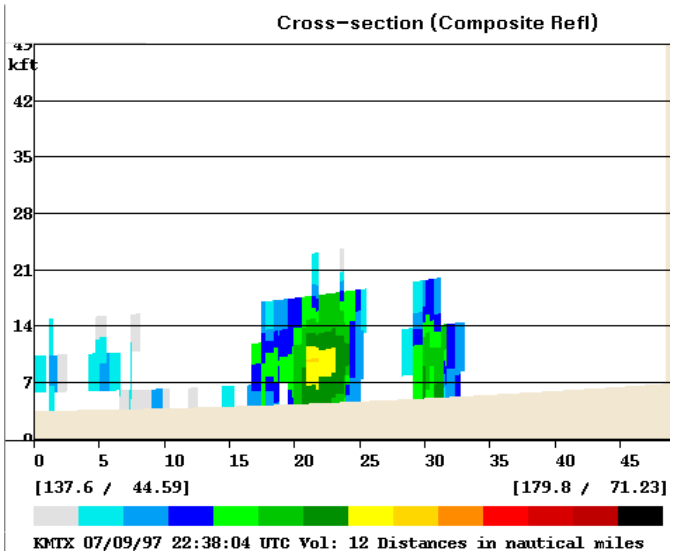

Figure 3-8. Reflectivity cross-section through a dry microburst-producing storm taken from the KMTX WSR-88D 09 July 1997 - 2238 UTC

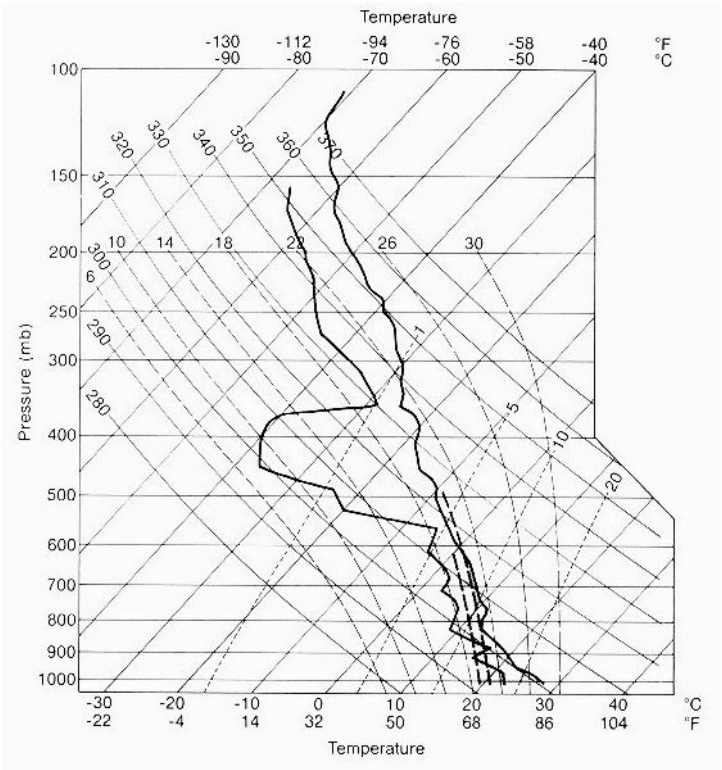

Figure 3-9. A typical wet microburst sounding showing dry midlevel air and steep lapse rates closer to ground.

significant midlevel dry air (see Fig. 3-9). Taking the difference of theta-E between the surface and the layer of minimum theta-E in the midlevels often reveal values exceeding 25^{o}K for days with severe

wet microbursts (Atkins and Wakimoto, 1991). A steep lapse rate below the LCL is important to minimize the inhibition for the downdraft to result in strong outflow. However, the height of the LCL is not as important as with the dry microburst example.

Hybrid Microbursts

Hybrid microburst forcing is a combination of both midlevel and low-level forcing. Environments that support hybrid microbursts have both significant CAPE, large theta-E differences from surface to midlevels, and high LCLs with adiabatic subcloud lapse rates. In a sense, hybrid microburst environments represent the middle of the microburst sounding spectrum. It could be said that most microburst soundings are hybrids. .A hybrid microburst sounding is characteriized by a deep boundary layer (high LCL), significant CAPE (>500 J/kg), and a midlevel dry layer (Fig. 3-10).

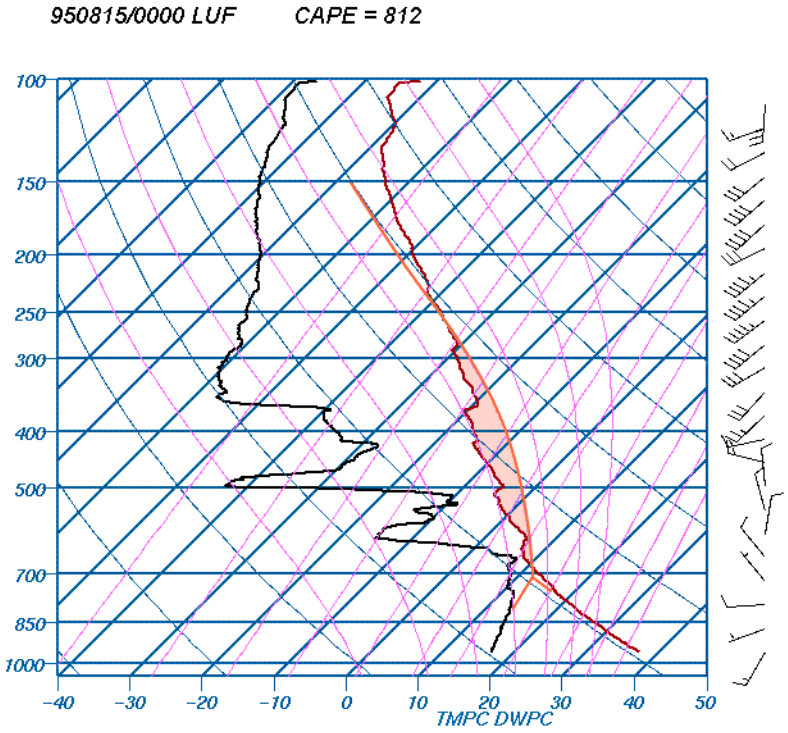

Figure 3-10. A hybrid microburst sounding showing midlevel dry air and a deep, mixed layer below the LCL. This is taken from Phoenix, AZ 0000 UTC, 15 August, 1995.

Storm Signatures of Wet and Hybrid Microbursts

Downdrafts are initiated when an elevated reflectivity core provides enough precipitation loading to overcome the initial updraft. After initiation, the dry air entrainment helps to maintain or strengthen the downdraft. Figure 3-11 shows a hybrid microburst-producing storm at the time when the precipitation loading of a young updraft reaches the point of initiating a downdraft.

The descent of a strong precipitation core is a precursor signal of a downdraft as shown in Figure 3-12. **The bottom edge of a descending reflectivity core is a likely location for the bottom of the downdraft.**

As the downdraft commences, midlevel radial convergence also develops as air flows into the downdraft source. The convergence often peaks when the downdraft is about to reach the ground (Fig. 3-13). Therefore, this feature gives very little lead time.

Some pulse storms collapse as the downdraft commences. This can be reflected in time trends of VIL, storm top, POSH, and most importantly the height of maximum reflectivity. **A simultaneous decrease in cell-based VIL and Z_{max} is a strong signal for a downburst.** Since you must wait till the end of a volume scan for these time trends, there is little lead time before the downburst commences at ground. **In addition, the lack of any signals of storm collapse does not indicate a lack of a downburst.** More often than not, the downburst phase of a storm coincides with the maximum vertical extent of the precipitation core, which then corresponds to the peak in cell-based VIL, POH, and POSH. The Z_{max} may not need to collapse either. **Therefore, do not depend on a**

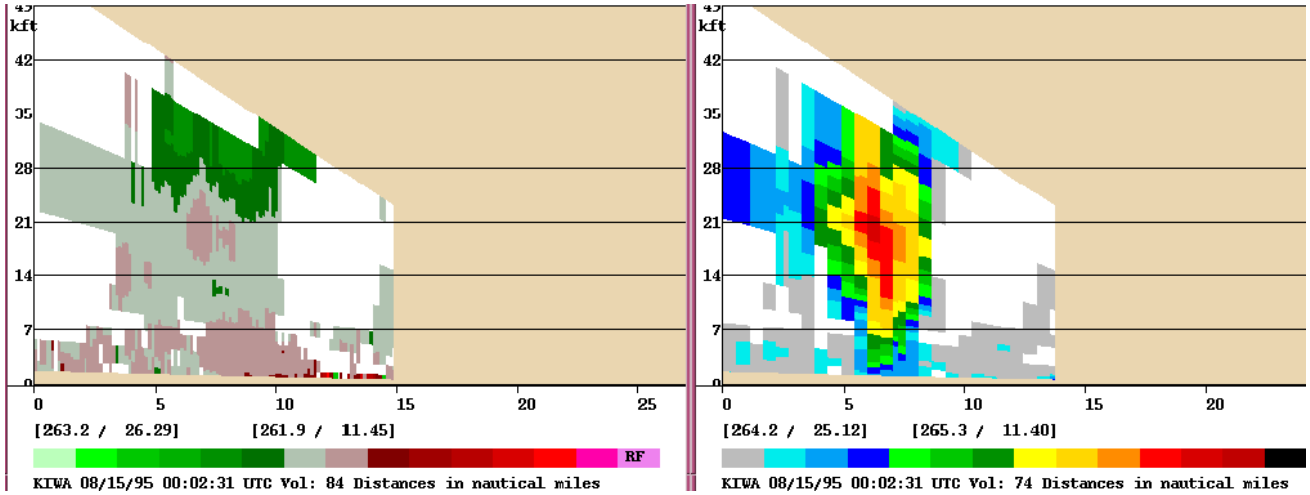

Figure 3-11. Velocity and reflectivity cross-section near the initiation time of an elevated downdraft from KIWA, 15 August, 1995 - 0002 UTC.

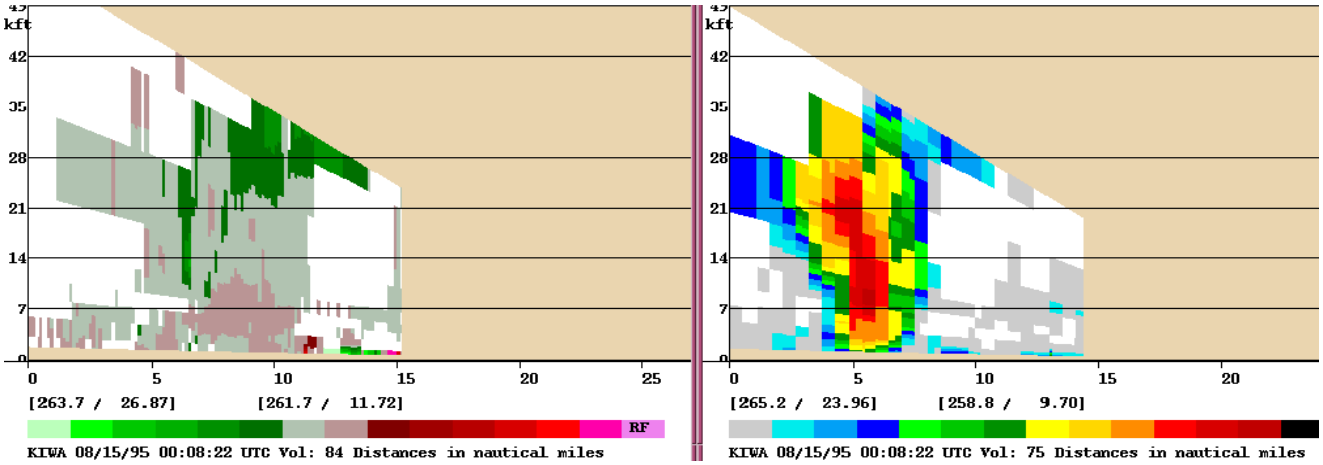

Figure 3-12. Velocity and reflectivity cross-section from KIWA, 15 August, 1995 - 0008 UTC.

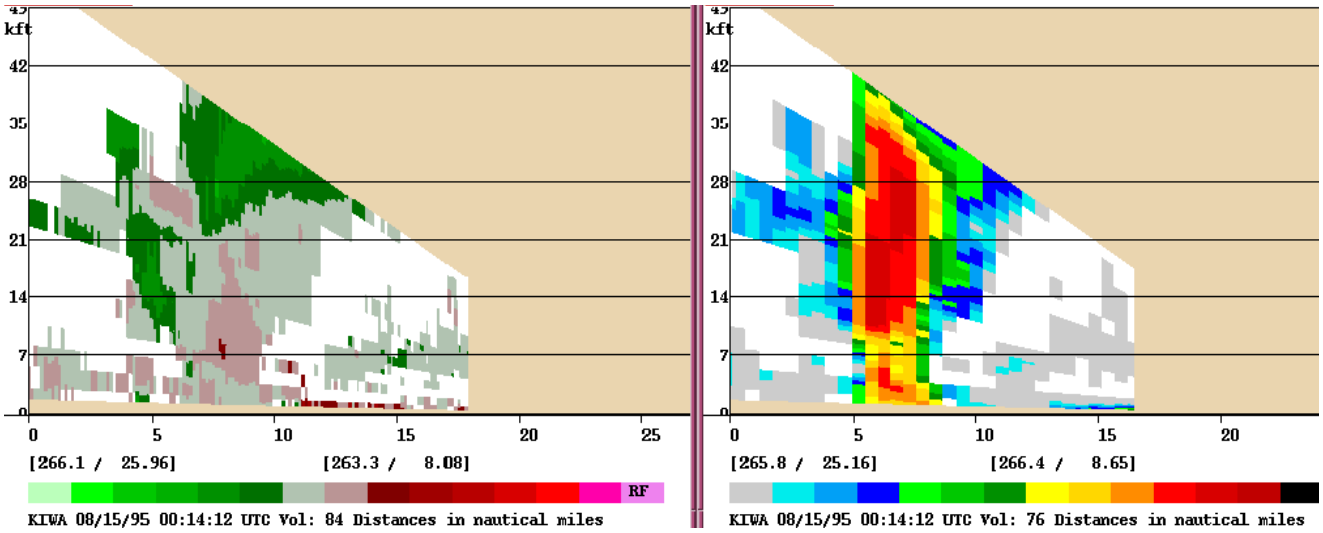

Figure 3-13. Velocity and reflectivity cross-section from KIWA, 15 August, 1995 - 0014 UTC.

storm collapse signature as a signal for a downburst event.

Hail Size

The radar is capable of effectively inferring the presence of a hail in pulse storms using several techniques (NOTE: there is a direct observation of hail when a WSR-88D signature is present called the “three body scatter spike” or hailspike. More on the hailspike in the section on moderate to strongly sheared cells). For the vast majority of pulse storms, a warning forecaster must infer the presence of large hail using a variety of techniques including **a higher than normal elevated reflectivity core, high VIL and VIL density, the presence of low-level reflectivities > 60 dBZ, and high values of Probability of Severe Hail (POSH)**. Notice that this does not include large hail signatures associated with supercells including a mesocyclone and a Bounded Weak Echo Region (BWER).

Elevated Reflectivity Core

For large hail to form in a pulse storm, the initial updraft should be intense. Increasing updraft intensity results in the ability to keep growing hailstones within the updraft for a longer period of time. Observed from radar, the first indication of an abnormally intense updraft is a higher and stronger elevated reflectivity core than typical during the initial stage of a pulse storm. **In particular, reflectivities > 55 dBZ in colder than -20^{O}C air strongly indicate hail. Increase the reflectivities in the sub -20^{O}C air and the odds of large hail increase dramatically.** Therefore, it is important to know which height corresponds to the -20^{O}C level (Witt et al. 1998).

Vertically Integrated Liquid (VIL) and VIL Density

VIL can be useful in comparing storm intensity amongst adjacent storms in a similar environment. Generally more intense updrafts yield

higher values of VIL with peak values during the storms mature phase. VIL is **not** a good indicator of severe hail or of the presence of hail of any size for a given storm. This is due to several factors, including:

- **Upper cap of 56 dBZ.** The original intent of the VIL algorithm was to *eliminate the contributions of hail* into the vertical integration. Any reflectivity greater than 56 dBZ is truncated back to 56 dBZ for VIL calculations. Thus, a storm with 75 DBZ from 10,000-20,000 feet equally contributes to VIL as a storm that has 56 dBZ from 10,000 to 20,000 feet even though the storm with 75 dBZ is clearly far more severe. Using VIL to diagnose the hail threat does not make sense.
- **Environmental dependence.** The VIL parameter is highly dependent on the thermodyanmic profile of the environment. This can vary greatly on any given day and across a single radar umbrella.
- **Fast storm motion**. VIL calculations that are displayed graphically in AWIPS are grid-based. Thus, storms may appear strongly tilted to the radar and VIL will be vastly underestimated.
- **Interpolation at storm top and down to the surface.** The algorithm interpolation can lead to great errors especially at near and far distances from the radar.

VIL Density

VIL can be normalized by division with the storm top height to yield VIL density (Amburn, 1996; Cerniglia and Snyder 2002; Blaes et al. 1998). VIL density is created by dividing the VIL by the echo top in meters to get the value kg/m^3. Multiplying by 1000 produces a manageable number in g/m^3 (dividing VIL by echo top in km also yields

a density of g/m^3). This parameter attempts to eliminate the problem of changing VIL thresholds using the depth of the storm as a proxy for the height of the freezing level. Short, high reflectivity storms indicate that a strong updraft exists and the hail production zone is lower providing less transit time for melting hail before reaching the ground. For pulse storms, severe hail is likely as the VIL density exceeds 3.28 in the Northeast US (see Table 3-2). This value (3.28) coincidentally occurs when the storm top in kft equals the VIL in kg/m^2. **Other studies arrive at numbers between 3.28 to 3.5 for a rough large hail threshold**.

VIL Density ($g\ m^{-3}$) at or above	POD	FAR	CSI
3.75	0.800	0	0.800
3.50	0.920	0.080	0.852
3.28	0.422	0.107	0.893
3.25	1.00	0.107	0.893
3.00	1.00	0.286	0.714
2.75	1.00	0.375	0.625
2.50	1.00	0.432	0.568

Table 3-2: VIL density vs. POD, FAR and CSI for severe hail. Adapted from Cerniglia and Snyder (2002).

Cautions About VIL Density

There are significant difficulties in correlating hail sizes (>0.75") to VIL density. Edwards and Thompson (1998) show that a large range of reported hail sizes are associated with large values of VIL normalized by equilibrium level or maximum parcel level (Fig. 3-14). Therefore, anticipating very large hail given a storm with very high VIL density likely will result in disappointment, especially in pulse severe storm cases. **We recommend not using VIL or VIL density alone for estimating hail threat.**

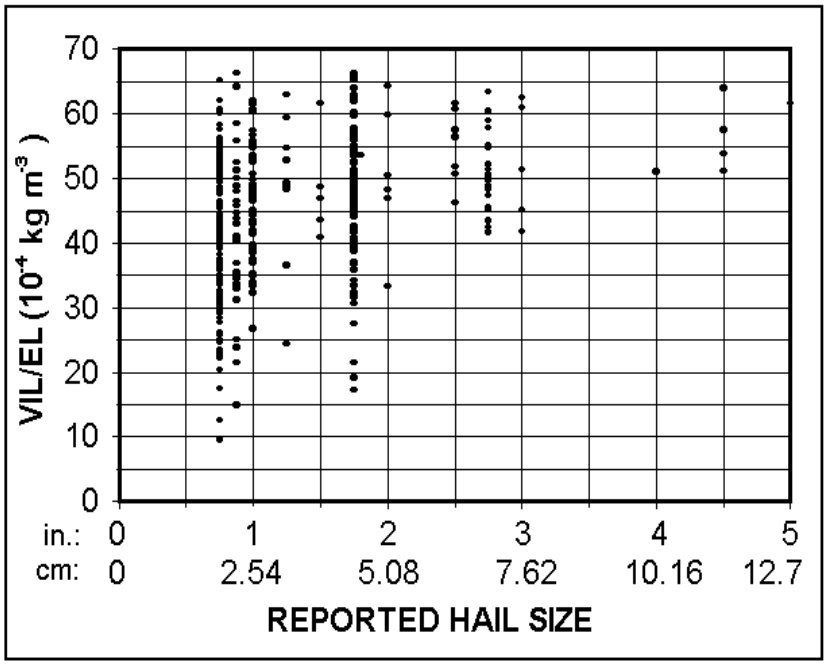

Figure 3-14. VIL normalized by Equilibrium Level (EL) from proximity soundings vs. reported hail size. Adapted from Edwards and Thompson (1998).

High Low-level Reflectivities

Reflectivities of 60 dBZ in the lowest slice strongly suggest the presence of hail (Witt, 1996). However, the same reflectivity could be the result of large concentrations of small hail or fewer but severe sized hail. Therefore, investigate all aspects of storm structure before assessing severe hail potential.

POH and POSH

The Probability of Hail (POH) and the Probability of Severe Hail (POSH) heavily depends on the integrated amounts of reflectivity above the 0^{o}C and -20^{o}C levels. POSH is especially dependent on the vertically integrated amount of reflectivities exceeding 45 dBZ above the -20^{o}C level (Witt et al., 1998). The performance of both POH and POSH is optimized during sheared cool season storms. **The process by which POSH was developed tends to overestimate its probabilities in weakly sheared pulse storm environments**. Conversely, in storms over high terrain, POH and

POSH may underestimate their values as they do not account for topography.

Objective 8b

Identify the most likely period of a cell lifetime for non-mesocyclonic tornadoes.

Tornadoes in Weak Shear Environments

Pulse severe storms are capable of producing significant tornadoes given an **adequate supply of low-level vertical vorticity and a strong enough updraft**. These processes are not dynamically driven by the traditional mesocyclone and thus do not depend on strong vertical wind shear for their existence.

Figure 3-15 illustrates the evolution of pulse storms that produce non-mesocyclonic tornadoes. Consider a sharp surface boundary with strong horizontal directional shear. **The directional shear across the boundary may breakdown into a series of misocyclones. A young pulse storm updraft superimposed on top of one of these misocyclones stretches the preexisting vorticity quickly into tornadic scales**.

Because the origin of the rotation in these features is close to the ground, radar may easily overshoot the circulation unless it is within 50 km. The diameter and lifetime of these misocyclones are small (<2 km, 5-15 min) also limiting the ability of radar to resolve their velocity structures. This process creates a difficult job for Doppler Radar to provide adequate lead time of pulse storm tornadoes.

Favorable conditions leading to the formation of a pulse storm tornado include:

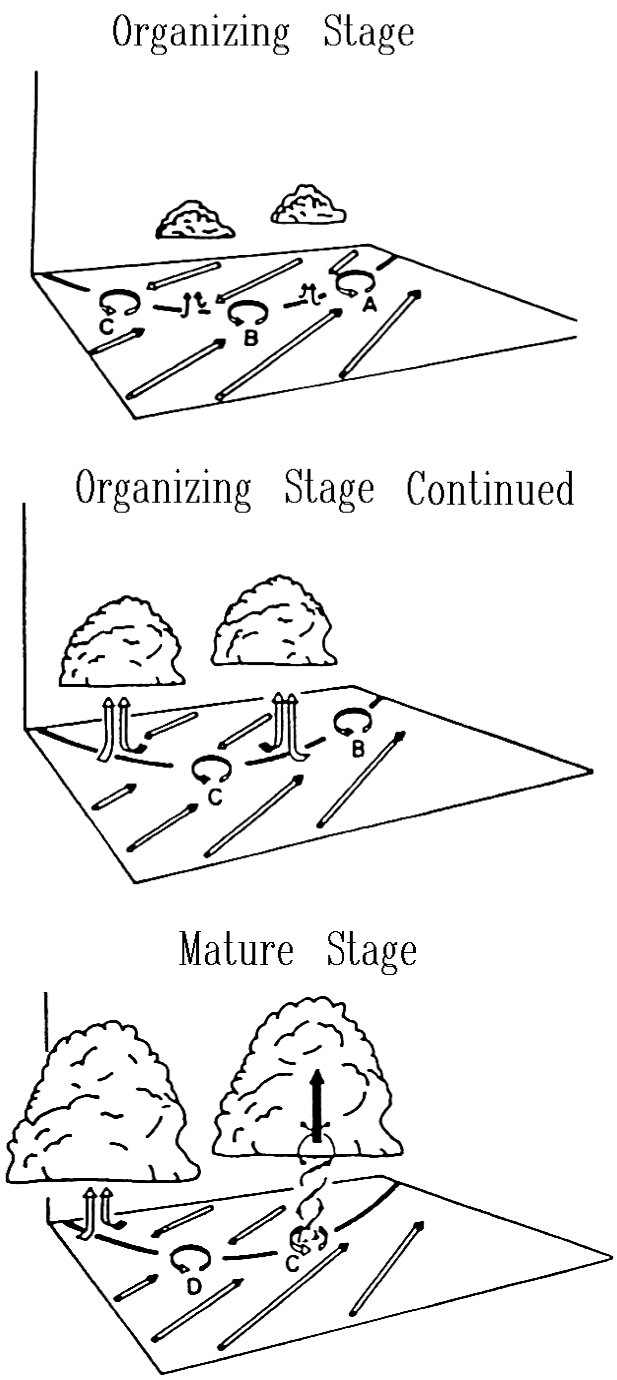

Figure 3-15. A schematic evolution of pulse storm tornadoes. Adapted from Szoke et al. 1984.

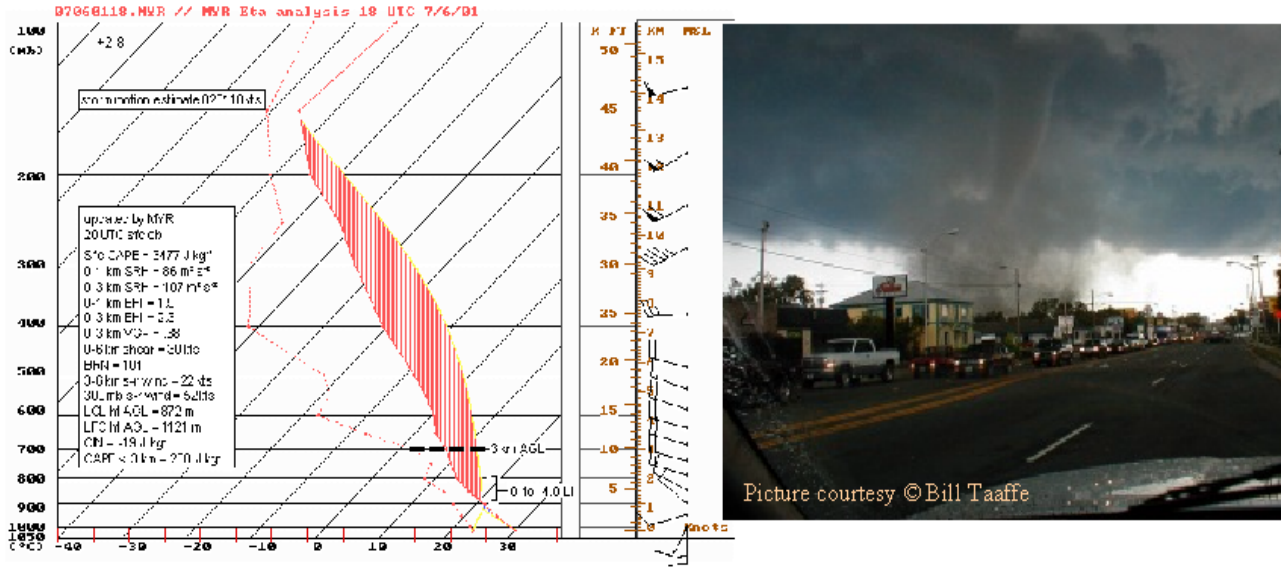

Figure 3-16. An example of a favorable sounding for weakly sheared tornadoes. This figure is adapted from Davies (2002).

- **An environment with steep lapse rates,strong surface heating and no CIN** (Fig. 3-16)
- **A well defined boundary** marked by a fine-line in reflectivity, velocity discontinuity in base velocity, or a cumulus line visible from satellite. **The boundary should have significant vertical vorticity**. Note that 10 m/s of shear across a 1 km wide boundary carries the same vorticity as a moderate mesocyclone, (10^{-2} s^{-1}). Ideally, the boundary and cell motion should be nearly equivalent. Boundary collisions are also common regions of pulse storm tornadoes (Fig. 3-17).
- **Colliding or intersecting boundaries with high potential for vertical vorticity production is an area to be closely monitored** (Wakimoto and Wilson, 1989).
- **A rapidly growing updraft situated close to or over the boundary**. Be especially alert for tornadoes when the updraft forms an elevated reflectivity core.

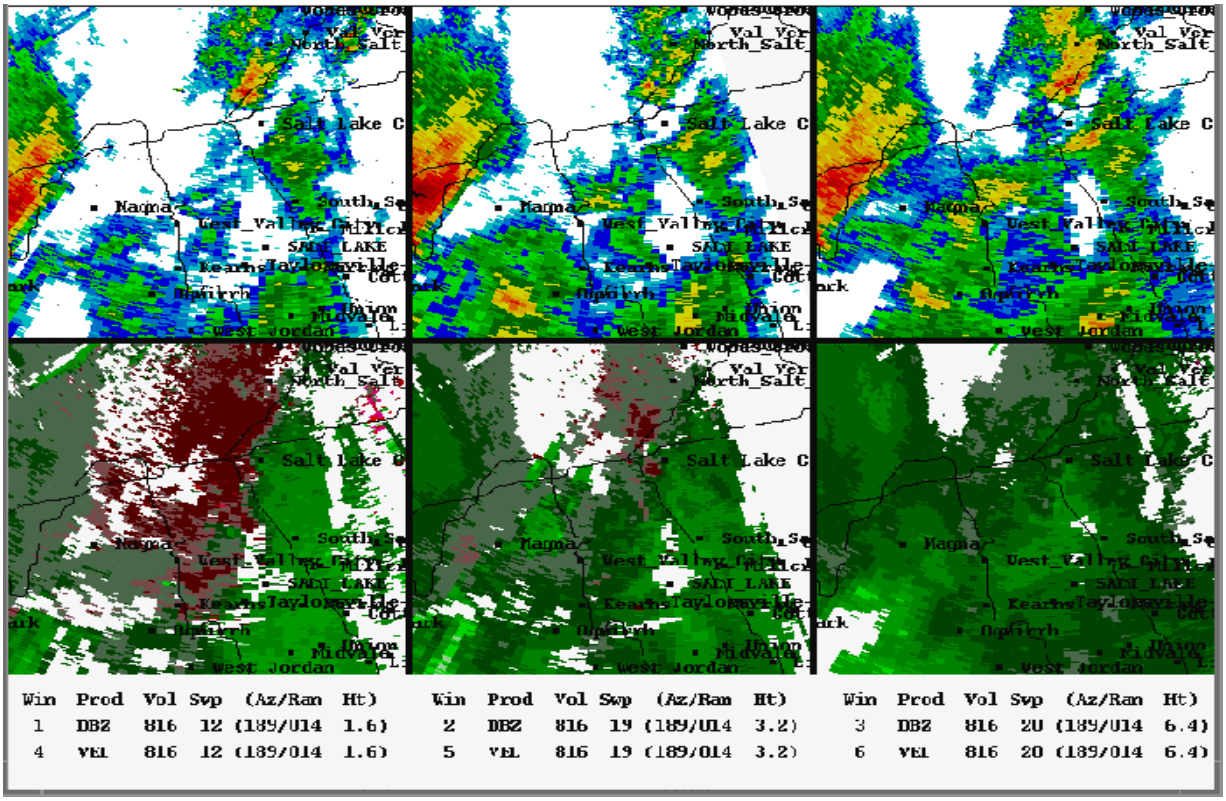

Figure 3-17. A six panel from the Terminal Doppler Weather Radar in Salt Lake City from 11 August 1999 tornado event. The velocity image in the lower left panel shows the boundary with mesocyclonic shear from which a developing updraft rode on top eventually developing a tornado.

Heavy Rain Potential

There are two considerations in assessing heavy rainfall potential: The instantaneous rainfall rate potential, and the duration of heavy rain.

Rainfall rate is a function of:

- **Updraft strength**
- **Water content of the air entering the updraft**
- **Dominat mode of precipitation production**

These are parameters that go into measuring upward **moisture flux**. However, the percentage of the upward moisture flux that gets returned as precipitation at ground-level is defined as **precipitation efficiency**. Given a highly efficient storm, precipitation rates can easily exceed 4”/hr, even given updrafts too weak to produce hail. Because

it is impossible to measure precipitation efficiency directly, it is important to be cognizant of the parameters that govern how efficient a storm becomes.

Favorable Conditions for High Precipitation Efficiency

Characteristics that help increase precipitation efficiency of pulse storms, ironically, are similar to those that inhibit strong downdrafts. **Parameters favorable for highly efficient storms include**:

- **High midlevel tropospheric relative humidity**. Lateral dry air entrainment would be minimized helping to preserve the cloud water content of the updraft.
- **Deep warm cloud layer**. The most efficient pulse storms depend on a deep layer of warm cloud that supports collision-coalescence of raindrops (Beard and Ochs, 1993). The warm cloud layer depth is measured from the LCL to the freezing level. Many intense flash flood producing storms occur with warm cloud layers exceeding 10 kft. For example, the Ft. Collins flash flood producing storm carried an updraft barely strong enough to produce lightning, yet had a deep warm cloud layer. The result was a rainfall rate of 2-4”/hr (Fig. 3-18).
- **Wide updrafts** reduce dry air entrainment.
- **A close group of storms** improves precipitation efficiency by interstorm seeding and higher storm-induced relative humidities. Watch for multiple storms in close proximity to improve odds for an efficient storm.

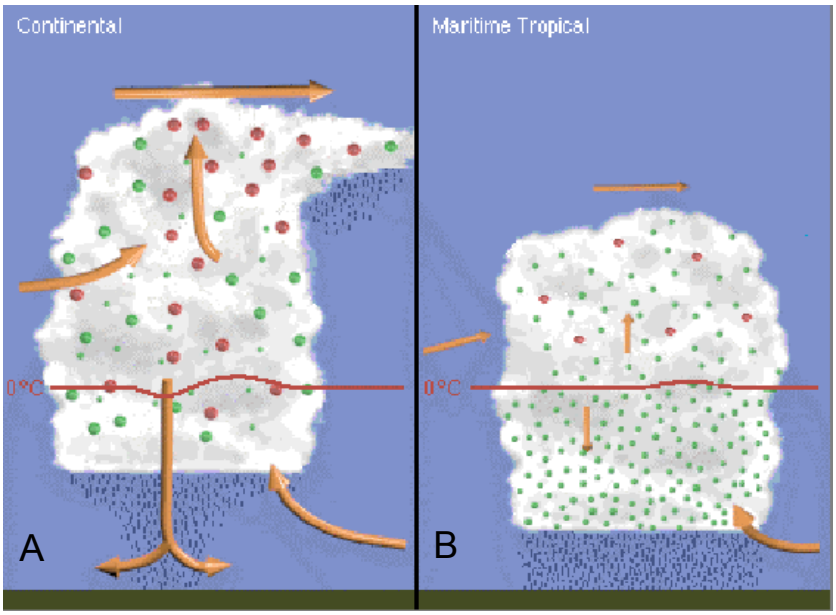

Figure 3-18. Schematic of a cell with A) a small warm cloud layer, and B) a large warm cloud layer (COMET, 2000).

Signature of a Storm with Significant Warm Cloud Microphysics

If the storm is producing much of its rainfall from warm rain processes, the default Z/R relationship may underestimate rainfall rate. These storms are marked by deep warm clouds, little lightning and increasing reflectivities from the freezing level to the LCL. Cloud top temperatures are not remarkably cold (>-40^{o} C). In addition, the low centroid reflectivity of these storms may cause the Z/R relationship to underestimate the rainfall rates as the 0.5^{o} slice ascends above the LCL (Fig. 3-19).

The more anomalously high the mean mid tropospheric RH, inflow mixing ratio, and warm cloud depth are for a particular area, the more likely a storm will be to produce high rainfall rates that may quickly overwhelm a drainage basin.

Objective 9

Identify the typical environment, structure, and evolution of supercells.

The Effects of Shear on Storm Structure

As the vertical wind shear begins to increase, important changes occur to convective cells,

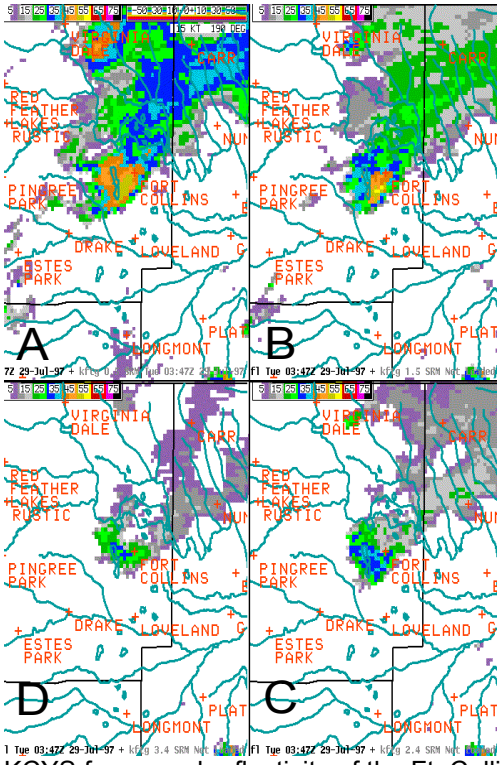

Figure 3-19. KCYS four-panel reflectivity of the Ft. Collins Flash flood-producing convective storm at 0342 UTC, 28 July 1997. The four panels are: A) 0.5°, B) 1.5°, C) 2.4°, and D) 3.4°

increasing the threat of severe weather. Several of these changes help to increase updraft strength and longevity, including:

1. **Horizontal separation of the updraft and downdraft** helps to reduce precipitation loading in the updraft. This process is aided through increasing storm-relative flow, which accompanies shear.
2. **Shear increases the odds that updraft motion matches that of the gust front**. Updraft is continually assisted by ascent along the gust front and maintains access to the inflow.
3. **The onset of updraft rotation increases updraft strength** through dynamic pressure forcing. More on this topic will be discussed later.

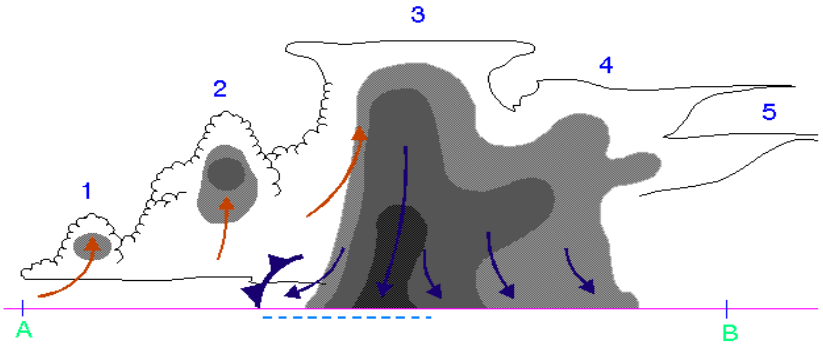

Figure 3-20. A schematic multicell storm cross-section in the direction of the shear vector (from A to B). Each cell undergoes an evolution similar to pulse storms.

4. **Storm-relative low-level inflow** is more intense, increasing low-level convergence along the gust front and, therefore, strengthening the updraft. A strong gust front is necessary to develop strong convergence.

Storm Evolution in Moderate Shear

As shear increases (i.e. the 0-6 km shear) to 10-20 m/s, the gust front produced by the initial cell becomes more likely to initiate new convection. Assuming that the first updraft developed in a relatively isolated mode, its gust front most likely **enhances ascent of potentially unstable environmental air on the side experiencing the strongest convergence.** As a result, **the next updraft pulse is likely to be stronger than the first one**. A classic, multicell cluster storm begins to take shape. In moderate shear cases, the updraft pulses may move forward onto the cold side of the gust front, and may still suffer from excessive precipitation loading, both of which act to limit their life spans. However, new updrafts constantly replace the old ones along the gust front. The result is a successive series updraft pulses in different stages of development (Fig. 3-20), the decaying cells forming anvils, while fresh updrafts with elevated cores continue to develop on the right rear flank.

Updraft Strength in Moderate Shear

Updraft strength in a storm experiencing moderate shear is stronger than in one in weak shear due to better updraft-downdraft separation, lower boundary-relative storm motion, and better storm-relative low-level inflow.

Remember that individual updrafts are still affected by dry air entrainment, and some precipitation loading. Therefore, the same considerations that aid strong updrafts apply for both weakly and moderately sheared storms.

Since multicell storms consist of groups of individual cells, and can occur in most combinations of shear and instability, further discussion of their morphology, motion and radar interpretation is deferred to the last section in this lesson.

Storm Evolution in Strong Shear

As updrafts encounter an increasingly sheared environment (e.g., 0-6 km shear >20 m/s), they become enhanced by:

- **increased updraft/downdraft separation,**
- **lower boundary-relative storm motion,**
- **stronger storm-relative low-level inflow,**
- **increased nonhydrostatic upward directed pressure forcing due to updraft rotation.**

Updrafts last longer as precipitation loading is weaker, and updraft rotation helps to weaken dry air entrainment. If an updraft begins to persist for longer than an individual air parcel takes to traverse it, and it is well correlated with significant rotation, the updraft is then called a **supercell**.

Objective 10

Identify the effects of shear on storm propagation.

Supercell Evolution, the Origins of Rotation and Deviant Motion

The origins of rotation and storm motion deviant to the steering layer wind can both be explained by how the updraft is influenced by vertical wind shear. There can either be unidirectional or directional vertical shear in supercell environments. Fundamental origins of rotation and propagation are shared by both straight and curved sheared environments. However, there are important differences in the origins of supercell rotation and propagation between unidirectional and directional vertical shear. These differences will be covered in this section.

The Origins of Rotation in a Straight Hodograph.

We can visualize vertical shear as a continuous series of vortex lines oriented horizontally. A good analogy is a sheet of rolling logs. **As an updraft extends into a sheared environment, horizontal vorticity tilting acts to create two vertical vortices (Figure 3-22).** The strength of these vortices depends on the strength of the shear and the intensity of the updraft. Facing toward the direction of the shear, from left to right in Figure 3-21, on the right (left) side of the updraft lies a cyclonic (anticyclonic) vortex. Initially in Figure 3-21 , the vortices lie along the periphery of the updraft, and thus contain no updraft within them. In other words, the updraft and vorticity are not correlated.

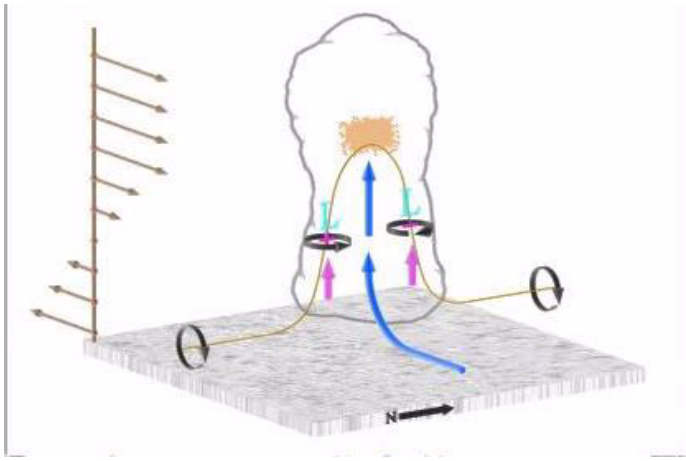

Figure 3-21. Schematic of dynamically driven low pressure forming on either side of an updraft. From COMET (1996).

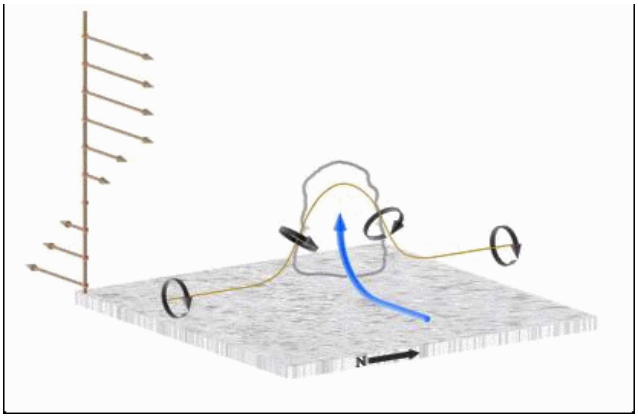

Figure 3-22. Schematic of an updraft tilting vortex lines in westerly shear. Adapted from COMET (1996)

Dynamically Driven Low Pressure in Each Vortex

Both counter rotating vortices create a dynamic low, as air is accelerated (spun) away from the core of each vortex. The faster the rotation, the lower the pressure in the center of rotation. **Since tilting of the originally horizontal vorticity is most pronounced where the updraft is strongest (at midlevels), the vertical vortices are most intense there.** With the dynamic pressure at its lowest aloft, an enhanced upward directed pressure gradient force promotes the development of new updraft within their centers of rotation (Fig. 3-21). The effect is a widening of the updraft and increasing correlation between updraft and rotation on both flanks.

Deviant Supercell Motions in Straight Shear.

The greatest tilting of horizontal vorticity occurs right and left of the shear vector. **This means that the development of rotation and new updrafts also occur to the right and left of the shear vector.** Precipitation developing in the middle of the widening updraft acts to develop a downdraft which, in turn, helps to split the widening updraft into two parts (Fig. 3-23). **The cyclonically (anticyclonically) rotating member moves to the right (left) of the shear vector.** Since both the cyclonic and anticyclonic updrafts experience similar upward dynamic pressure forcing, they are

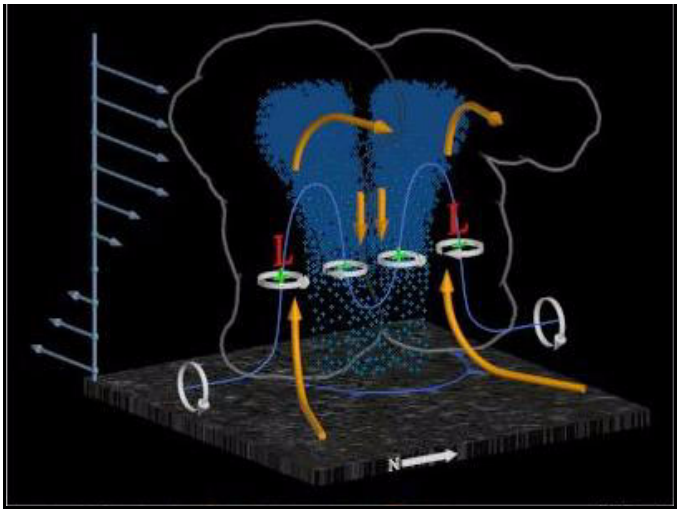

Figure 3-23. Schematic of downdraft formation and subsequent retilting of vortex lines downward. Adapted from COMET (1996).

equally strong supercells in a straight hodograph environment.

Once the supercell is deviating off the hodograph, it experiences streamwise vorticity, and storm-relative helicity in its inflow layer. Tilting of the streamwise vorticity into the updraft immediately produces vertical vorticity well correlated with updraft.

Curved Shear Origins of Rotation

The processes that develop rotation in the unidirectional hodograph, also apply to curved hodographs. However, a curved hodograph implies that streamwise vorticity and helicity are available for the updraft to directly ingest upon its initial growth. Instead of the rolling log analogy to describe the vorticity in the environment, here the analogy is the thrown spinning football. This analogy represents the available streamwise vorticity that merely needs to be tilted into the vertical by the updraft in order for rotation and updraft to be well correlated. Therefore the evolution from ordinary cell to supercell is much quicker.

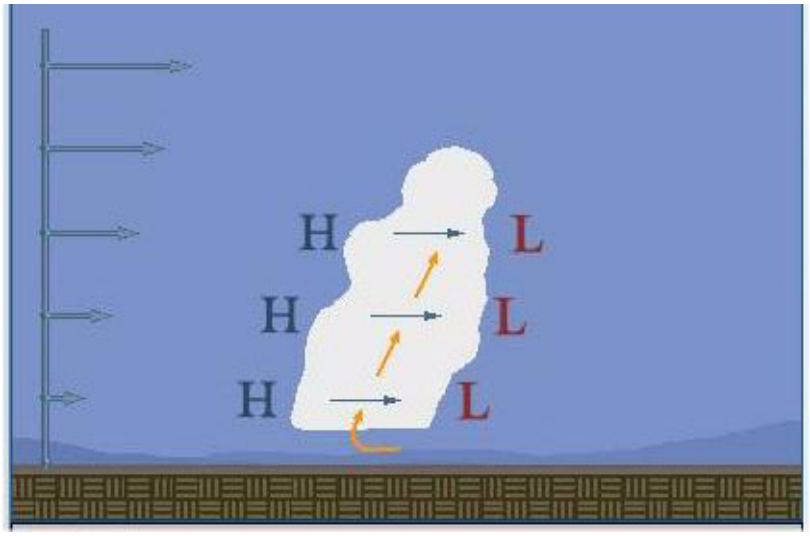

Figure 3-24. A schematic of updraft tilting through differential dynamic pressure induced by unidirectional shear. Adapted from COMET (1996).

Deviant Motion in Curved Shear.

While the same processes that promote deviant motion in unidirectional hodographs will work in curved hodographs, the interaction of the changing shear vector with height will result in additional nonhydrostatic vertical pressure gradient forcing that promotes growth on only one flank of an updraft. This additional process is related to the same processes that force an updraft to tilt in the presence of vertical shear. On the upshear side of an updraft, high dynamic pressure forms as a result of partial flow blockage, while low pressure forms on the other side (Fig. 3-24) forcing the updraft to tilt.

When the shear profile changes with height (Fig. 3-25), so do the locations of the dynamic pressure maxima and minima. **For example, in an environment with clockwise turning shear with height, the lower parts of an updraft will experience relative high (low) pressure on the upshear (downshear) side. In the example hodograph (Figure 3-25), the relative high is on the south side of the updraft at low levels because of a northerly shear vector (Figure**

3-26). At higher levels, the shear vector pointing south would produce a relative low on the south side of the updraft. The result is an upward directed pressure gradient force that causes new updraft development and therefore, storm propagation to the right of its original motion. Meanwhile, the left side of the updraft would experience a downward directed dynamic pressure gradient force weakening, or even destroying, the side of the updraft containing the anticyclonic member of

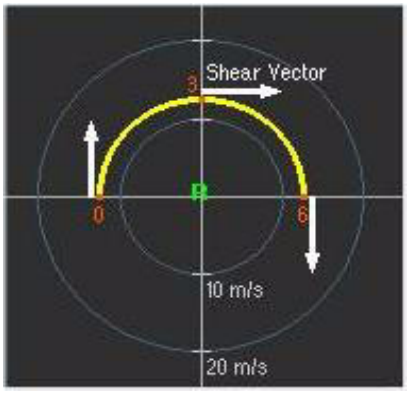

Figure 3-25. A schematic 180° curved hodograph resulting in the dynamic pressure perturbation structure shown in Figure 3-26.

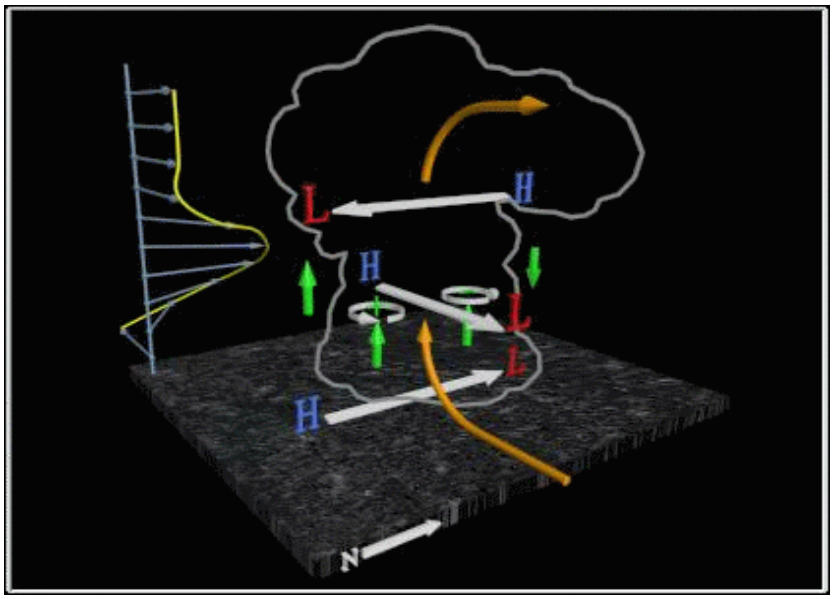

Figure 3-26. A schematic storm structure resulting from the hodograph in Figure 3-25. The labels, L and H, represent dynamic perturbation pressure minima and maxima respectively. The green arrows represent vertical motions forced by the vertical perturbation pressure gradients. Adapted from COMET (1996).

the rotational couplet. This is why a left-moving storm, given the hodograph in Figure 3-25, would be suppressed.

Objective 11

Describe how to anticipate the motion of supercells.

Plotting Supercell Motion

To plot the location of the right- and left-moving members of the supercell pair on a hodograph, draw a line perpendicular to the 0-6 km shear vector that passes through the 0-6 km mean wind. The right- (left-) moving member will be located on the line 3-8 m/s to the right (left) of the wind shear vector along your line. An example of a linear hodograph (Figure 3-27) shows where to place the right- and left-moving pairs of a splitting storm. The COMET module, *A Convective Storm Matrix*, contains more examples of estimating deviant storm motion from unidirectional hodographs.

Two Methods of Estimating Supercell Motion

There are two methods for estimating supercell motion for which to be aware. The “Old Supercell method” and the ID method , which is the preferred technique, are presented next.

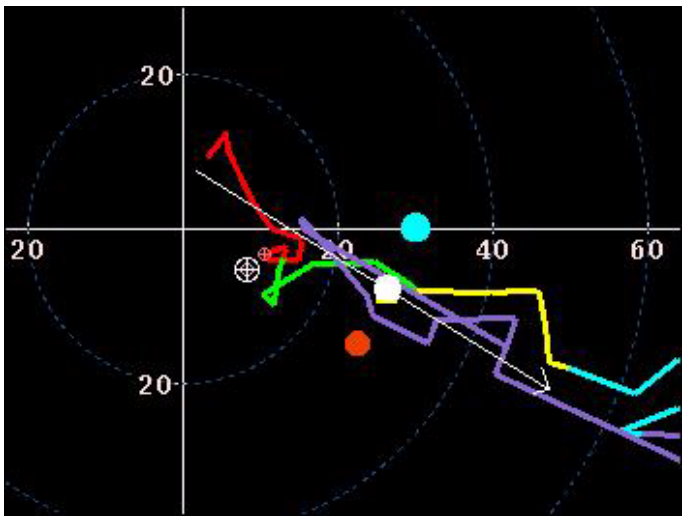

Figure 3-27. Motion of the cyclonic and anticyclonic rotating supercell plotted as a red and cyan dot respectively on a hodograph. The thin white arrow represents the 0-6 km shear vector and the white dot is the 0-6 km mean wind.

The Old Supercell Motion Method

In the past, forecasters often based supercell motion on the 30R75 (Maddox, 1976) or 20R85 (Davies and Johns, 1993) rules. **The 30R75 rule estimates the cyclonically rotating supercell motion by adding 30° to the right of the 0-6 km steering layer flow direction and 75% of the speed**. The 20R85 rule was an adjustment for those supercells embedded in very strong flow. Unfortunately, these estimations are non-physically based and only apply in the Northern Hemisphere with the typical counterclockwise turning hodographs. The AWIPS skew-T program still uses this technique to estimate SRH.

The Internal Dynamics (ID) Method

Bunkers et al. (2000) developed a better method called the **ID method (Internal Dynamics)**, which uses the mechanisms by which updraft and shear interact to cause deviant motion. **This method can be used to calculate storm motion for both the cyclonically and anticyclonically rotating supercells resulting from a storm split**. The ID method is Galilean invariant allowing for its use in atypical hodographs (i.e., westerly shear with northerly mean winds). To estimate supercell motion using the ID method, the following steps work well:

a. Plot the 0-6 km non-pressure-weighted mean wind. An example in Figure 3-28 shows the mean wind as a red dot.

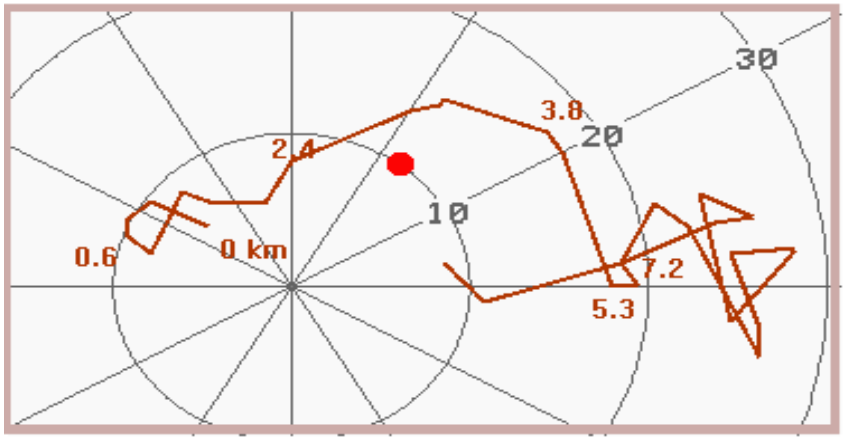

Figure 3-28. A sample hodograph with the 0-6 km mean wind plotted as a red dot. Each ring represents 10 m/s.

b. Draw the shear vector from the mean wind in the lowest 0.5 km to the mean wind from 5.5-6 km (Fig. 3-29).

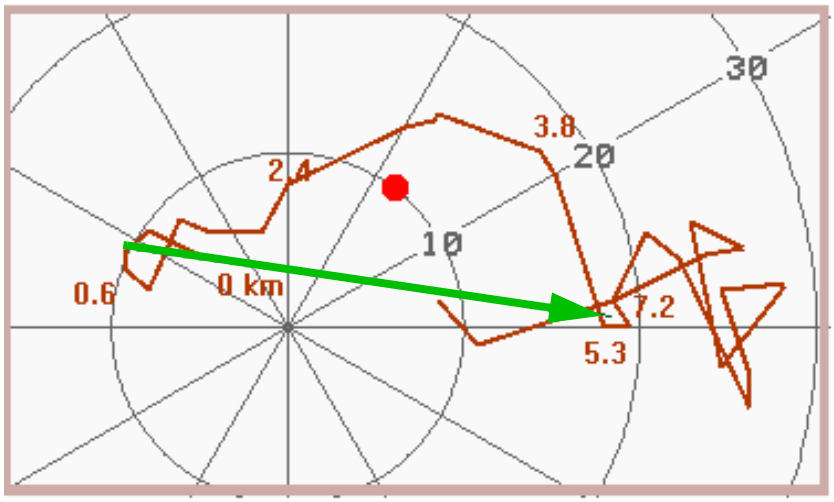

Figure 3-29. Same as Figure 3-28 except the 0-6 km shear vector is added as a green arrow.

c. Draw a line orthogonal to the shear while passing through the mean wind (Fig. 3-30). Note that the shear vector can be placed anywhere on the hodograph as long as it retains the same direction and magnitude.

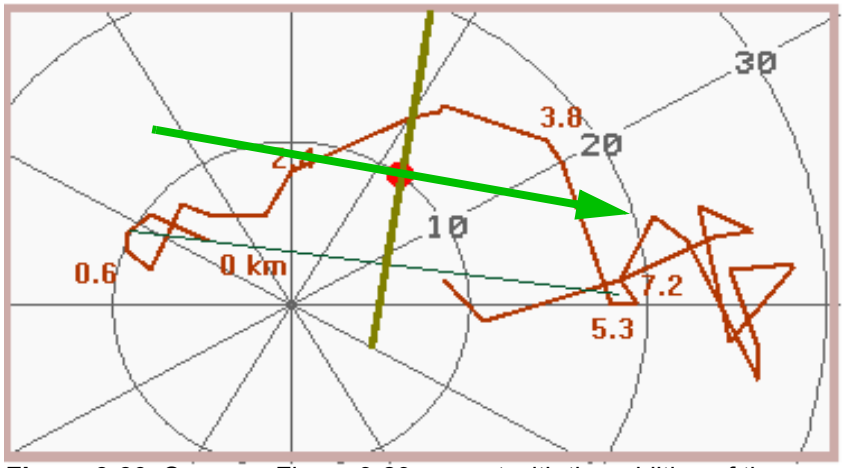

Figure 3-30. Same as Figure 3-29, except with the addition of the shear-normal line passing through the 0-6 km mean wind (red dot).

d. The right- (left-) moving supercell is drawn 7.5 m/s to the right (left) of the shear vector where shear vector intersects the shear-orthogonal line at the 0-6 km mean wind. Note that the storm motion remains on the shear-orthogonal line (Fig. 3-31).

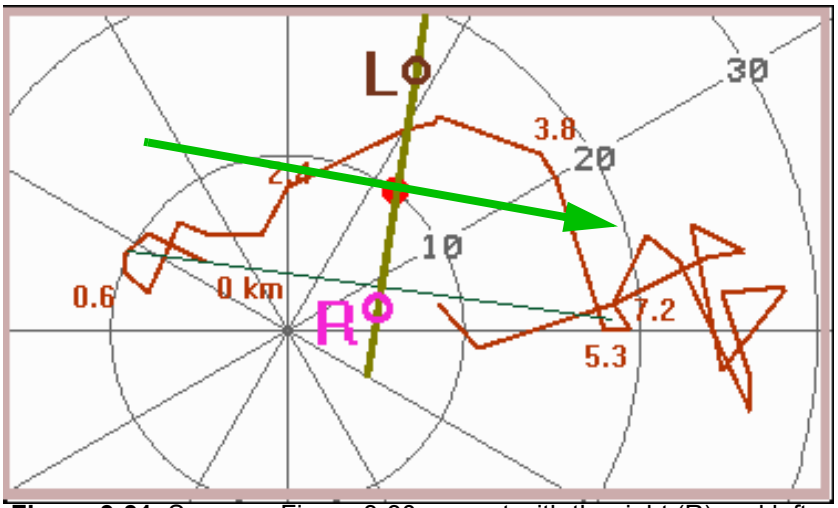

Figure 3-31. Same as Figure 3-30, except with the right (R) and left (L) moving supercells added.

Magnitude of Deviant Motion and Other Issues

Although the ID method is physically-based, there still exists uncertain knowledge on what the deviant motion vector should be. Currently, the 7.5 m/s value is chosen as the most representative value for a large population of observed supercells. Until more is known about how to modulate the deviant motion vector in a physically-based way, there will be differences between observed and predicted supercell motions. It is known that supercells may preferentially propagate along boundaries or other sources of updraft forcing resulting in a motion vector different than that predicted by the ID method. Additional errors may result between observations and predictions because of errors in our analysis of vertical wind profiles.

Identify radar reflectivity characteristics of supercells.

Objective 12

Reflectivity Structure of a Supercell

Supercell storms have characteristic reflectivity signatures that are unique to this class of storms. The signatures of a supercell include:

- **A low-level reflectivity notch on the low-level inflow side of the cell** (point N in Figure 3-32). This signature indicates the presence of a very strong updraft with enhanced low-level inflow. If the storm is close to the radar, a surface gust front may be seen wrapping into the region of the notch. Inflow notches are the most common feature in supercells. However, they can likewise occur in non-supercell storms.
- **A hook echo is a common feature of supercells with strong mesocyclones** (point. H Figure 3-32). Precipitation wrapping around a midlevel circulation can produce a hook echo. Low-level rotation may also wrap falling precipitation from the main forward flank core. Descent of rainfall embedded within a rear-flank downdraft may also produce the hook echo. Hook echoes vary widely in appearance as will be discussed in the next section on supercell types.
- **A weak echo region (WER) is very common for most supercells**, even those with weak mesocyclones (labeled WER in Figure 3-32 and Figure 3-33). **A WER should be persistent (>5 minutes), and be capped by high reflectivities (>45 dBZ) with the top of the weak reflectivities between 8 and 20 kft AGL. WERs are common features of severe storms in vertically sheared environments.** WERs not capped by strong reflectivities imply weak or no updraft, such as an overspreading anvil layer. **In addition, the WER should be**

adjacent to the part of the low-level reflectivity core containing strong reflectivity gradients and on the storm-relative low-level inflow side. Be careful to take into account storm motion which may induce an spurious WER in the direction of storm motion for fast flow events.

- **A Bounded Weak Echo Region (BWER) is a less common feature associated with strongly rotating supercells with intense updrafts** (BWER in Figure 3-32 and Figure 3-33). The presence of a BWER is almost always associated with severe weather of some type. However, a BWER is not necessarily present in all supercells. Look for BWERs to begin between 8 and 25 kft AGL.

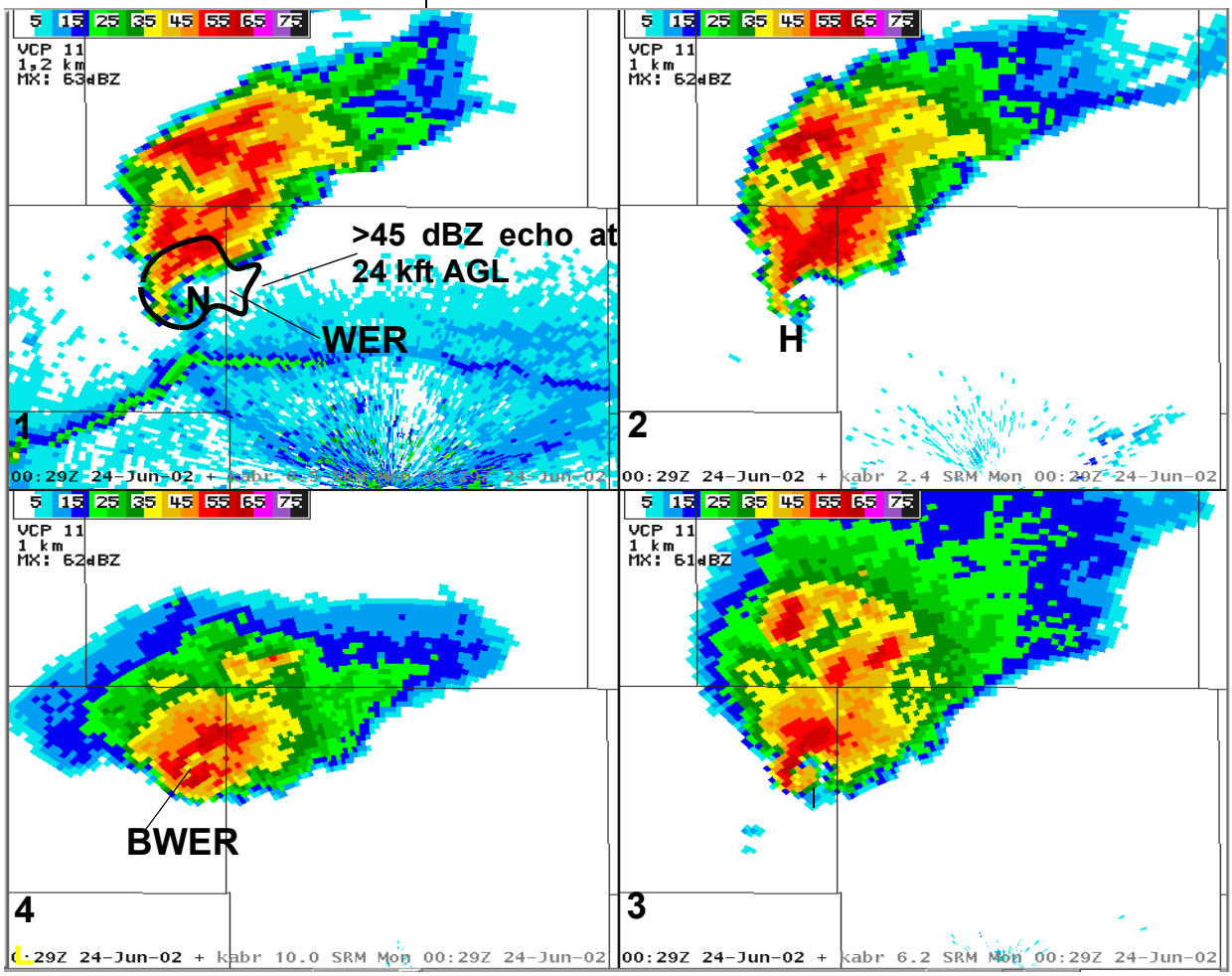

Figure 3-32. Supercell reflectivity example with the following elevation slices: 1) 0.5° - 1.5 kft, 2) 2.4° - 5.5 kft, 3) 6° - 14 kft, and 4) 10° - 24 kft AGL. The labels are explained in the text.

They are capped by very high reflectivities as the strong updraft begins to generate large hydrometeors around the -20C level. The BWER is thought to form as a result of the intense updraft inhibiting any large hydrometeors from forming until near the anvil level. Precipitation wrapping around the mesocyclone envelopes the central intense updraft forming the BWER.

Radar Signatures may not Tell the Whole Story

As alluded to previously, not all of these reflectivity structures are apparent in all supercells. The radar resolution may be too coarse to identify small scale, or shallow features such as hook echoes and BWERs at far ranges, especially for mini supercells. Inflow notches, and enhanced reflectivity gradients may be resolved to greater distances,

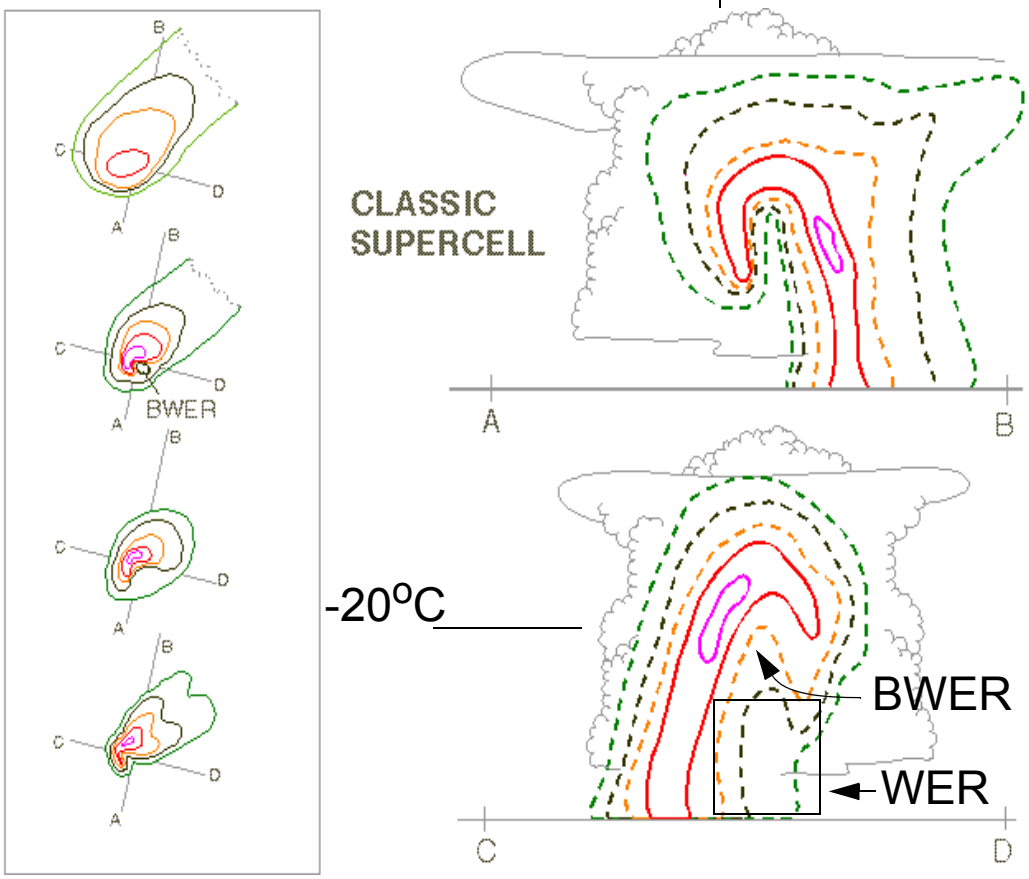

Figure 3-33. A schematic of a supercell thunderstorm with two cross-sections, A-B and C-D. The box represents the Weak Echo Region (WER).

though there will be times when these are also poorly sampled.

Objective 13

Identify the criteria for determining the presence of a mesocyclone.

The presence of a mesocyclone is the most important signature that defines a storm as a supercell. **By definition, a mesocyclone is a small-scale rotation closely associated with the updraft of a convective storm that meets or exceeds established criteria for shear, vertical extent and persistence**. Each of these criteria will be discussed.

Basic Mesocyclone Structure

Mesocyclone velocity structure is similar to that of a Rankine Combined Vortex (Figure 3-34). The core of the mesocyclone rotates as a solid body with the tangential velocity proportional to radius. Beyond this core, the velocity decreases exponentially with increasing radius from the mesocyclone center. Since only the radial velocity

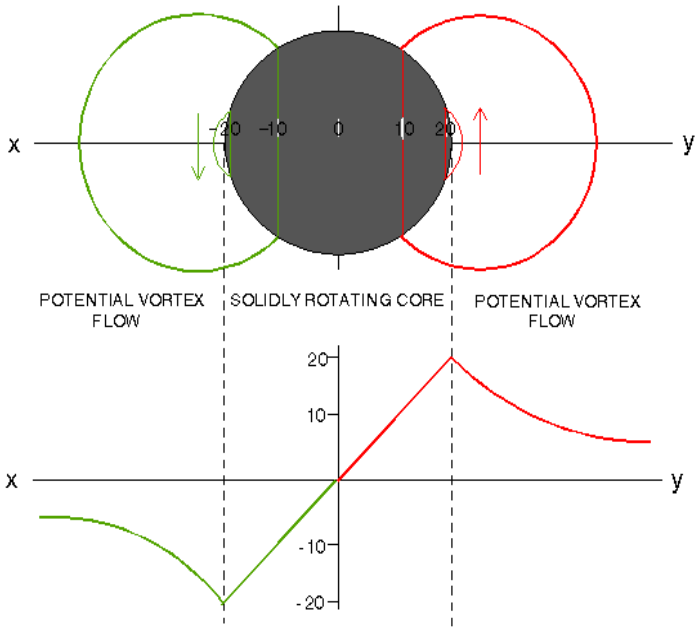

Figure 3-34. A schematic of a mesocyclone showing the velocity profile as a Combined Rankine Vortex.

component is visible from Doppler radar, only the radial components of the velocity can be detected, and therefore, the mesocyclone appears as a couplet of inbound and outbound velocity (see Figure 3-35)

Mesocyclone Recognition Criteria

To establish the validity of a mesocyclone, we use a set of criteria for shear persistence and vertical depth. A circulation feature is labeled a mesocyclone when:

- **The core diameter (distance between the maximum inbound and outbound velocities) is < 5 nm**, and
- **The rotational velocity ($V_r = |V_{min}| + |V_{max}|) / 2$) equals or exceeds minimal mesocyclone strength. V_{min} (V_{max}) is the minimum (maximum) radial velocity in the circulation.**
- **The feature persists for at least 10 minutes.**

The inputs into calculating V_r should represent the maximum outbound and inbound veloci-

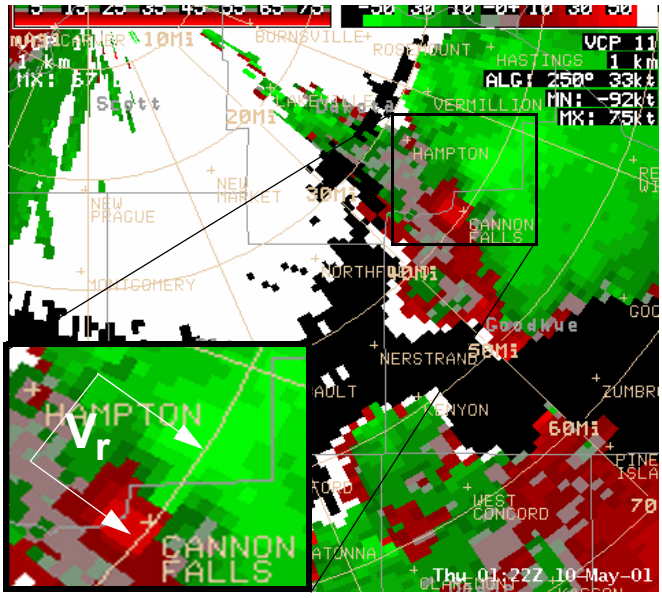

Figure 3-35. Example of a mesocyclone from Minneapolis, 0122 UTC, 10 May 2001. The mesocyclone is located in the upper right hand side of the figure. The inset is explained in the text.

ties as illustrated by the inset in Figure 3-35. Note that the inbound and outbound velocities that contribute to the calculation of rotational velocity should be measured using mid-range values of the data levels in the 4 bit velocity or SRM products. However, for the 8 bit products, the data increments are only one knot. V_r calculated from the standard or high resolution products will be close but not equal.

V_r shear is calculated by dividing V_r by the distance between V_{min} and V_{max}. It can be easily calculated using AWIPS using the V_r shear tool. Values are on the order of 10^{-2} s^{-1} for mesocyclones. However, V_r shear can change by orders of magnitude just by changing the baseline distance without any actual increase in mesocyclone intensity. **Therefore, V_r shear should be calculated with great caution and consistency through successive volume scans**. Estimating mesocyclone strength from V_r alone is just as valid as that from V_r shear.

Note that estimating mesocyclone strength is more representative when assessing V_r from multiple levels rather than one alone.

Establishing a minimal rotational velocity threshold requires knowledge of the distance of the feature, and the size of the supercell. **As radar sampling resolution degrades either by distance or by circulation size, the warning forecaster must reduce the minimal rotational velocity that discriminates mesocyclones from weaker circulations**.

The vertical criteria are required because of the number of shallow circulations uncorrelated with updrafts. Deep, vertically correlated

circulations are most likely associated with updrafts because of vertical vortex stretching and advection of vorticity by the updraft.

From the latest findings of the Tornado Warning Guidance 2002 project (TWG, 2002), only 3% of all mesocyclones are associated with tornadoes. **9% of moderate to strong mesocyclones are tornadic. However, the majority of mesocyclones are associated with some type of severe weather.** Refer to the TWG home page at:

http://www.wdtb.noaa.gov/resources/PAPERS/twg02/index.html

Significant tornadoes may follow the development of a strong mesocyclone by 20 to 30 minutes. **However, for about 50% of all tornado events, the mesocyclone provides no lead time to tornadogenesis**.

Mesocyclone Lifetime

Mesocyclones typically undergo a life span where there is an organizing stage, mature stage and dissipating stage.

Organizing Mesocyclone

The **typical organizing mesocyclone** begins at the level of maximum tilting or in the **midlevels of an updraft**. The mesocyclone then begins to build downward and upward. The midlevel mesocyclone is dominated mostly by updraft. **If the radar is close enough to the circulation, a convergent signature may be detected in the lowest slices**.

Mature Mesocyclone

The mature stage of a mesocyclone is associated with the greatest rotational velocities, deepest vertical extent, and greatest potential for severe weather.

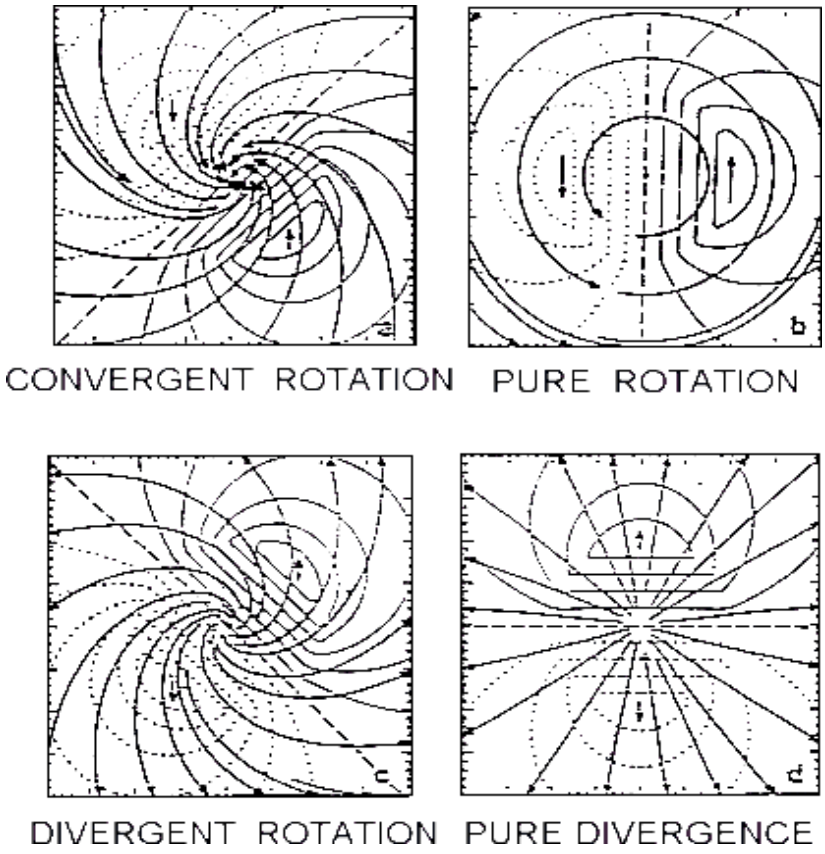

Figure 3-36. Vertical structure of a mature mesocyclone. Radial velocity inbound (outbound) are labeled as solid (dashed) countours. The streamlines represent horizontal velocity.

A mature mesocyclone has significant low-level convergence (panel 'a' in Fig. 3-36 and panel 1 in Figure 3-37), nearly pure rotation at midlevels (panel 'b' in Fig. 3-36 and panel 2 in Figure 3-37), divergent rotation at upper-levels (panel 'c' in Fig. 3-36), and nearly pure divergence at storm top (panel 'd' in Fig. 3-36). The example in Figure 3-37 does not show the divergent part of the mesocyclone. Most mesocyclones may not show all four parts of the mesocyclone vertical structure shown in Figure 3-36.

The lower half of a mature mesocyclone is occupied by the rear flank downdraft, usually on its trailing side. The rear flank downdraft can be marked by the presence of strong localized convergence between the inbound to outbound velocities

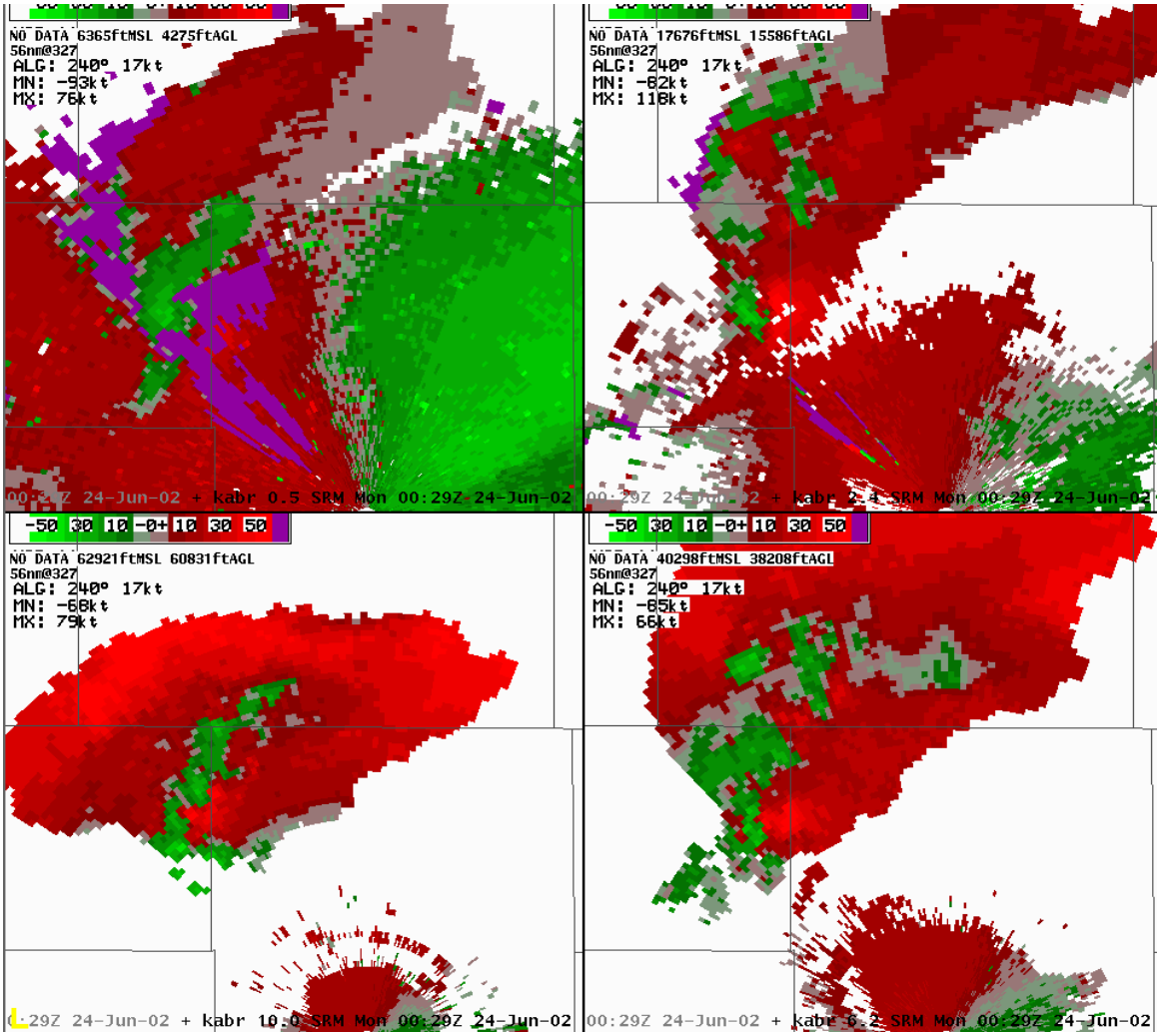

Figure 3-37. Similar to Figure 3-32, except this one depicts Storm Relative Velocity.

(labeled RFD in Fig. 3-37).This convergence should not be mistaken for the transition from in- to outbound velocities in a symmetric vortex. **Remember that mature mesocyclones are partly occupied by an RFD which may extend for several kilometers above ground-level.**

Decaying Mesocyclone

In the decaying phase of a mesocyclone, the convergent rotational signature in the low-levels gradually transitions to that of divergent rotation as outflow begins to dominate. Mesocyclone depth decreases as does the maximum rotational velocity. **If the mesocyclone is tornadic and undergoes a dissipating stage, the tornado could**

persist for a period of time after all evidence of the parent mesocyclone has dissipated.

Cyclic Mesocyclones

A supercell may produce more than one mesocyclone during its lifetime. The first mesocyclone typically takes the longest time to mature as the supercell remains outflow deficient. **Successive mesocyclones mature much more rapidly as they have the advantage of stronger lifting and vortex tilting from a stronger gust front** (see Fig. 3-38). The life spans of successive mesocyclones may or may not be longer than the first one.

The first mesocyclone extends to low-levels as the RFD reaches the ground. When the RFD matures, the outflow wraps cyclonically around the center of circulation, eventually closing it off from the inflow. **If the RFD is thermodynamically unstable, the primary mesocyclone can continue for an extended time**. However, the leading edge of the gust front associated with the RFD can quickly produce successive updrafts and mesocyclones

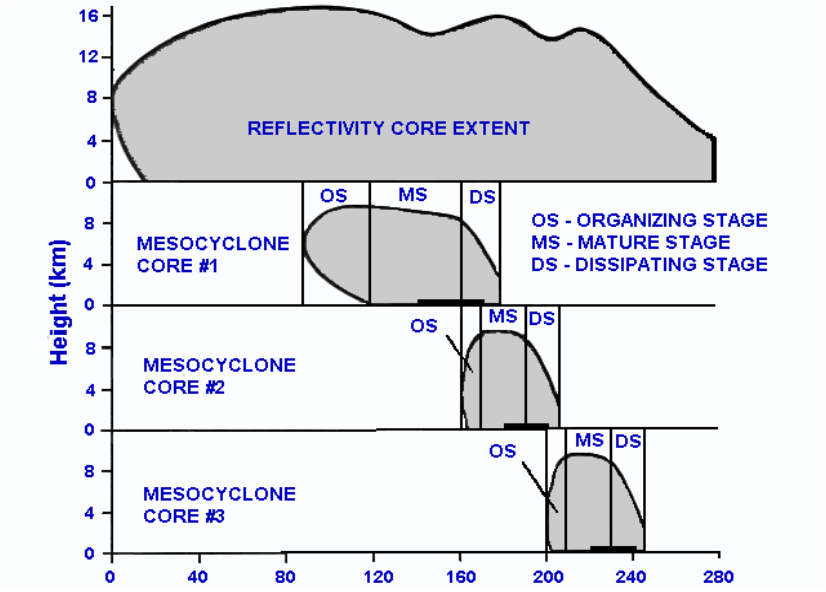

Figure 3-38. Time-height evolution of reflectivity core extent (top), and mesocyclone cores (bottom) in a supercell. Solid bars indicate tornado occurrence. The figure is adapted from Burgess et al. (1982).

owing to increased convergence and vertical low-level vorticity. In turn, the successive mesocyclones become wrapped by local RFD enhancement, and the process continues for possibly several hours. A family of tornadoes is produced in this fashion from one supercell.

Objective 14

Describe the environmental, structural and evolutionary differences that can produce low precipitation, high precipitation and classic supercells.

The Supercell Spectrum

Supercells are grouped into three different structural classes depending on the amount of precipitation contained within the core, and where the mesocyclone is located with respect to the main core.

The Low-Precipitation Supercell

Low Precipitation (LP) supercells are generally dominated by updraft with little precipitation reaching the ground. These storms are visualized by exposed updrafts and translucent to nearly transparent precipitation cores. The relative lack of precipitation leads to poor downdraft formation and thus these storms could be said to be outflow deficient. LP supercell updrafts often show significantly strong midlevel mesocyclones. However, low-level mesocyclones are rare owing to the lack of a well defined RFD. There is rarely a hook echo, and most of the precipitation is carried well downstream of the updraft by the storm-relative upper-level winds. Maximum reflectivities in LP storms can be weak. However, the reflectivity maximum likely consists of a few large hailstones (see Fig. 3-39).

LP supercells require significant instability and shear. However, other conditions help to reduce precipitation efficiency. Relatively dry boundary air

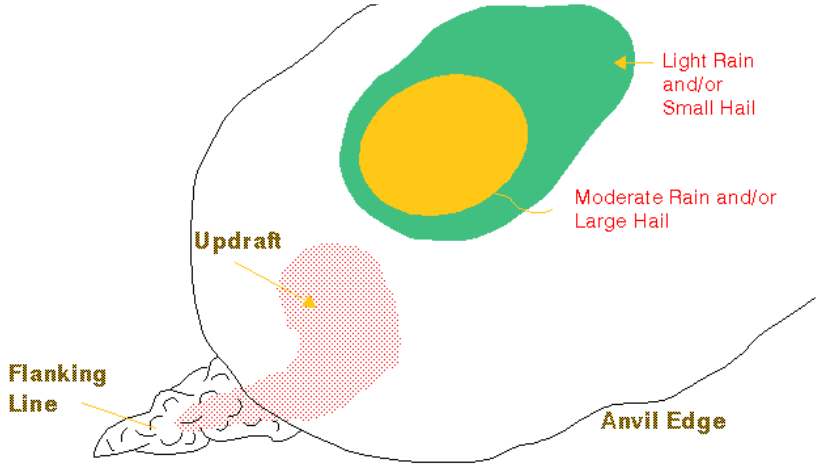

Figure 3-39. A top view LP supercell schematic.

reduces available moisture and adds to entrainment, but LP storms can also exist where boundary layer moisture is high. **Additionally, very high storm-relative anvil-layer winds (>30 m/s) transport rising hydrometeors well away from the updraft before they descend out of the anvil layer (Rasmussen and Straka, 1998).** Hydrometeors may have little chance of recycling back into the updraft, especially if the midlevels are dry.

LP storms have a propensity to produce very large hail but little rainfall, and because of little potential for downdraft formation, significant tornadoes are rare. LPs can transition into classic supercells rapidly, thus it is important to pay close attention for any structural changes such as the development of a well defined hook echo or increased reflectivities either aloft or near the surface.

Classic Supercells

Classic (CL) supercells generate enough precipitation to be able to produce enough downdraft for a moderately strong outflow. A sufficient amount of precipitation is available to wrap around the mesocyclone to create a hook echo. However, the majority of precipitation falls

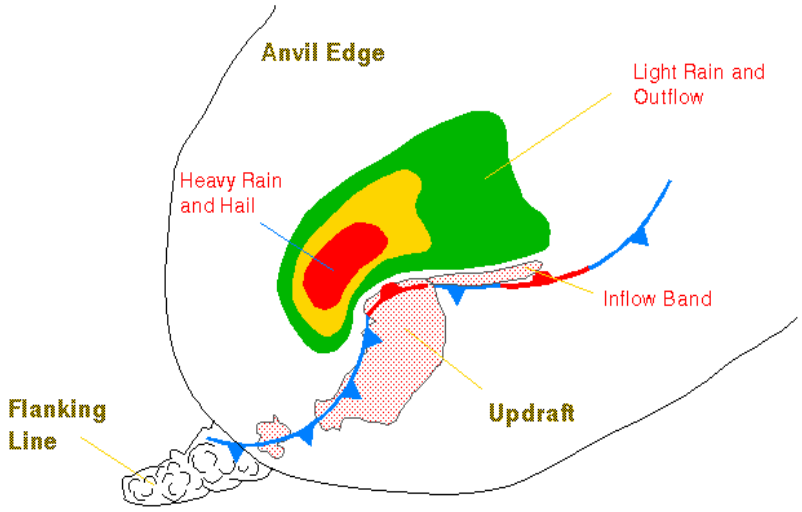

Figure 3-40. A top view Classic supercell schematic.

into the core ahead of the mesocyclone. The RFD is stronger with a CL than with an LP and therefore, low-level mesocyclogenesis is more likely. The result is a greater threat of severe weather from winds and tornadoes (Fig. 3-40).

CL supercells occur in moister environments than are typical for LP storms. Storm-relative, anvil-layer winds are likely to be lower for CL supercells (mainly between 18 and 30 m/s).

These supercells produce the majority of long-lived tornadoes. They are also the common cyclic tornado producer.

High Precipitation Supercells

High Precipitation (HP) supercells are the most common of all supercells. They are highly efficient precipitation producers and often produce strong downdrafts and outflows. Large amounts of precipitation are available to wrap around the mesocyclone, producing a large, high reflectivity hook. Occasionally, the RFD gust front associated with the hook is intense enough to generate strong convection along its leading edge (Fig. 3-41). The result is that the

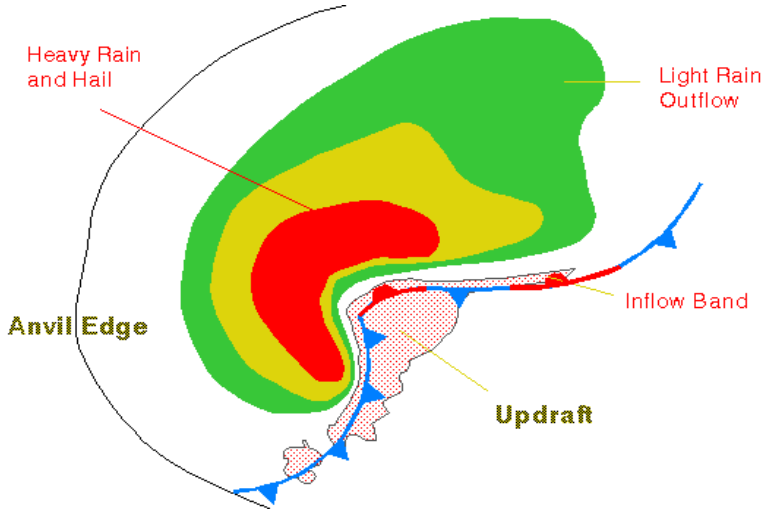

Figure 3-41. A top view HP supercell schematic.

strongest core can be behind and to the right of the mesocyclone path. Occasionally, this process leads to supercells evolving into bow echoes. There is a wide variety of possible HP supercell configurations (Fig. 3-42), however, they all share traits common to all supercells - a mesocyclone well correlated with an updraft and longevity.

The mesocyclone is usually well sampled by radar owing to the high reflectivities in the hook. Spotters in the field often have a difficult time observing the mesocyclone area most favorable for tornadogenesis.

HP environments typically show more boundary layer moisture than that of LP or even CL. However, high boundary layer moisture is not necessary for an HP. **Another possibility includes low anvil-level, storm-relative flow (<18 m/s) to allow precipitation to reseed the updraft improving precipitation efficiency.** A supercell can turn HP if it is being seeded by aggressive cells on its flanking line or adjacent storms.

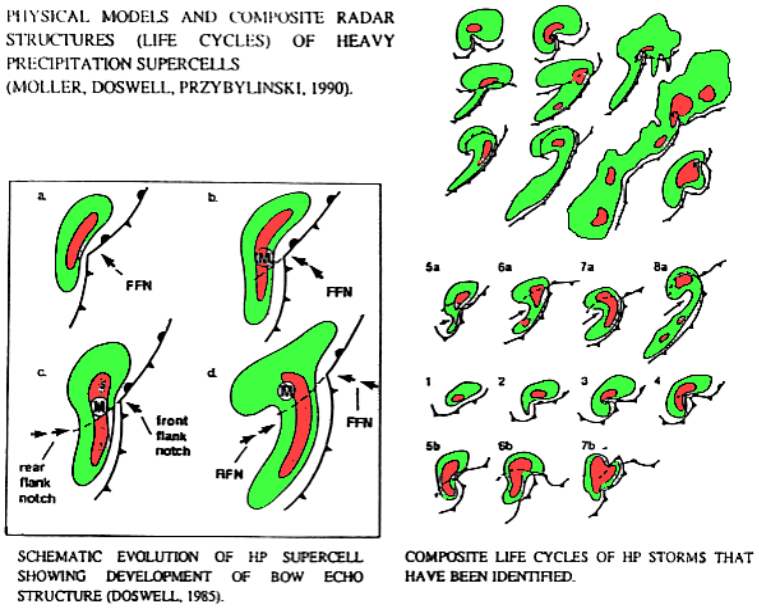

Figure 3-42. A variety of documented HP supercell reflectivity configurations. Adapted from Moller et al. 1990; Doswell, 1985.

HP storms carry all threats of severe weather including strong tornadoes. However, the threats of large hail, damaging winds and flash flooding are greatly enhanced with HPs.

Mini Supercells

As supercells can vary in the amount of precipitation falling around the mesocyclone, they can also vary in width and height. There can be low-topped supercells with wide mesocyclones, or high-topped supercells with narrow mesocyclones. **By definition, a mini supercell is one that is low topped and consists of a narrow mesocyclone. Low topped supercells can reach anywhere from 20-30 kft AGL. Mesocyclone diameters in mini supercells typically are less than 3 nm.**

There are no structural differences between low topped and normal-sized supercells. There are differences in the expected severe weather. Giant hail (>2.5”) is rare because of limited extent of the updraft into the hail growth zone, and smaller horizontal dimensions of the updraft. **Poor radar sampling of small mesocyclones means that it is**

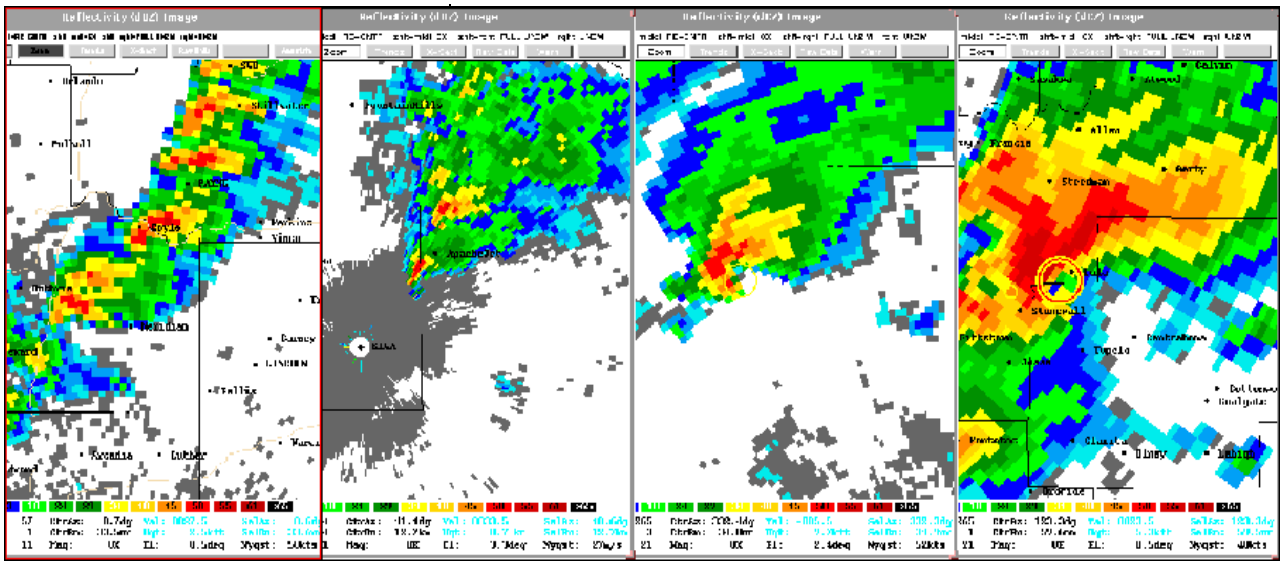

Figure 3-43. A spectrum of supercell types from mini supercells in the left three panels compared to a typical supercell on the right. Each supercell in the right three panels is producing a tornado. The yellow and red circle near the hook on the right panel is an automated mesocyclone detection. Adapted from Stumpf (1995).

more difficult to measure high rotational velocities. To illustrate this point, the main supercell in each panel of Figure 3-43 is tornadic, yet only the largest supercell (right panel) was large enough for the radar to resolve a mesocyclone. Therefore, it is important to recognize mini supercells and be more sensitive to the fact that weak circulations (V_r < 30 kts) can carry a significant tornado risk (Prentice and Grant, 1996).

Left-moving Supercells

Left-moving supercells typically rotate anticyclonically and are a by-product of the original storm split. They are structurally a mirror of the right-mover. Very few left-moving supercells produce tornadoes, and for reasons that are poorly understood they may produce long swaths of giant hail. As long as the hodograph is relatively straight, the left-mover can be as strong as the right-mover. Note that the reflectivity structure of a left-moving supercell infers the updraft to be on the left side of the core as shown by the enhanced reflectivity gradient and concavity on the north side of the northern supercell in Figure 3-44. In the

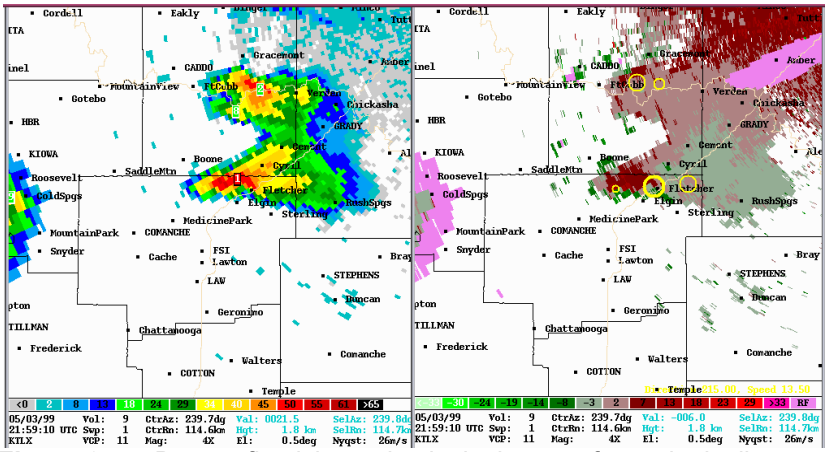

Figure 3-44. Base reflectivity and velocity image of a cyclonically (bottom) and anticyclonically (top) rotating supercell pair from 03 May 1999 - 2159 UTC.

same figure, the velocity pattern shows anticyclonic shear in the left-mover.

Objective 15

Identify the common signatures in supercells that can be used to detect severe winds, large hail, tornadoes, and heavy rainfall.

a. **Identify three major radar signatures for determining large hail.**

b. **Describe the criteria for defining a tornado vortex signature.**

c. **Describe two major meteorological contributors that contribute to a flash flooding threat from supercells.**

General Updraft and Volumetric Signatures

Before analyzing specific severe weather threats (e.g., hail and wind), it is important to take advantage of the volumetric radar data available to analyze the three-dimensional nature of storms. Lemon (1980), derived a methodology for volumetric discrimination between non-severe and severe convection. It focuses on how the updraft modulates the shape of the reflectivity echo. Since updraft strength is an important controlling factor in severe weather, analyzing the 3-D shape of the reflectivity core is important. **A weak updraft in a**

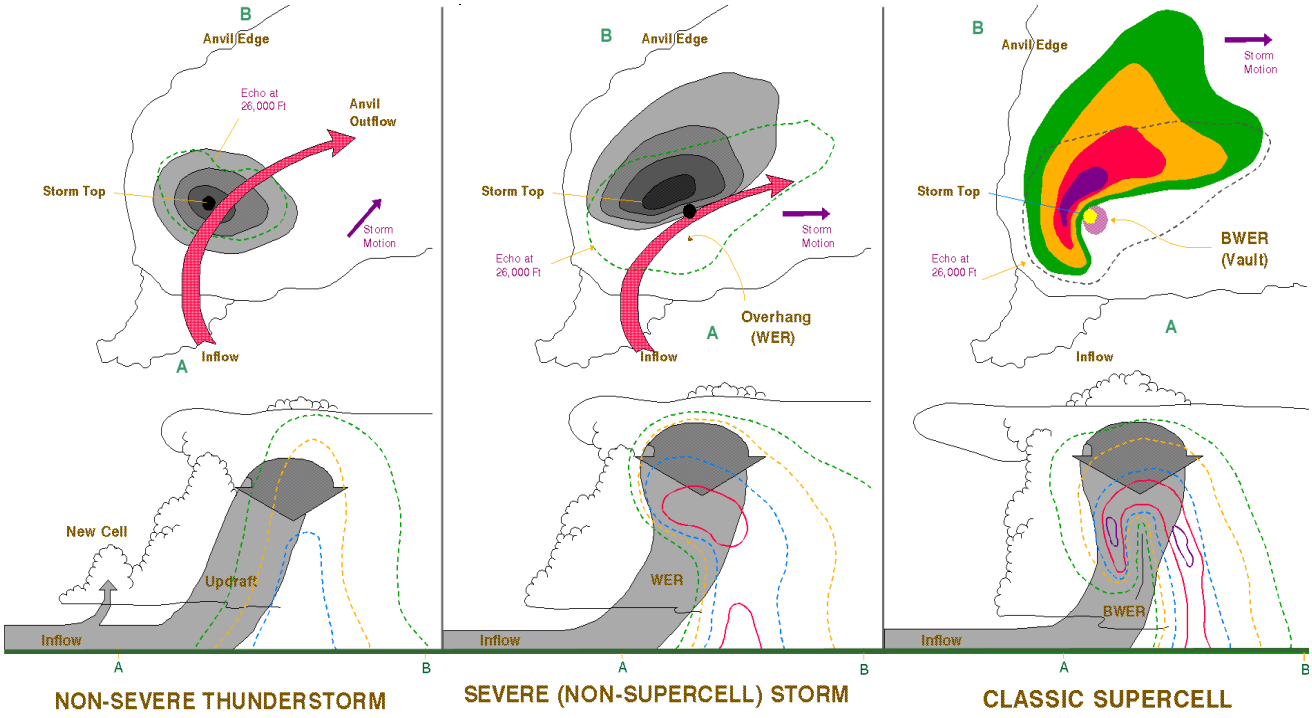

Figure 3-45. Reflectivity structure of (A) weak updrafts, (B) strong updrafts, and (C) strongly rotating updrafts, in a sheared environment. The small green letters in the top panels represent the endpoints of the cross-sections in the lower panels (Adapted from Lemon, 1980).

sheared environment slopes downwind and is typically unable to suspend any precipitation (Fig. 3-45a). As updraft strength increases, it becomes more erect and is able to suspend a heavy core of precipitation resulting in the WER (Fig. 3-45b). The most intense updrafts are erect and may exhibit a BWER if strongly rotating (Fig. 3-45c).

The base of a severe updraft is typically located under the WER and BWER and next to strong reflectivity gradients and inflow notches. These areas show substantial low-level convergence, and with weak updrafts, it is more difficult to pick out the updraft base.

The updraft signatures discussed previously may result in different severe weather types depending

on the storm environment. Here are a few examples:

- A BWER in a nearly saturated, warm sounding (e.g., a tropical cyclone) is unlikely to infer the presence of large hail because the environment is too warm at the top of the BWER.
- An environment with a low equilibrium level supporting mini supercells may indicate to the forecaster that BWERs may be too small to detect beyond a close range.
- A tall supercell environment may exhibit strong storm top anvil-layer winds and dry air. In this case, LP storms may show relatively light reflectivities compared to the size of the hail they generate.
- HP supercell environments may lead a forecaster to expect that some storms may show WERs, and BWERs ahead of the main core with respect to the shear vector.
- Straight or anticyclonically curved hodograph environments favor left-moving storms with updraft signatures to the left of the main core.

Any supercell with motion deviant to the steering-layer flow is cause for increased concern for severe weather production.

High Winds

The same mechanisms that force pulse storm microbursts also apply to supercells. The unique downdraft forcing mechanism to supercells is the RFD. **The beginnings of an RFD are believed to be forced from evaporational cooling and possibly precipitation loading on the right-rear flank of a supercell. Low-level mesocyclogenesis adds a downward directed dynamic pressure gradient force to an RFD that can overwhelm all other downdraft forcing mechanisms.**

The high wind threat from an RFD is maximized when:

- **Low-level mesocyclogenesis occurs.** Watch for the development of a strong mesocyclone in the lowest slices. A descending mesocyclone core is a strong precursor to a severe RFD.
- **Heavy precipitation (> 50 dBZ)** within the hook can favor a severe RFD through precipitation loading and evaporational cooling.
- **A deep convergence zone (DCZ) exists on the backside of the mesocyclone.** Look for strong convergence with velocity differences over a few nm along the radial > 50 kts, and extending up to 15 kft or more (See Fig. 3-46.).
- **The same environmental parameters favoring hybrid or wet microbursts help to**

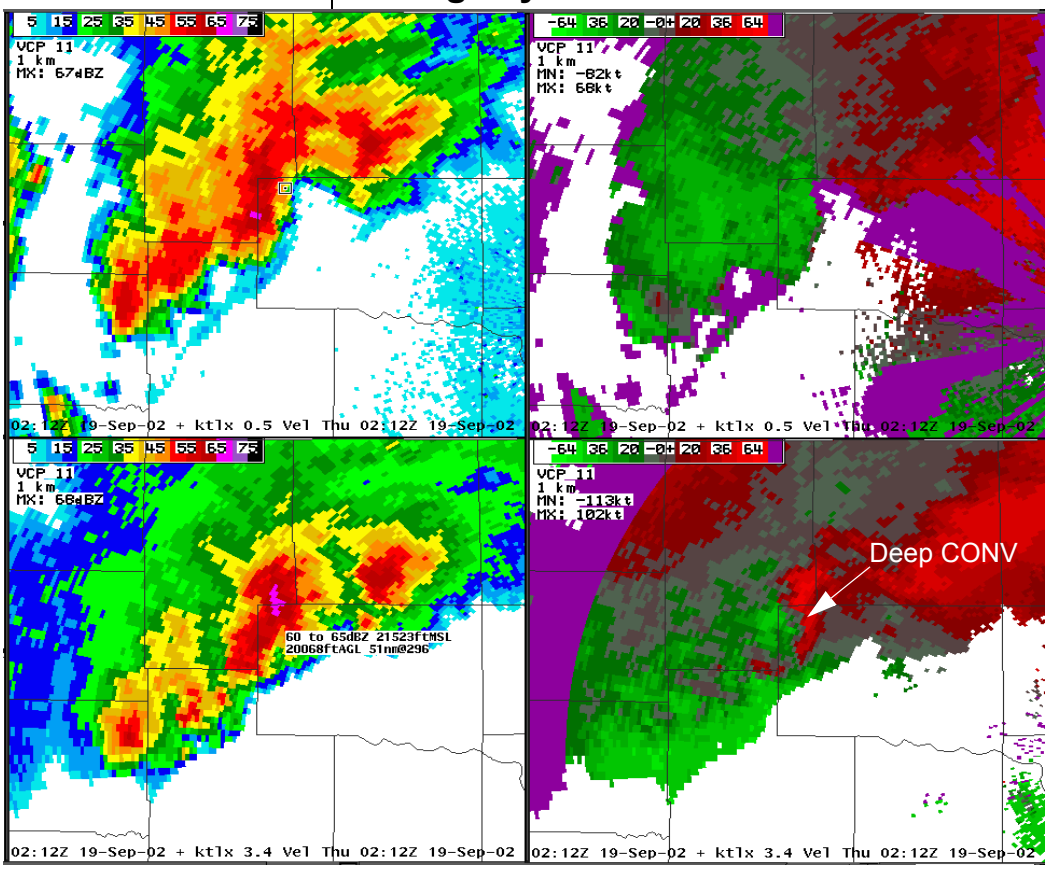

Figure 3-46. A velocity-reflectivity four panel of a HP supercell with deep convergence (labeled CONV). The top panels are 0.5^{o} and the bottom are 3.4^{o}.

encourage a severe RFD. However, they are not necessary if a strong low-level mesocyclone is developing.

The most damaging RFD winds likely occur with HP supercells just to the right of the primary mesocyclone track.

Objective 15a: Large Hail

Identify three major radar signatures for determining large hail.

All types of supercells may produce large hail. Giant hail (diameter > 2.5") is almost exclusively produced by supercells. **In general the following are large hail signatures**:

- **Significant Storm-Relative (S-R) flow**. S-R flow largely determines the trajectories of hail embryos across the updraft. These help feed a steady stream of hail embryos into the main updraft. Supercells with upwind flanking lines and upwind anvils have a steady supply of hail embryos (graupel). Embryos can also fall into the updraft from the upwind anvil overhang.
- **Large amounts of buoyancy in middle-to-upper-levels**. Steep midlevel lapse rates ensure that the environment favors strong updraft in the hail growth region where temperatures are between -10 and -30^{o}C.
- **A significant mesocyclone**. Dynamic pressure drops, especially in a strong midlevel mesocyclone, accelerate the updraft in the hail growth region. It can also provide a "stagnation point" increasing the residence time of growing hailstones in an updraft.
- **A sustained updraft with a large WER or BWER**. Studies have shown that above the top of the WER/BWER is the location where growing hailstones are suspended in the core

of a strong updraft. A WER or BWER suggests that these hailstones are subject to a massive influx of cloud water, especially if in the hail growth region. A large WER or BWER means that there is a large area, and more time, for suspended hail to grow before cascading into the core. Remember that a WER or BWER is topped by intense reflectivities in order for it to be associated with updraft. A great majority of giant hail events are associated with BWERs.

- **As inferred above, a broad updraft favors large hail** since the hail embryo trajectories will be exposed to updraft for a longer period of time.
- **Elevated high reflectivities, especially above the -20^{o}C level**. See hail signatures for pulse storms.
- **The HDA algorithm output works very well for supercells**.
- **A three-body scatter spike (or hailspike) is a direct detection of large hail in an updraft using 10 cm radar**. The presence of this signature is enough to issue a severe thunderstorm warning. A hailspike forms as incident energy from the radar is reflected off the hail, down to the ground, then back up to the hail and back to the radar. The radar, confused by the delayed return of the echo, believes it to be coming from further away (Fig. 3-47).

Fig. 3-48 shows that the hailspike typically appears in elevated slices. Increasing the height above the surface of the intense hail core increases the length of the spike. Hailspikes have low reflectivities of 15-25 dBZ, low radial velocities, and high spectrum widths.

Storm Top Divergence

Strong storm top divergence can be considered for assessing large hail potential. Check for scans

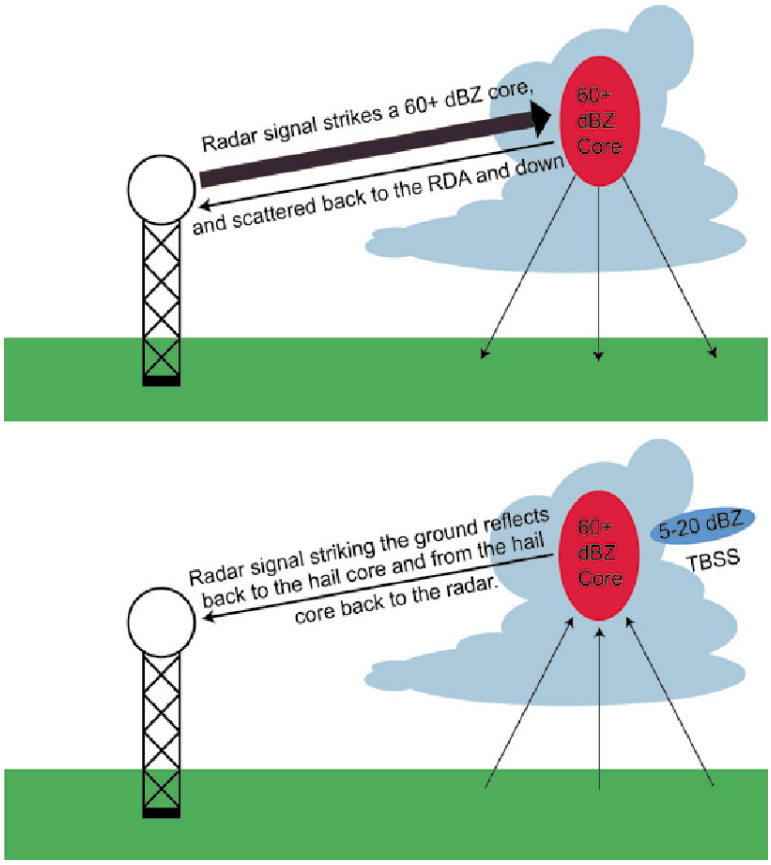

Figure 3-47. A schematic of a three-body scatter spike.

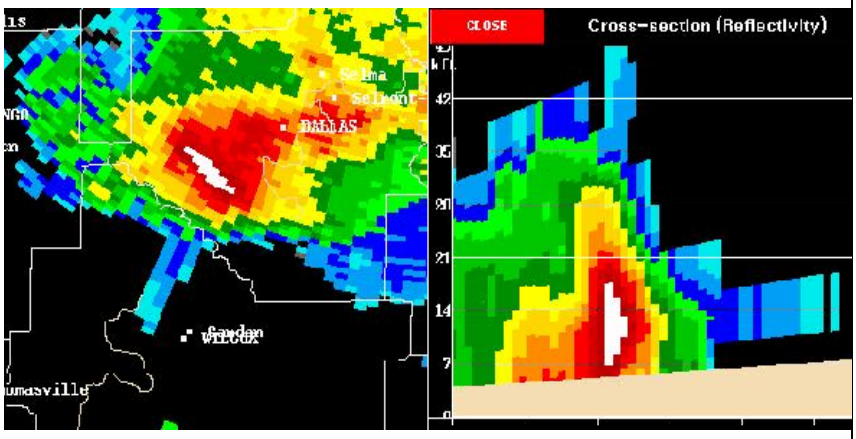

Figure 3-48. An example of a three-body scatter spike showing that the highest reflectivities contain large hail.

that cut through the storm summit only, and examine the maximum inbound and outbound velocities. **Storm top divergence is shallow and easily missed by radar, thus it is considered to be an unreliable large hail indicator**. The presence of strongly divergent flow at storm top (say

$|V_{out}| + |V_{in}| > 75$ kts) does indicates a strong updraft. Because of viewing problems, this technique should only be used to diagnose hail threat after examining base reflectivity and the HDA.

Signals Indicating Less Likely Hail Production

Signatures that may show a supercell is a poor hail producer are:

- **Supercells in moist environments with weak lapse rates in the midlevels** just below the hail growth layer (-10^{o} C to -30^{o} C layer).
- **A shallow supercell with a weak reflectivity core above the -20^{o}C level**.

Objective 15b: Defining TVS

Describe the criteria for defining a tornado vortex signature.

Mesocyclonic tornadoes develop as a result of processes within a supercell mesocyclone that help to develop vertical vorticity at ground-level. Although little is known about the fundamental processes that lead to near surface vertical vorticity, there is general agreement that the mesocyclone and the attendant RFD play important roles. Observations have shown that tornadogenesis follows the formation and strengthening of the low-level mesocyclone and the RFD descent to ground. The RFD outflow produces significant vertical vorticity along the gust front with strong positive vertical vorticity on its left side, beneath the mesocyclone updraft. Convergence and stretching of the positive surface vorticity are presently believed to be the final steps to tornadogenesis. More buoyant RFDs allow the updraft to more efficiently stretch the vertical vorticity into a tornado (Markowski et al., 2002).

The tornadogenesis process traditionally manifests itself on radar as an increase in rotational

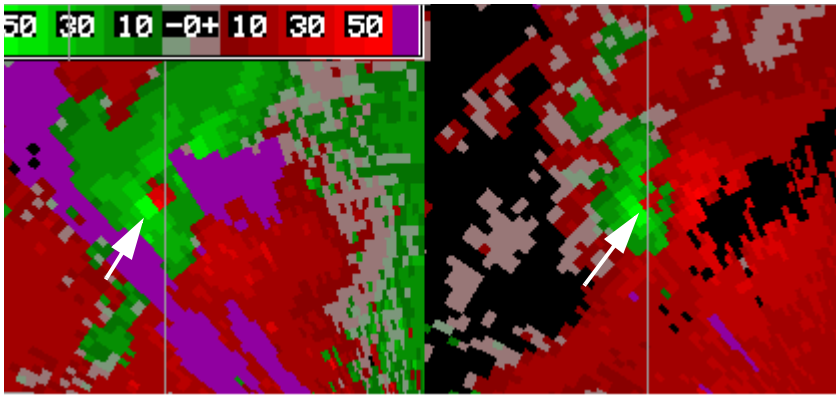

Figure 3-49. Example of a Tornado Vortex Signature (TVS) from 23 June 2002 - 0039 UTC marked by the white arrow. The left (right) panel is the 0.5^{o} (2.4^{o}) slice.

velocity in the mid- and/or low-levels. **The tightening of the mesocyclone is common, which often leads to the development of a Tornado Vortex Signature (TVS)**. Note in this section, we refer to the TVS as one defined by the operator, not an algorithm.

A Tornado Vortex Signature (TVS)

The TVS is a gate-to-gate azimuthal shear possibly associated with tornadic rotation that meets or exceeds established criteria for shear, vertical extent and persistence (Fig. 3-49). A TVS can be described as a tornadic velocity profile superimposed on a large mesocyclone. Let's elaborate more specifically on the TVS criteria.

TVS Gate-to-gate Velocity Difference

Since a TVS is defined by strong gate-to-gate azimuthal shear, we assume that measuring the velocity difference between two adjacent gates gives a good measure of its shear (see Fig. 3-50). **Therefore, the velocity difference (DV) is,**

$$\Delta V = \left|V_{min}\right| + \left|V_{max}\right|,$$

where DV, V_{min} and V_{max} are defined in Fig. 3-50. Because the distance between two adjacent gates increases as the distance to the

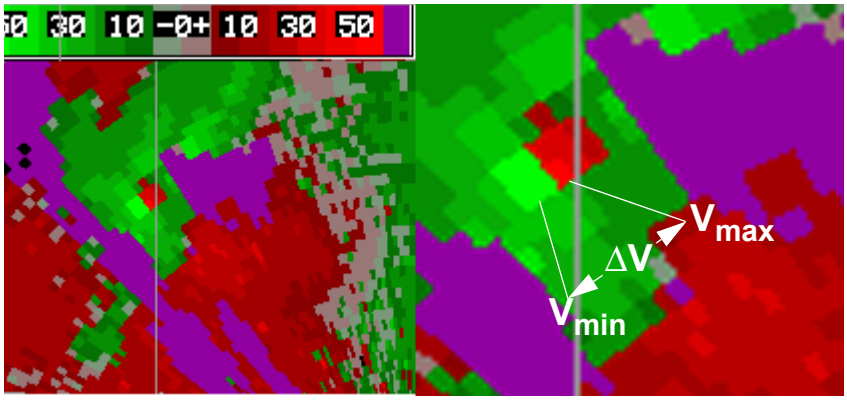

Figure 3-50. Close-up of a TVS showing where velocity difference is calculated from two adjacent gates.

radar increases, DV is not really equivalent to shear. However, to simplify the process, we still use DV and account for how decreasing resolution can affect the relationship between DV and shear (more on this later). There are two DV calculations that are typically calculated:

- **The DV measured in the lowest slice is called the Low-Level Delta V, or LLDV**.
- **The maximum DV for all slices containing a TVS is called Maximum Delta V (MDV)**.

The criteria for determining whether LLDV or MDV satisfy a TVS criteria depends on how likely it is to be associated with a tornado. This likelihood depends on a great many parameters, including storm type, environment, and distance to the radar. Comparing the likelihood that a certain LLDV and MDV are associated with a tornado, we look at False Alarm Rate (FAR), Probability of Detection (POD), and Heidke Skill Score (HSS) from a study of thousands of TVSs of all storm types across the country (Fig. 3-51). The HSS score compares FAR, POD, missed detections and correct nulls to show the best values for LLDV and MDV (TWG 2002). **Results show significant skill score values are reached when LLDV exceed 20 m/s (40 kts) and MDV exceed 30 m/s**

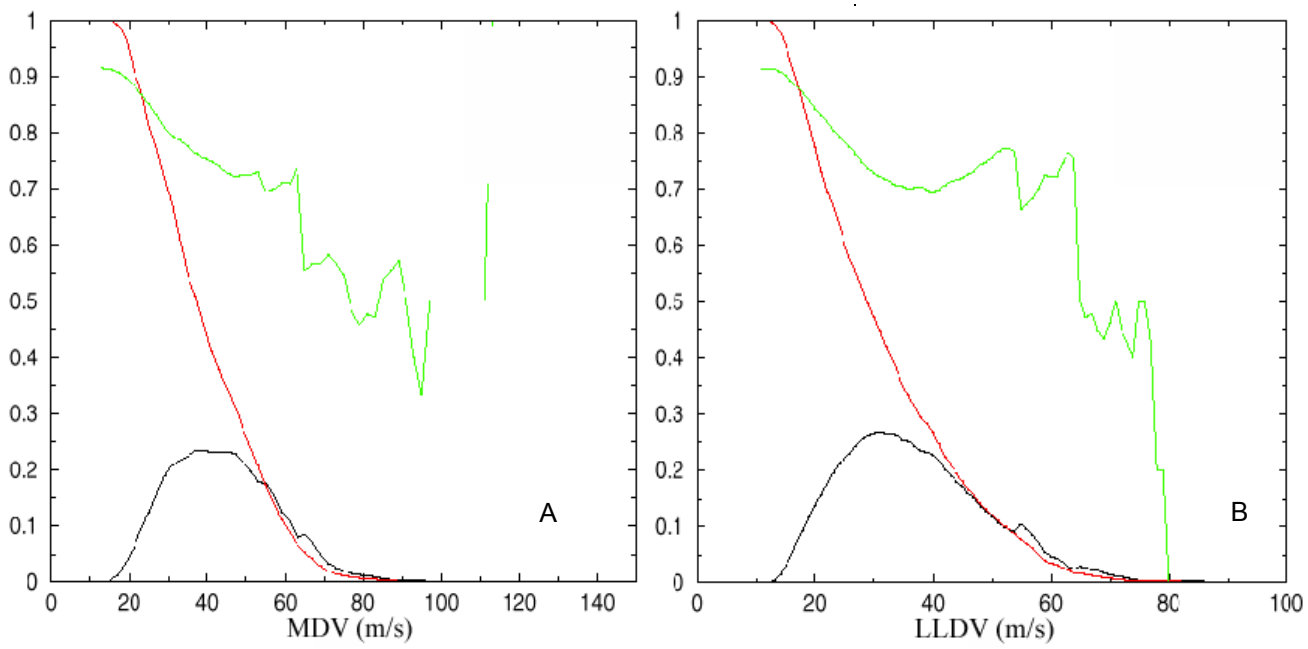

Figure 3-51. Skill scores of a) TVS MDV and b) TVS LLDV values being associated with a tornado as measured by FAR (green curve), POD (red curve) and HSS (black curve). Adapted from TWG, 2002.

(58 kts). The TDA algorithm default parameters are LLDV= 25 m/s and MDV=36 m/s. As these values increase, the likelihood of a tornado also increases.

TVS Depth

At least some vertical continuity should be seen in a TVS so that there is high probability that an updraft is present in the circulation. **For most events, the depth should be at least 1500 m (4900 ft)**. Low-topped supercells typically do not have deep TVSs, even if tornadic. Sometimes only the lowest elevation angle contains the gate-to-gate rotational signature in tornadic low-topped supercells.

Persistence

In order to reduce the possibility of a circulation that randomly becomes vertically coordinated, you should ensure that the TVS persists for at least five minutes. Some legitimate TVSs may become tornadic in less time. We suggest that if a gate-to-gate velocity signature forms in close proximity to a mesocyclone or a strong

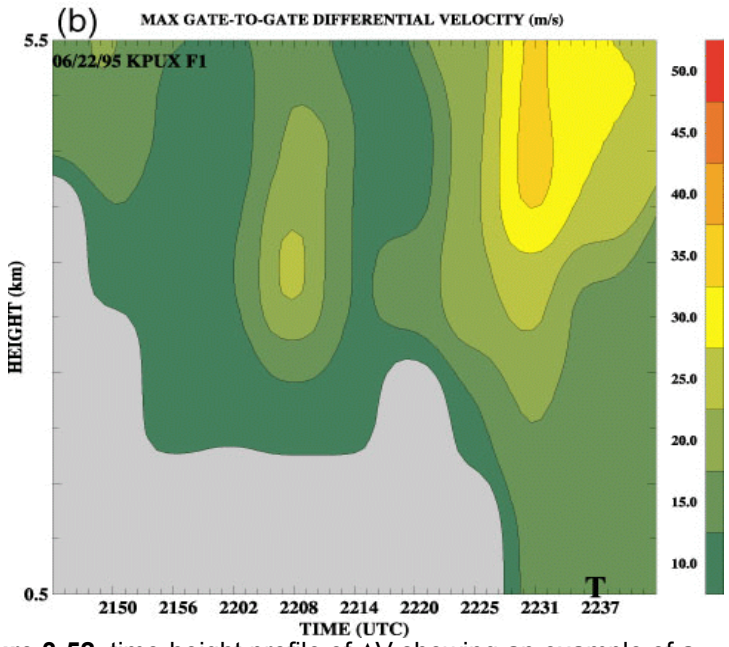

Figure 3-52. time-height profile of ΔV showing an example of a descending TVS. The "T" represents tornado time (Trapp et al. 1999).

updraft signature, persistence may not be a requirement to call it a TVS.

TVS Evolution

Descending TVS

In a traditional mesocyclone evolution, the TVS originates in the midlevels and then descends to the ground over time as the mesocyclone strengthens below (Fig. 3-52). This process allows for the maximum lead time in a tornado warning.

Non-descending TVS

Recent studies (Trapp et al., 1999; Atkins and Wakimoto, 1995) have indicated that not all mesocyclone-induced TVSs descend from midlevels to reach the ground. **About half originate at low-levels and then extend upward**. Often, this non-descending paradigm is associated with subsequent mesocyclones in cyclic supercells, or in supercells with very strong low-level shear, possibly from an outflow or other type of boundary. Non-descending TVSs occasionally originate within supercells over a boundary containing strong verti-

cal vorticity (Wakimoto and Atkins, 1996). Warning lead time depends on monitoring the trend of the low-level TVS shear and picking the right threshold. Non-descending TVSs will be discussed further in the section on multicell squall lines.

TVS Performance vs. Range to Radar

TVS detections are limited in range owing to degraded radar sampling with range. However, a comparison on the statistical performance of TVSs to detect tornadoes vs. range to radar indicates that there is little range degradation out to 150 km (~78 nm) (Fig. 3-53). These results show that other factors could be more important than radar range degradation - at least within the first 150 km. Therefore, there is a strong need for spotters regardless of range to the nearest radar.

What is a TVS Really Detecting?

The TVS in Fig. 3-54 is showing a small circulation that is still much larger than a significant close-

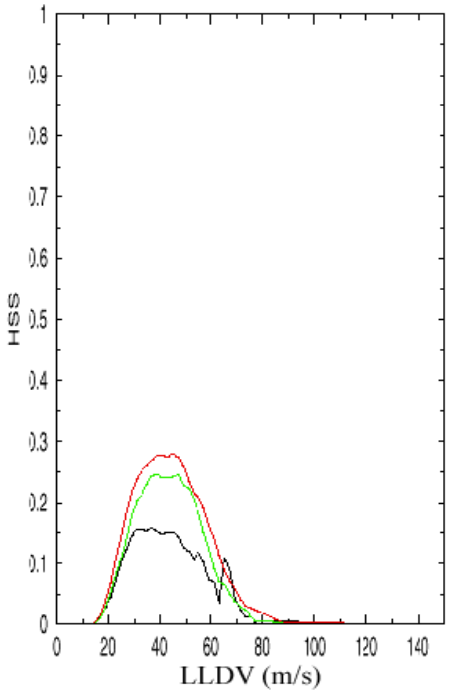

Figure 3-53. Ability for TVSs of all storm types to detect tornadoes as a function of LLDV and range from the radar. The black curve represents the HSS for a range of 0-50 km, red represents 51-100 km, and green, 101-150 km. From TWG, 2002.

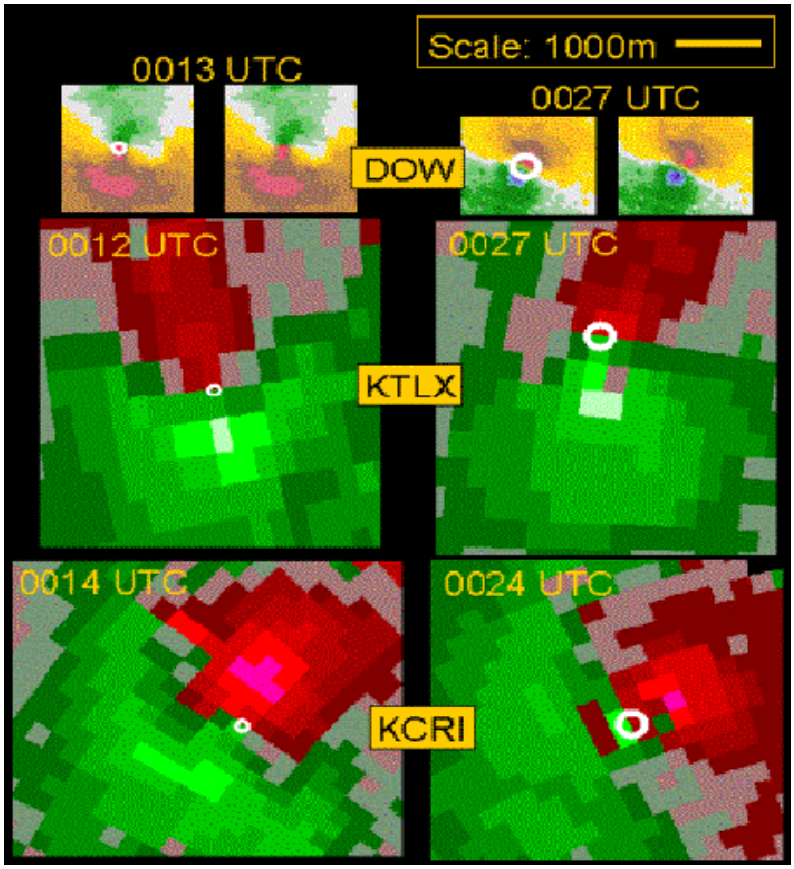

Figure 3-54. A comparison of radial velocity patterns of the 03 May 1999 OKlahoma City tornado between the Doppler on Wheels (DOW), KTLX, and the experimental WSR-88D, KCRI. The DOW is resolving the tornado whose radius of maximum winds is marked by the white circle, which then is overlaid on the other two radars. The tornado at 0012 (0027) UTC, is 200 (500) m in diameter (after Magsig et al. 2000).

range tornado as depicted by the high resolution Doppler on Wheels (DOW) data. At low-levels, the TVS likely represents part of the intensifying mesocyclone inside the wrapping RFD (Fig. 3-55). The RFD axis is usually closely aligned with the axis of the wrapping hook echo. The low-level air-flow inside the hook/RFD gradually increases with decreasing distance to the circulation center.

Tornado Warning Guidance

Since a major tornado is still small compared to the size of the gate-to-gate velocity signature that makes up the TVS, we cannot depend on the radar to directly detect a tornado. In

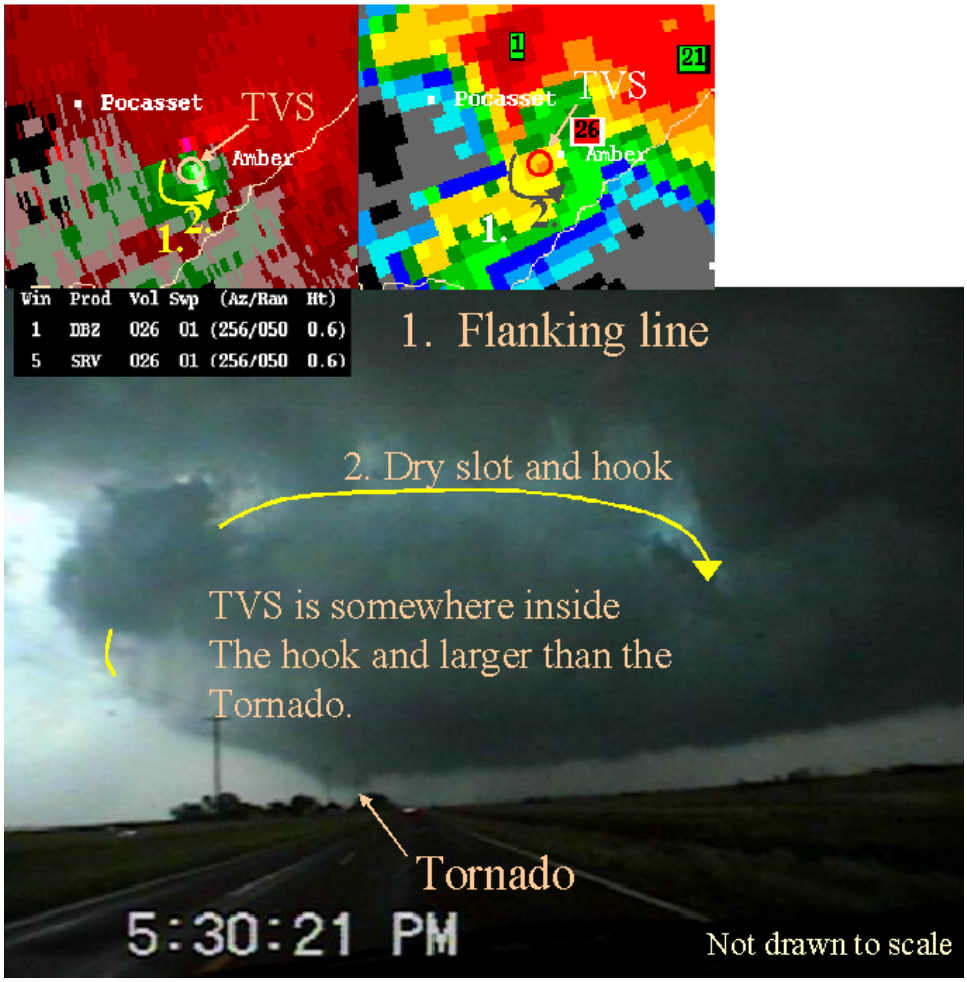

Figure 3-55. Comparison between radar observable features associated with a TVS and that from the ground facing north. The numbers in the photograph correspond to the numbers in the radar reflectivity and velocity insets on top.

order to be successful in issuing tornado warnings, radar, environmental, and spotter data must be used to improve your knowledge of what is really happening with the storm. When considering a tornado warning, it is important to assimilate the relative contributions of several data sources pertaining to tornado formation and persistence. We'll now discuss these aspects of tornado warning guidance: environment, rotational signatures, and updraft strength.

Environment

Additional environmental parameters to that of supercells seem to be needed for enhanced tornado probability. **Mesocyclone-induced tornado**

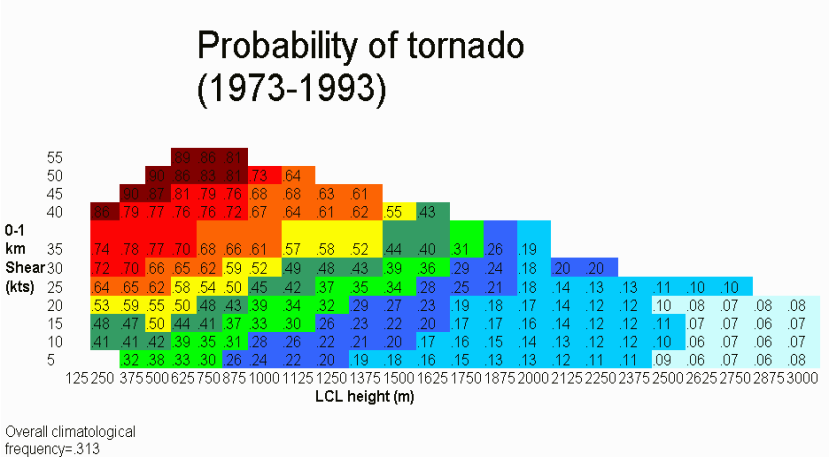

Figure 3-56. A smoothed probability of a tornado as a function of LCL and 0-1 km shear within a proximity to an observed sounding given the presence of CAPE. The results are based on 30 years of climatological data. Based on Brooks and Craven, 2002.

environments favor strong 0-1 km shear and a low LCL (Fig. 3-56). The shear helps to strengthen low-level mesocyclones. The low LCL ensures that the RFD is still potentially unstable as it helps create vertical vorticity (Markowski et al., 2002). **The LCL and shear should be in an environment that promotes strong low-level updraft acceleration (i.e., low CIN and strong low-level convergence)**.

Boundaries are regions that can be locally favorable for tornadic supercells. Look for these types of boundaries:

- **Subtle boundaries with backed winds and good SBCAPE providing a good clue of increased low-level shear, low LCL and little CIN (Fig. 3-57), and**
- **boundaries with strong vertical vorticity in supercell environments**.

Supercells can stretch environmental vertical vorticity along boundaries at least as effectively as pulse cells and provide little forewarning of tornadogenesis.

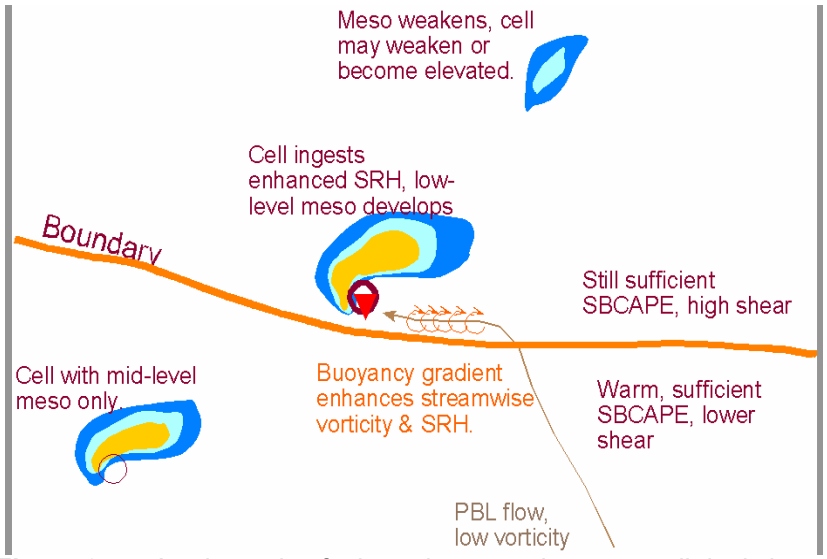

Figure 3-57. A schematic of a boundary-crossing supercell depicting favorable parameters for tornadogenesis.

Rotational Signatures

Based on the National Severe Storms Laboratory Mesocyclone and TVS algorithm performance, 30% of all TVSs (LLDV>25m/s, MDV>35m/s) are associated with tornadoes (TWG, 2002). However, if the TVS is within a significant mesocyclone, the chances go up to 34% (TWG 2002). **Look for improved odds of tornadic potential when there is a well developed mesocyclone in conjunction with a TVS**.

Mesocyclones with strong tornadic potential have accelerating inflow signatures. Sometimes, the RFD and hook will appear to wrap around and occlude near the tip of the hook as low-level mesocyclogenesis commences.

Lower your thresholds of what you consider a significant mesocyclone or TVS in mini supercells. As mentioned previously, velocity signatures are weaker and smaller in mini and/or low topped supercells, but can nevertheless produce significant tornadoes.

Strong Updraft

If storm has a BWER as well as both a TVS and a mesocyclone, the chances of a tornado jump to 39%. Evidence of a strong updraft in the lowest half of a storm provide even more support that a low-level circulation can be stretched into a tornado. **BWERs are rare, but if visible, there is an enhanced threat of a tornado when coupled with a strong mesocyclone and/or TVS**. **However, you should not depend on a BWER to consider a tornado warning**.

Remember that favorable parameters for tornadic supercells should be thought of as interrelated. For example, if there is a BWER, a TVS and a mesocyclone in an environment of low LCLs, steep low-level lapse rates, and no CIN, the odds for tornadogenesis are much higher than if the same three signatures were in a poor environment.

Other Considerations in TWG

As a tornado nears the end of its life cycle, the parent mesocyclone, and even the TVS contract to the point of becoming unresolveable. **Do not terminate your warning prematurely. Allow 15 minutes for the end stage of a tornado**.

Be careful not to terminate a tornado warning for a supercell with a weakening mesocyclone/TVS signature that is rapidly approaching or already within a favorable tornado environment. The supercell may just be in the process of producing a new mesocyclone, or the mesocyclone may be contracting into a tornado. In some cases, the collapse of a BWER, lowering of the storm top, and shrinking of the mesocyclone

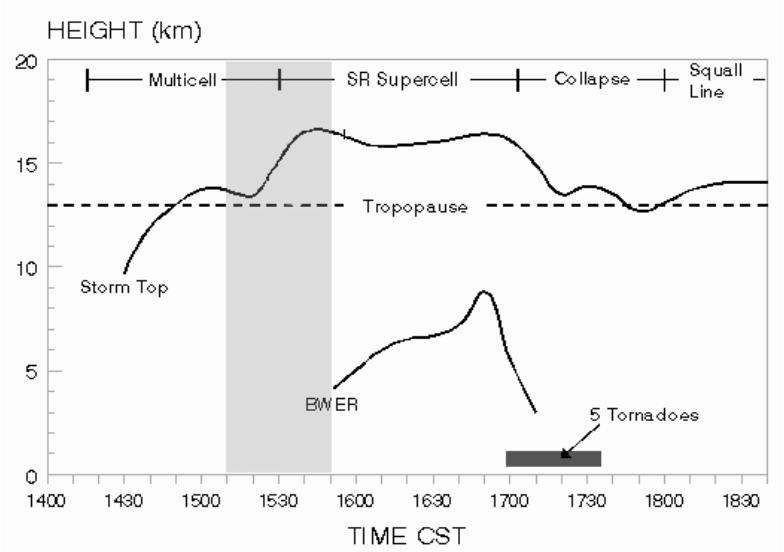

Figure 3-58. Evolution of a supercell exhibiting a collapsing BWER and storm top preceding its tornadic phase. Shading between 1510 and 1550 indicates the period of storm splitting (Adapted from Burgess, 1974).

diameter may mean tornadogenesis is underway (Fig. 3-58).

Tornado and Mesocyclone Motion in Cyclic Supercells

Account for differing tornado motions than storm motions, especially if a supercell is cycling. An old mesocyclone with tornado can move up to 10 miles left of the main supercell path (Fig. 3-59). Cyclic tornadogenesis appears to occur after the RFD to the right of a mature mesocyclone surges forward enhancing convergence at its leading edge as shown in Figure 3-60. The locally enhanced convergence helps initiate a local updraft which then tilts horizontal vorticity into the vertical. In a short time, a new mesocyclone forms on the head of the RFD surge while the old one continues motion to the left. The old mesocyclone often begins to move left of the main supercell either as a result of outflow from the main core pushing it rearward or from inflow locally pushing the RFD gust front backward.

Storm Mergers

Be aware that mergers of a non-tornadic supercell with a gust front increases the possi-

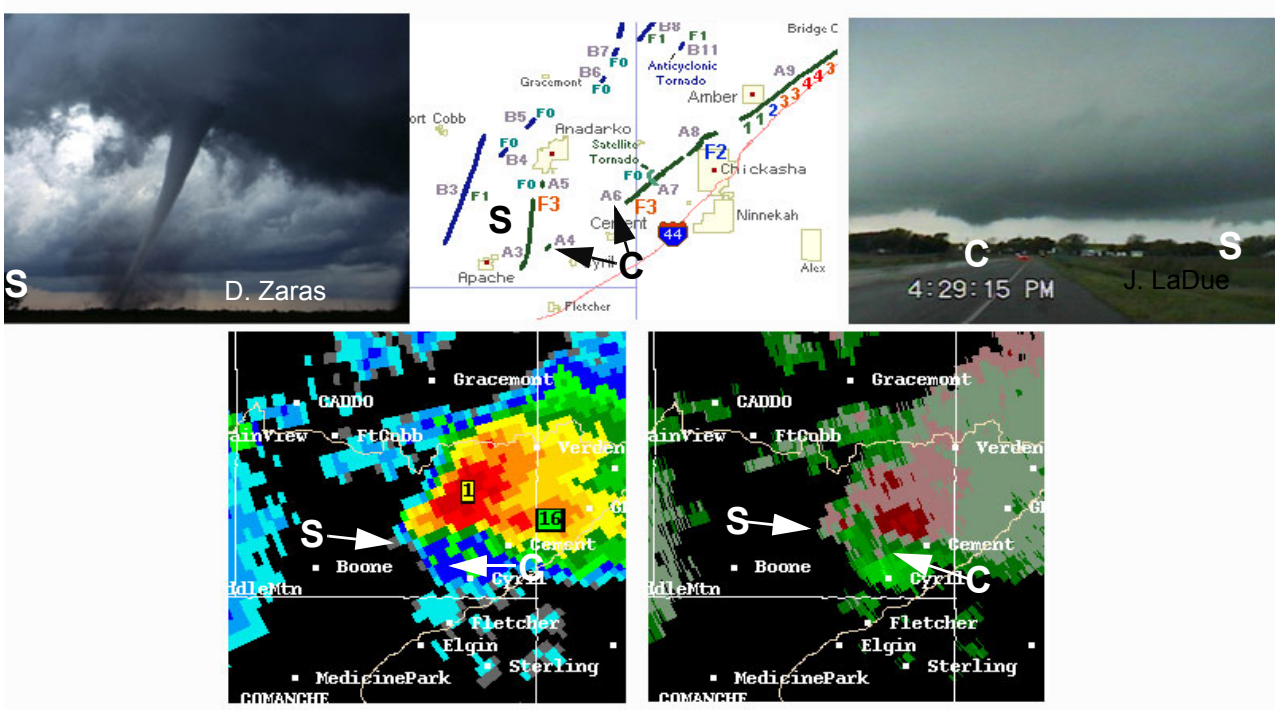

Figure 3-59. Two mesocyclones, each producing a tornado on 03 May 1999. The tornado labeled S, refers to the Stecker tornado and is the one moving left of the main supercell track. The mesocyclone labeled C, refers to the Cyril mesocyclone which goes on to produce a series of long-tracked tornadoes as it follows in the same direction as the parent supercell.

bility of a tornado. A wide range of possibilities have been found to occur from this type of merger, but precisely what leads to tornadogenesis or failure is poorly understood. A non-tornadic supercell interacting with a neighboring gust front may have an enhanced RFD which produces a tornado, ingest and tilt a high amount of streamwise vorticity to produce a tornado, or in many cases, no tornado occurs at all after merging with a nearby gust front**.** Additionally, collisions between left- and right-moving supercells may or may not assist tornadogenesis. **The key lies in attaining a heightened awareness of the possibility of a tornado when you see an impending storm merge with another storm or gustfront.**

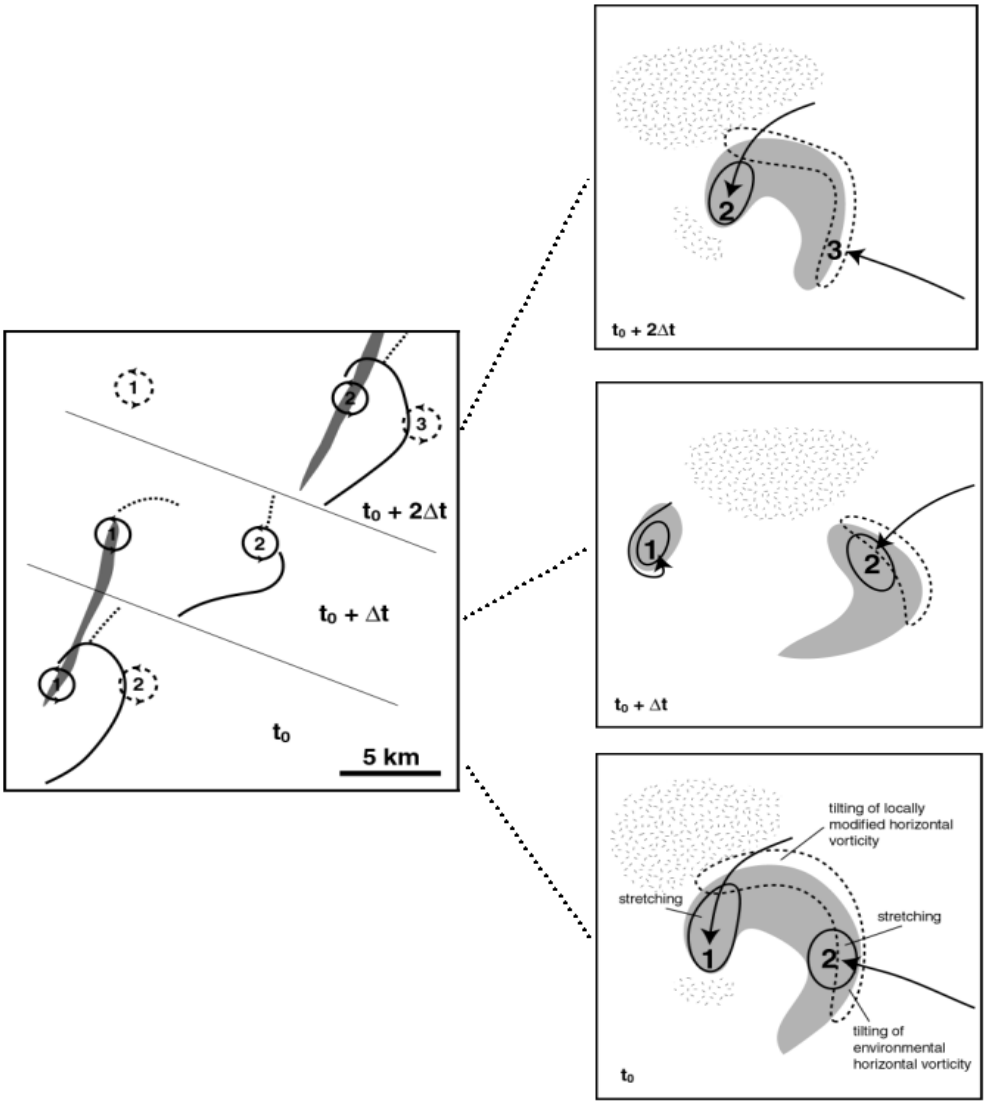

Figure 3-60. Schematic at low levels of cyclic supercell tornadogenesis. In the left-hand panel, the numbered circles identify vortices, and the thick lines indicate wind-shift lines. Tornado tracks are shaded. On the right, shading indicates updraft, and the spotted pattern indicates downdraft. Dashed (solid) outlines indicate regions of production of cyclonic vertical vorticity by tilting of horizontal vorticity (stretching of vertical vorticity). Arrows indicate vortex-relative trajectories. The time between successive tornadoes (2Dt) is ~20 min (Dowell and Bluestein, 2002).

Objective 15c: Flash Flooding Threat from Supercells

Describe two major meteorological contributors that contribute to a flash flooding threat from supercells.

Heavy rainfall from supercells, as with ordinary cells, depends on the instantaneous rainfall rate and expected duration. The instantaneous rainfall rate is, in turn, a function of precipitation efficiency and upward moisture flux. Heavy rainfall duration is largely determined by storm motion.

Rain Rate Parameters for Supercells

The following parameters from Davis (2002) are factors for production of extreme rain rates in supercells:

- **Low-level mixing ratio.** This is typically exceptionally high in supercell environments, and thus favors flash flooding.
- **Strong wind shear.** Supercell environments typically have very strong wind shear, which would increase entrainment. Thus, this is not always favorable for flash flooding. However, rotation in a supercell updraft tends to keep its core relatively undiluted, preserving the moisture supply of its source region.
- **Flanking line seeding.** Supercells with large flanking lines are provided a large seeding source for the main updraft.
- **Interstorm seeding.** This is especially important with neighboring supercells.
- **Deep warm cloud layer.** Some supercells will have a deep warm cloud layer, increasing the chance for flash flooding
- **Storm motion**. This is by far the most important parameter for the threat of flash flooding from supercells. HPs tend to move slower than the mean winds aloft, thus increasing the threat. However, some supercells move very fast. Thus, storm motion could either increase or decrease the flash flood threat. This needs to be examined on a storm-by-storm basis.

Moisture Inflow and Rainfall Duration

Precipitation efficiency is an important concept for pulse and multicell storms regarding the threat of flash flooding, but not necessarily for supercells. **Any supercell other than an LP can produce flash flooding if movement is sufficiently slow, even with very low precipitation efficiency.** CL and HP supercells possess extremely high values of moisture inflow, which overcome any deficien-

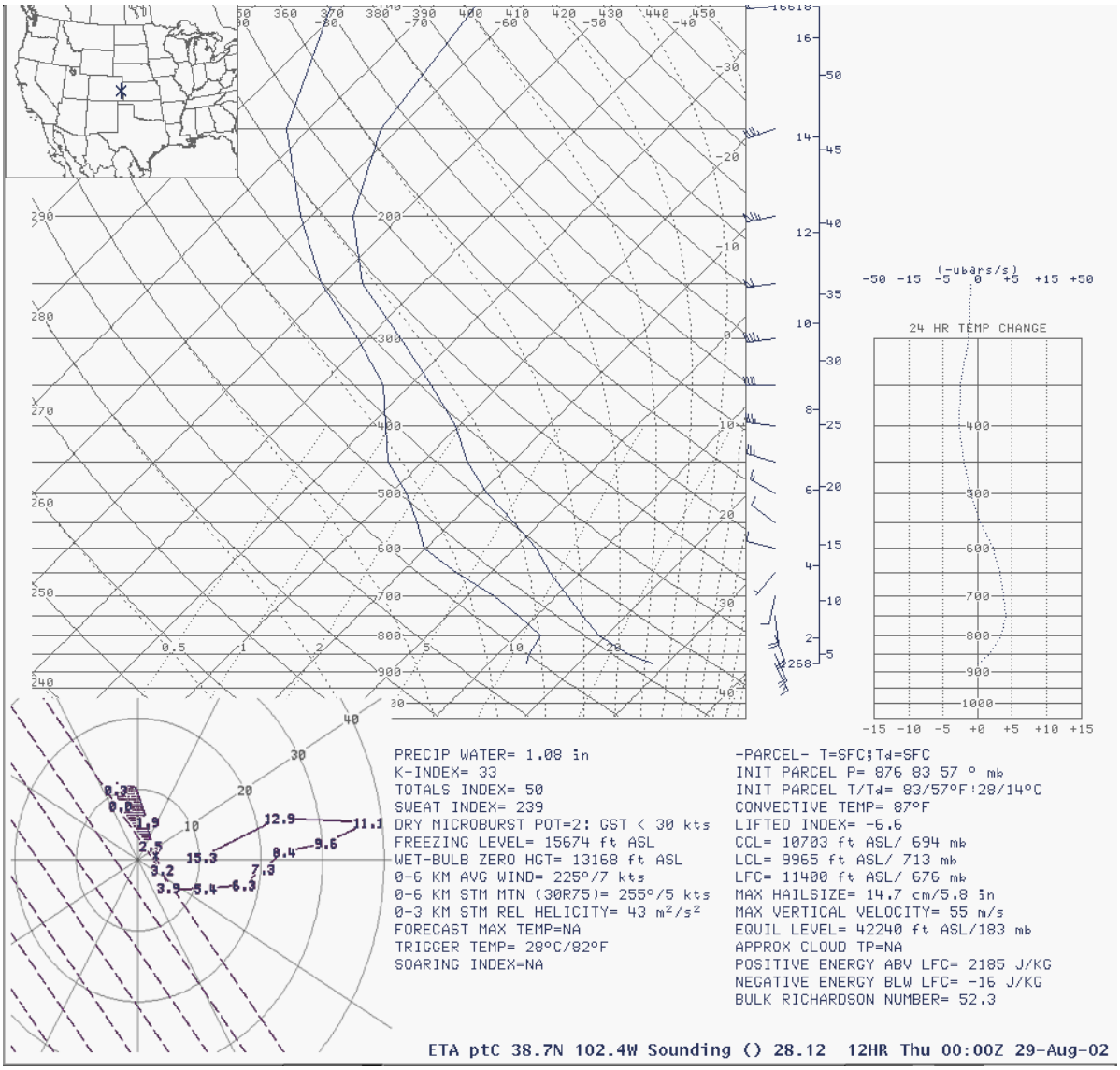

Figure 3-61. An ETA 12 hour forecast sounding from near Eads, CO for 29 August 2002, 00 UTC. Note that the sounding represents a typical high-plains supercell event. However slow supercell motion is suggested by this forecast.

cies in precipitation efficiencies. Generally, LP or CL supercells are very inefficient precipitation producers. However, with the tremendous moisture inflow, any slow moving supercell, other than LPs, can still produce precipitation rates that exceed 1-to-3 hour flash flood guidance in most cases. **Therefore, storm motion is the most important consideration for determining the flash flood potential of supercells.** An example atmospheric profile (an ETA forecast) conducive to flash flooding is shown in Figure 3-61. Even though the

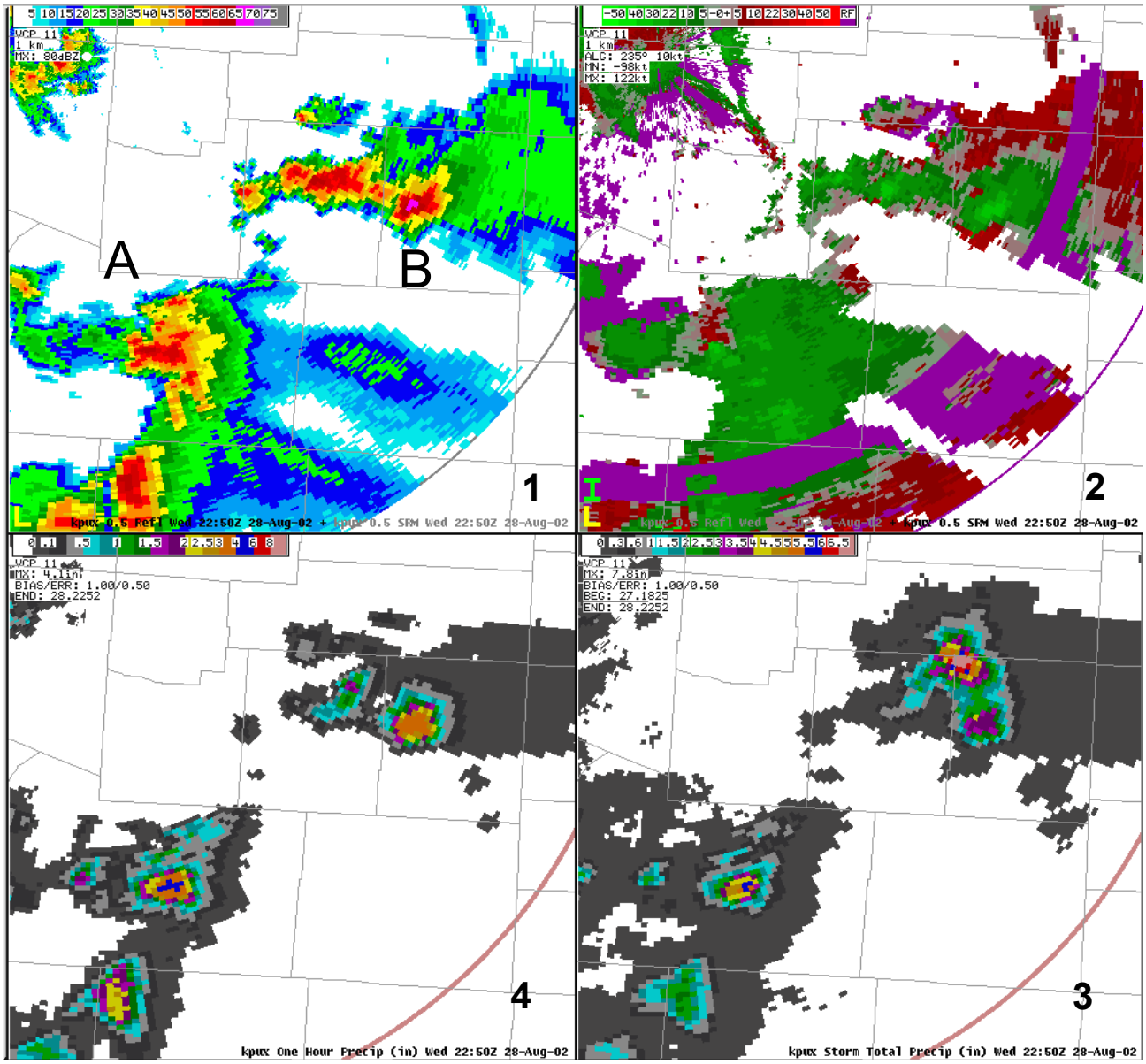

Figure 3-62. KPUX radar data of two supercells for near the same time as the forecast sounding in Figure 3-61. The panels are 1) base reflectivity, 2) storm-relative velocity, 3) storm total precipitation, and 4) one hour precipitation. The supercells (A and B) with small motion resulted in heavy precipitation and flash flooding.

sounding shows only modest low-level mixing ratios, slow supercell motion was suggested using the ID method (Bunkers, 1998). In combination with significant CAPE, these supercells produced heavy rainfall totals and several reports of flash flooding (see Fig. 3-62).

Objective 16

Identify multicell storm structures and evolutions including conceptual models, storm (system) motions, environments, and life cycles.

Multicell Storms introduction

Multicell storms are a common occurrence when deep, moist convection organizes in clusters, lines, or areas. **Multicells are defined in this text as a group of cells in close proximity sharing a common cold pool and precipitation area**. In Maddox's (1980) classification of Mesoscale Convective Systems (MCS), multicells could be thought of as belonging to both Linear and Circular types (Fig. 3-63).

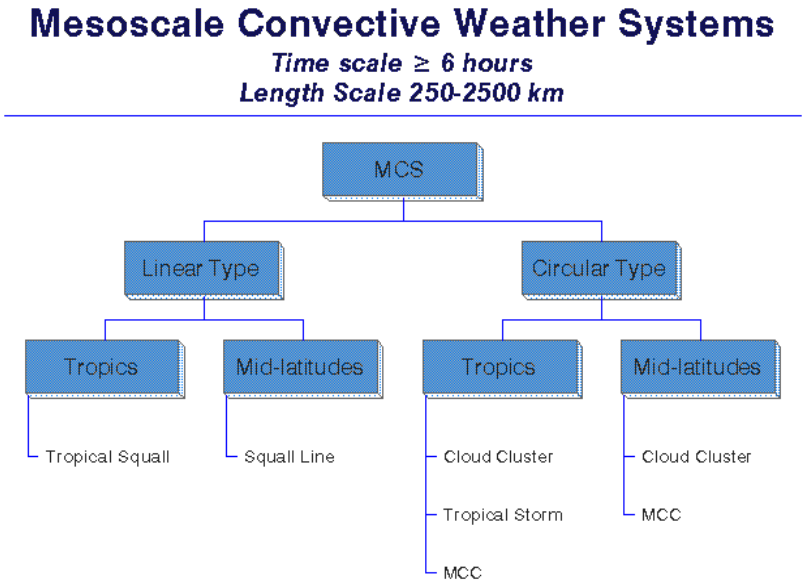

Figure 3-63. Schematic of mesoscale convective weather systems from Maddox (1980).

Some distinction is needed in the two classes to account for the unique three-dimensional attributes often found in MCSs. The uniqueness of MCS structure is based on the environmental conditions and longevity that tend to influence evolution of these large convective systems. These are examined in detail in COMET's web based instructional component, *Mesoscale Convective Sys-*

*tem*s: *Squall Lines and Bow Echoes*, available at this web address:

http://meted.ucar.edu/convectn/mcs/index.htm

The COMET MCS web module also explains the development of MCSs from initiation to mature phase. The module is strongly recommended reading to complement this Student Guide and associated teletraining session. Later in this lesson, we will review some of the environmental issues related to longevity of multicell complexes.

Conceptual Models of Squall Lines

The most common and extensively studied MCS is the squall line. Two of the more widely accepted conceptual models of the complex flow structure for squall lines are from Smull and Houze (1987); (see Fig. 3-64) and Biggerstaff and Houze (1991).

In the Small and House (1987) model of a mature MCS, development of the Rear-inflow Jet (RIJ) is attributed to midlevel, mesoscale areas of low pressure (labeled L3 & L4). The mesolow “L3”, which forms immediately behind the leading line convection, is a hydrostatically-induced negative pressure perturbation that develops under up-

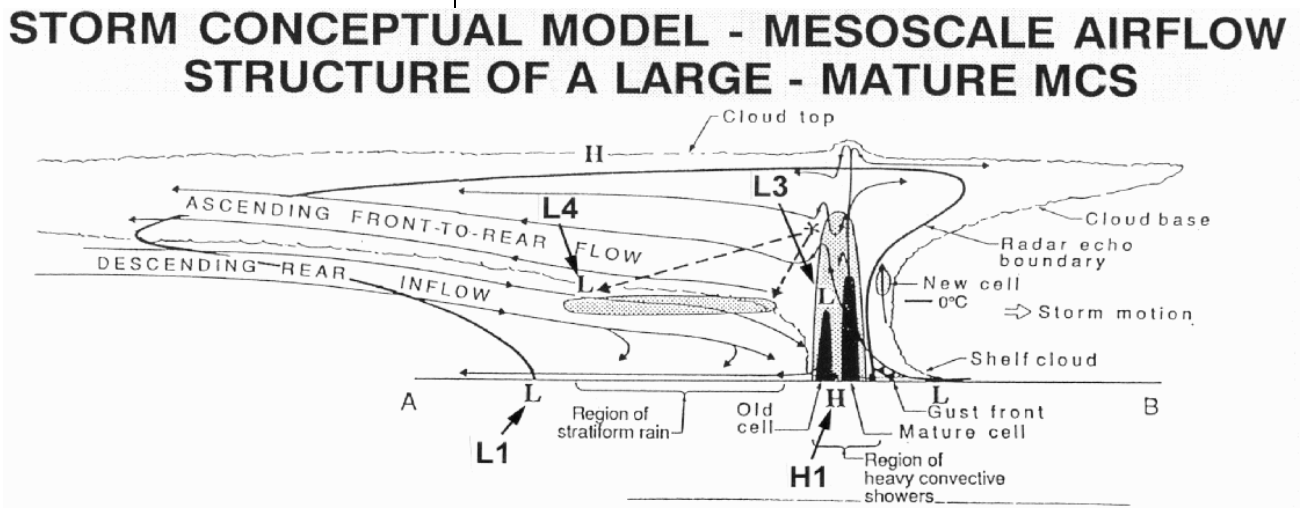

Figure 3-64. A conceptual cross-section of a mesoscale convective system. After Smull and Houze (1987).

shear tilted warm convective updrafts and above the evaporatively cooled downdrafts. Midlevel mesolow “L4” forms in the stratiform region in between the warm buoyant air which gets pulled rearward past the cool, dry descending air flow.

Although MCSs develop a number of ways, all mature systems contain convective and stratiform precipitation regions. The eventual MCS type is determined to a large extent by the environmental conditions in which it develops and the strength of the system cold pool. Parker and Johnson (2000) studied numerous MCSs and determined the distribution of hydrometers and stratiform precipitation shapes were largely a result of mean storm-relative winds. **The speed and direction of the environmental mid- and upper-level winds relative to system motion affect the resulting evolution of the MCS.** According to their studies, Parker and Johnson (2000) found MCS squall lines evolve into three major archetypes: **1) trailing stratiform, 2) leading stratiform, and 3) parallel stratiform**. The main distinction arises from storm-relative flow fields. The leading stratiform precipitation squall line archetype, which is typically slower-moving than trailing stratiform systems, is characterized by stronger mid- and upper-level storm-relative flow (often described as rear-to-front flow) than any of the other types (see Fig. 3-65). **The trailing stratiform squall line type has a sloped front-to rear flow produced by stronger system-relative flow in low-levels (and subsequent stronger low-level convergence along the leading edge)**.

Another convective type not covered in Fig 3-63 is the derecho. A derecho is defined by extremely

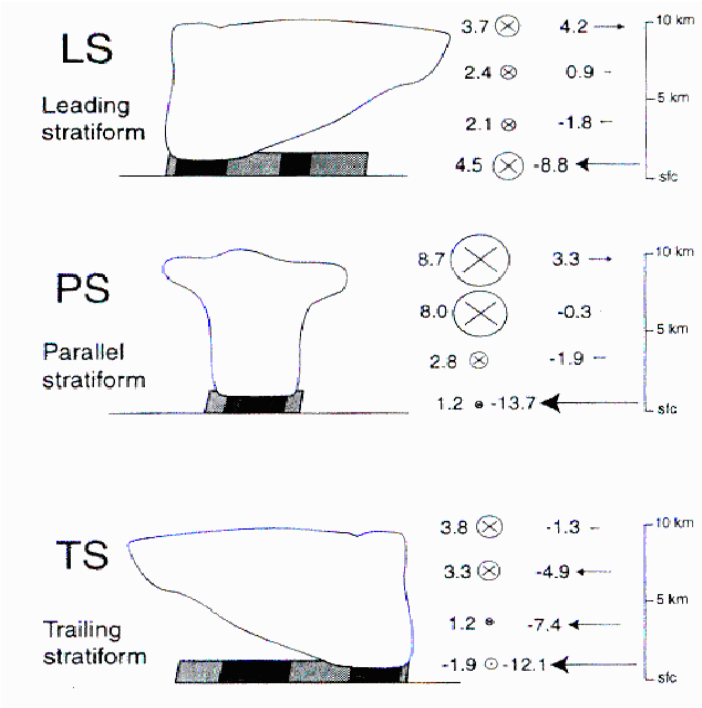

Figure 3-65. A schematic of three MCS archetypes based on their line-orthogonal storm-relative flow (after Parker and Johnson, 2000).

damaging straight line winds, and they typically exhibit motion faster than the mean wind.

Multicell Storm Motion

Multicell storms may consist solely of a complex of "ordinary" updrafts in different phases of growth and decay, or may contain embedded supercells. Since multicell storms contain such a wide variety of configurations, multiple mechanisms may exist for determining their movement. These mechanisms include, but are not limited to:

- **shear-cold pool interactions**
- **low-level convergence**
- **instability and moisture gradients**
- **three-dimensional boundary interactions**

Shear-cold Pool Interactions

Since multicell storms are observed more frequently as shear increases, the role of shear on multicell movement is important to consider.

Rotunno et al. (1988; henceforth referred to as RKW88) developed a theory, based on numerical simulations, to explain the process by which shear interacts with a multicell cold-pool boundary to enhance or suppress lifting. According to RKW88, preferential new cell development occurs on the flank of a multicell storm where the shear vector is directed in a positive sense relative to the orientation of the boundary.

Lifting of Air by Cold Pool

To further explain how shear is considered important, it is necessary to show how a cold pool initially lifts air without the presence of environmental shear. All cold pools have density gradients along their leading edge. This gradient in density induces a horizontal circulation with descending air on the cold side and ascending air on the warm side (Figure 3-66). The ascending air ahead of the gust front lifts up and over the cold dome. It then may become caught in the descending part of the circulation limiting its net vertical lifting. If the LFC is at the height of LFC1 (Fig. 3-66), convective initiation is likely. However, consider the lifting failing to reach a higher level, LFC2 (Fig. 3-66). Further lifting of the environmental air to LFC2 can only be realized if the cold dome depth increased at some distance away from the leading edge. Therefore,

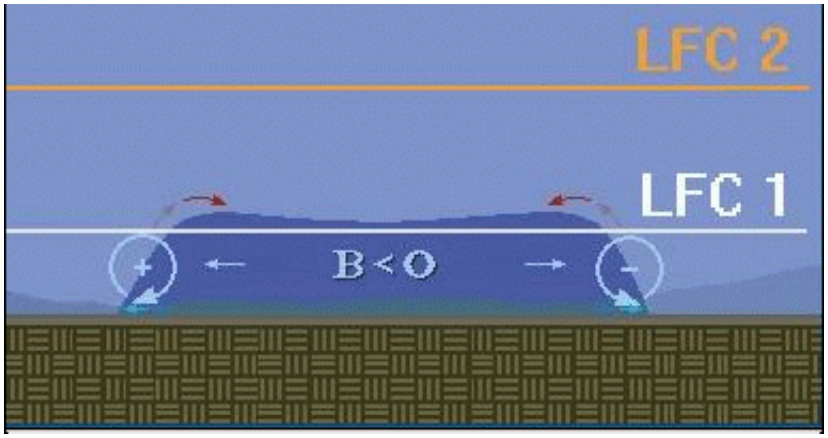

Figure 3-66. Depiction of lifting environmental air relative to two Levels of Free Convection (LFC). Adapted from COMET (1996).

in the absence of shear, and if all other factors are equal, no portion of a pre-existing cold pool is favored to initiate convection.

Shear and Cold Pool Lifting

Add shear to the environment and, according to RKW88, the shear interacts with the cold pool to increase (decrease) the lifting on the downshear (upshear) side. Take for example the situation where environmental shear is oriented downshear (or positively) with respect to the outflow boundary (Figure 3-67).

The positive horizontal vorticity inherent in the environmental shear and the negative horizontal vorticity along the boundary constructively interfere with each other to promote a vertically oriented deep lifting zone. Conversely, on the upshear side of a multicell cold pool (Figure 3-68), the environmental shear is now pointed in a negative direction with respect to the cold pool. In this case, the environmental horizontal vorticity destructively interferes with that of the cold pool boundary, decreasing the net vertical displacement of the lifted air.

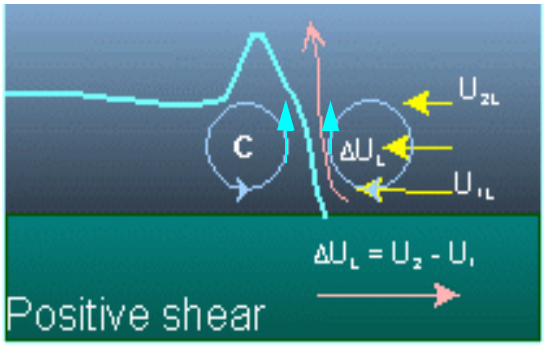

Figure 3-67. Schematic of positive environmental shear interacting with a cold pool boundary (blue perimeter). The yellow arrows indicate boundary-orthogonal wind vectors from U1 (bottom) to U2 (top). The value UL indicates the velocity difference and the orange horizontal arrow is the environmental shear vector. The red vertically pointing arrow represents a hypothetical environmental air parcel trajectory lifting over the boundary.

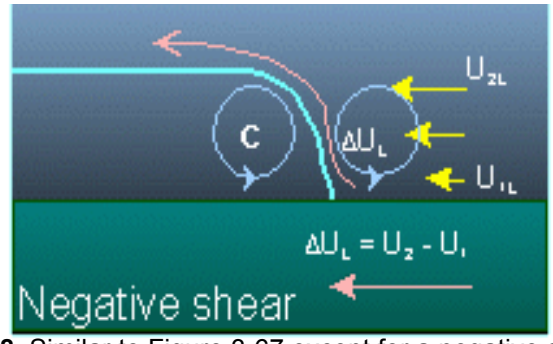

Figure 3-68. Similar to Figure 3-67 except for a negative shear example.

RKW Theory

In the framework of RKW88 theory, new cell development is favored on the downshear side of a multicell cold pool. The depth of the shear layer to be calculated when considering this theory is on the order of the depth of the boundary, approximately two kilometers.

Uncertainties in Shear-Cold Pool Lifting

There are some uncertainties when using the RKW88 theory for multicell propagation. One involves the proper depth of the shear and whether it should be a function of the LFC height, boundary height, or some other benchmark. RKW88 encourages using a shear layer around 3 km deep. However, their suggestion is based on idealized simulations. As will be discussed later, new theories argue for increasing the shear layer depth beyond that of RKW88 when attempting to describe squall line longevity (Coniglio and Stensrud, 2001). Also, we do not know how dominant this mechanism is at modulating multicell propagation, versus other mechanisms such as instability gradients, interactions with strong low-level winds, and boundary interactions. We will be discussing these considerations next.

Gradients in Instability

Gradients in instability can modulate the propagation of multicells, even without the shear/cold pool balance. Richardson (1999) successfully modeled

the effect an instability gradient has on the propagation of a multicell line. Not surprisingly, new cell development was favored on the side of the cold pool with a lower LFC. Eventually, the favored side produced a larger cold pool and continued propagation into the instability gradient as shown in Figure 3-69. **To summarize, Richardson (1999) showed the importance of forcing the multicell propagation vector toward higher regions of instability as measured by higher CAPE and lower LFC.**

System-relative Low-level Flow

Another factor that may affect multicell propagation includes strong low-level convergence and the location where the low-level jet intersects the cold pool boundary at the greatest angle. At this location, strong ascent of the low-level jet over the cold

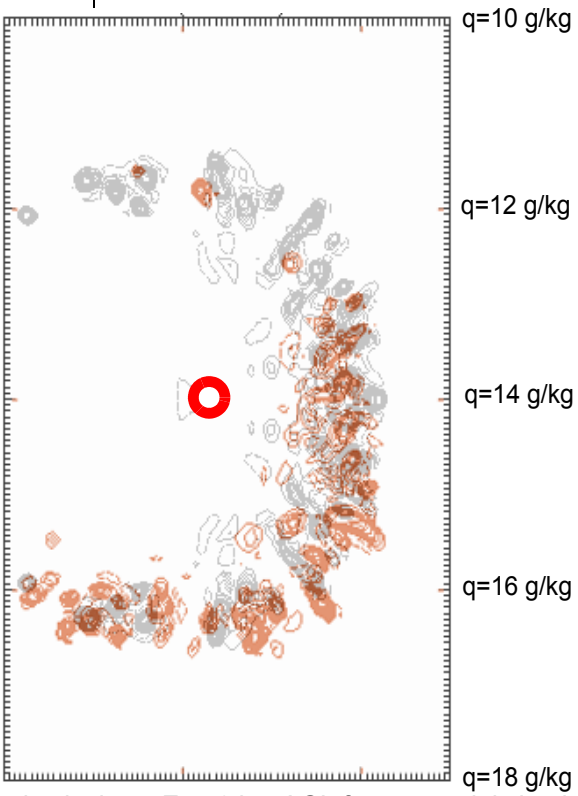

Figure 3-69. Contours of vertical velocity at Z=4.6 km AGL from a model simulation of multicell convection three hours after initiation. The gray contours are from a homogeneous mixing ratio run of 14 g/kg while the brown contours are from a model run with a southward directed gradient in mixing ratios whose values are labeled on the right side of this figure. The red circle is the location of storm initiation in a storm-relative frame of reference. Adapted from Richardson (1999).

pool promotes new cell growth and therefore, over time, the multicell complex begins to move with a component of motion toward the low-level jet. **In fact, Corfidi et al. (1996) found that back building Mesoscale Convective Complexes (MCC) propagation vectors were equal and opposite in magnitude to the presence of a low-level jet centered near 850 mb** (Fig. 3-70). When the propagation vector was added to the convective steering-layer flow, the total motion vector correlated well with the observed MCC motion. **Thus, the term 'Corfidi vector' was coined to describe the expected motion vector of an MCC.** The correct term is actually called the MBE vector (Meso-B Effects)(Corfidi, 1998). To estimate the MBE vector, add the mean 850-300 mb wind to the negative of the low-level wind at the level of the strongest wind (usually around 850mb). An example of this vector schematic is shown in Figure 3-71.

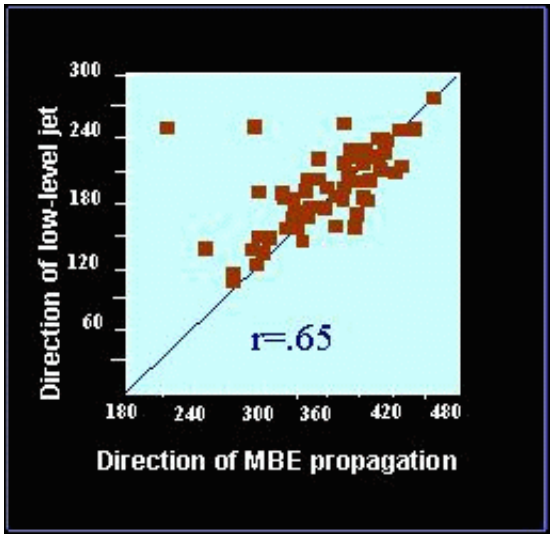

Figure 3-70. Scatter plot of Mesoscale Convective Complex observed direction of propagation and the 850 mb low-level jet direction. Adapted from Corfidi et al. (1996).

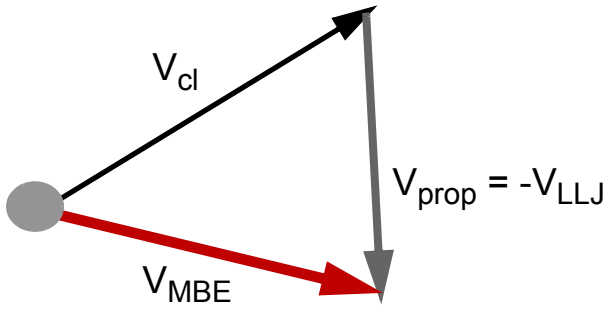

Figure 3-71. A schematic representation of the MBE vectors adapted from Corfidi et al. (1996). V_{cl} represents the mean convective steering-layer flow, V_{prop} is the propagation vector, V_{LLJ} is the low-level jet vector, and V_{MBE} is the motion of the back building mesoscale convective complex.

Initial Application of MBE Technique

Back Building multicell storms, which can also be long-lasting, usually result from a combination of environmental factors, some of which are related to the low-level jet impinging on the upshear side of the multicell system where surface-based instability is also present. This process focuses the propagation vector in the opposite direction of the advection vector (essentially, the mean cloud bearing winds) and enhances new updraft growth and overall system motion in the upshear direction. **Quasi-stationary convection often occurs when cell advection is mostly offset by cell propagation resulting in overall net multicell motion of approximately zero.** (see Fig. 3-72)

Limitations to Original MBE Technique

There are several limitations in using the original MBE vector technique. **A significant number of MCSs exhibit a rapid forward propagation component in the presence of low-level inflow that would yield a much different motion vector than the original MBE technique.** For example, a unidirectional vertical wind profile would typically yield very slow MBE vectors yet a significant number of MCSs exhibit rapid motions under this kind of wind profile. **Another limitation, or**

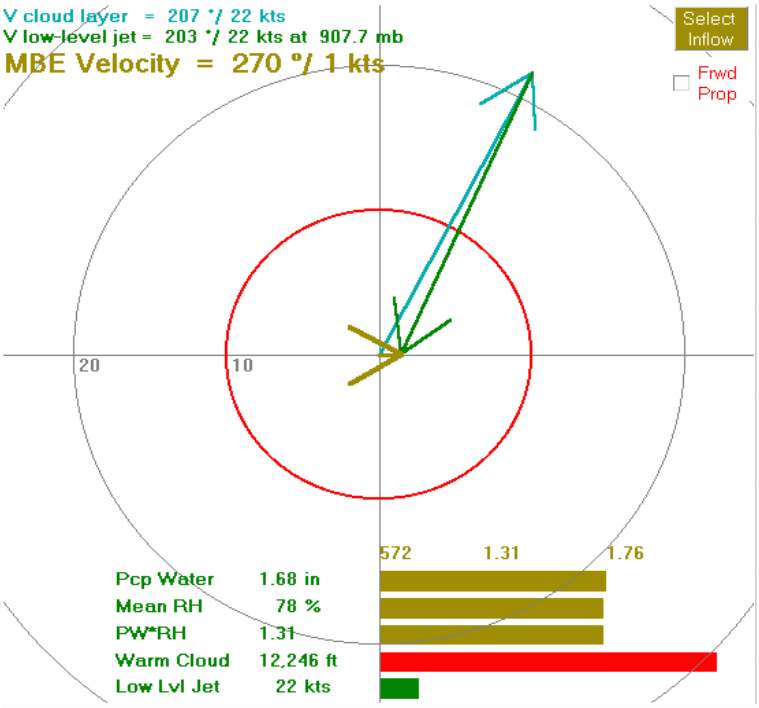

Figure 3-72. BUFKIT hodograph showing a very small MBE motion in a back building multicell scenario.

issue, is picking the proper depth in which to calculate a convective steering current. The mean wind should be representative of observed ordinary cell motions. If the analyzed mean wind disagrees, then the MBE vector calculations will be inaccurate. Also, the MBE technique assumes the existence of the low-level jet with maximum winds at the 850 mb level. If the low-level jet is maximized at a different level, the MBE technique may need to be adjusted to account for this variation. Finally, MCSs are large enough such that they may span a mesoscale gradient in wind fields. The MBE technique, applied in different areas of an MCS, may yield different results. One example would be a situation where the low-level jet is directed to only part of the MCS.

Modified Corfidi Technique for Downwind Propagating MCSs

Corfidi (2003) modified his original technique to account for systems which are strongly forward propagating in a unidirectional shear environment. In his most recent study, he examined MCSs that

moved faster than the mean 850-300 mb winds. To estimate the potential forward speed of such convective complexes, simply add the original V_{mbe} vector to the mean cloud layer wind (V_{cl}) as shown in Fig. 3-73. V_{mbe} provided by the original technique is, in fact, the negative of the gust-front-relative low-level flow for a boundary moving with the speed and direction of the mean cloud-layer wind.This technique assumes that cell propagation occurs along the direction of the low-level jet (forward propagation), along the downwind side of the cold pool. Anticipating which technique to use depends on the relative amounts of dry air at low and mid levels, location of strongest instability, and the orientation of the gust front with respect to the mean cloud-bearing winds.

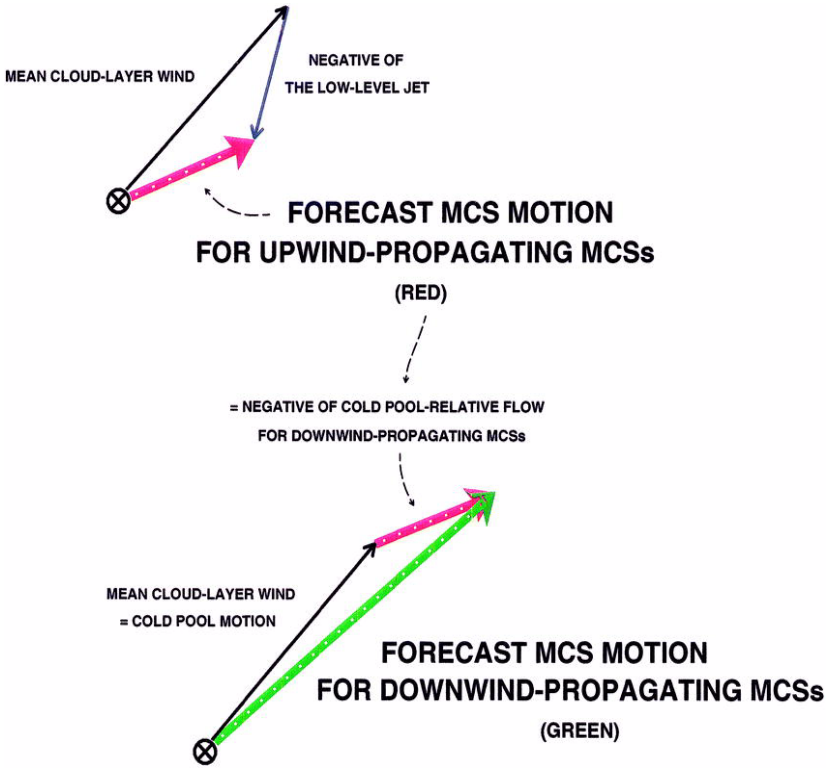

Figure 3-73. Modified Corfidi (2003) technique for estimating the motion of downwind -propagating MCSs. Original technique is red vector on top.

Forward and Backward Propagating System Threats

Back building multicell systems are notoriously heavy rain producers whereas forward propagating systems are more likely to produce damaging winds. A mesoscale boundary parallel to the steering layer winds can also affect the propagation process and enhance continuous redevelopment of convective cells in an upstream direction of the multicell complex. The cells in the line mature over the same location and thus, can produce flash flooding. Often, the low-level jet is positioned perpendicular to this boundary. An example of this was the 7 May 2000 heavy rain event in northeastern Missouri (See Glass et al., 2001). During this event continuous redevelopment on the upshear side of the multicell complex led to small net system movement and heavy rain in the same location (some places received over 17 inches!) over a period of 12 to 24 hours (see Fig. 3-74).

More on Forward Propagating MCSs

See the example sounding on the following page at Norman, OK (OUN) from 0000 UTC 28 May 2001 (Fig. 3-75). This is an excellent case illustrating a poor estimation of MCC motion using the original MBE vector technique. Note the large CAPE (4597 J/Kg), dry air in midlevels, and strong

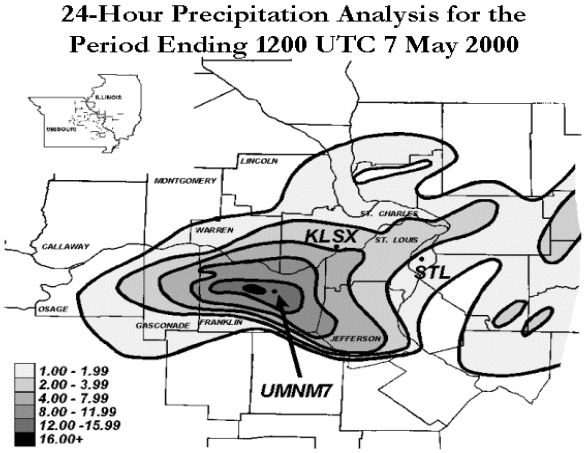

Figure 3-74. Heavy rainfall over Missouri caused by a back building MCS (Glass 2001).

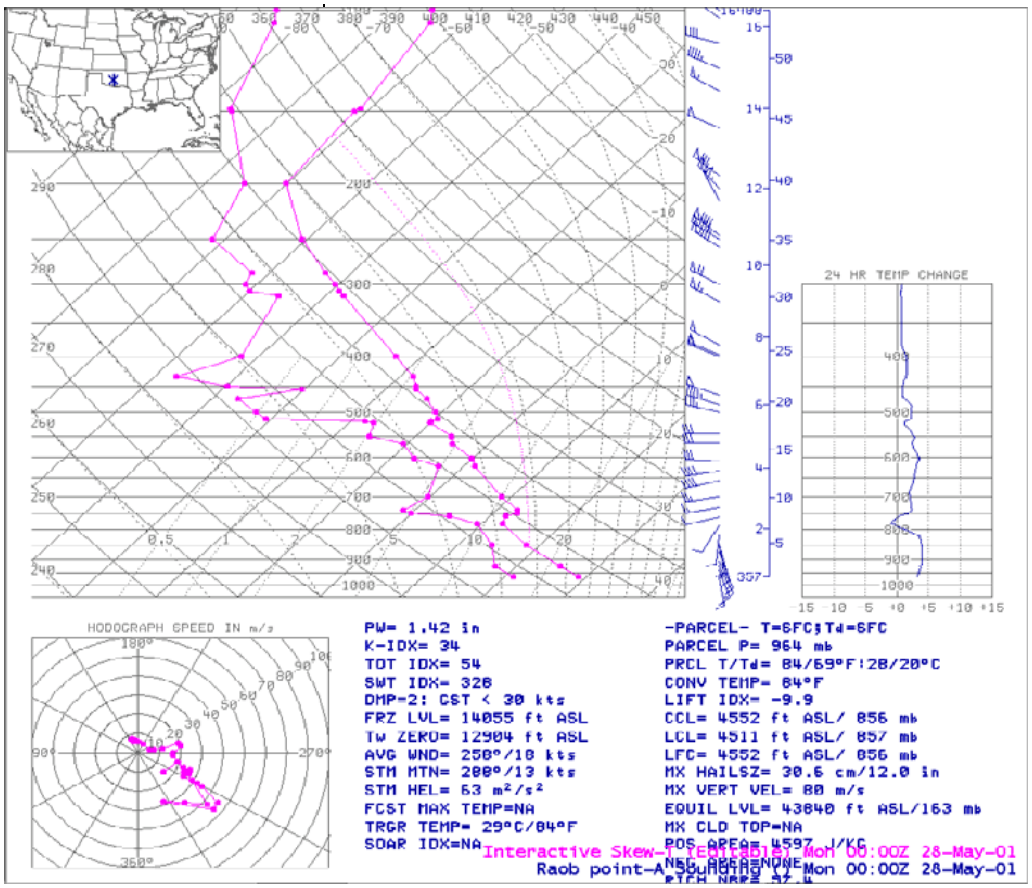

Figure 3-75. Sounding taken from Norman, OK on 28 May 2001 - 00 UTC.

mid and upper level winds (from W to NW at 50 to 80 kts in the 5-12 km AGL layer) in the observed sounding. Given the availability of dry air at both midlevels and in the sub-cloud layer, downdraft potential is quite strong. The resulting strong convectively driven cold pool that developed with the multicell storms in southwest KS and northwest OK (Fig. 3-76) moved southeastward with the gust front into a very unstable environment with strong low-level inflow from the southeast. Consequently, with both system-relative convergence and instability present in the downshear (SE) direction, the gust front led to new cell development and thus propagation was to the SE. With cell advection and propagation almost directly additive, the system accelerated at 50 to 60 knots towards the southeast and produced over fifty reported mesonet wind gusts of 60 mph or greater with hundreds

of reports of wind damage, many equivalent to F2 tornado damage (Miller, et al., 2002). **In these types of situations, there is a high potential for extreme system motion due to propagation effects in the downshear direction. It is thus very important to consider the direction of greatest system-relative convergence and distribution of surface-based instability when applying either MBE "Corfidi" techniques.**

Anticipating Forward Propagating MCSs

In order to correctly anticipate these type of forward propagating systems, one can analyze forecast hodographs and associated motion vectors. See the BUFKIT Eta model forecast sounding for OUN for 0400 UTC 28 May 2001 (Fig. 3-77). In the hodograph depiction in the upper left, the Corfidi vector for forward propagating systems is shown in red (301 deg, 65 kts), which is considerably larger than the result one would get from just con-

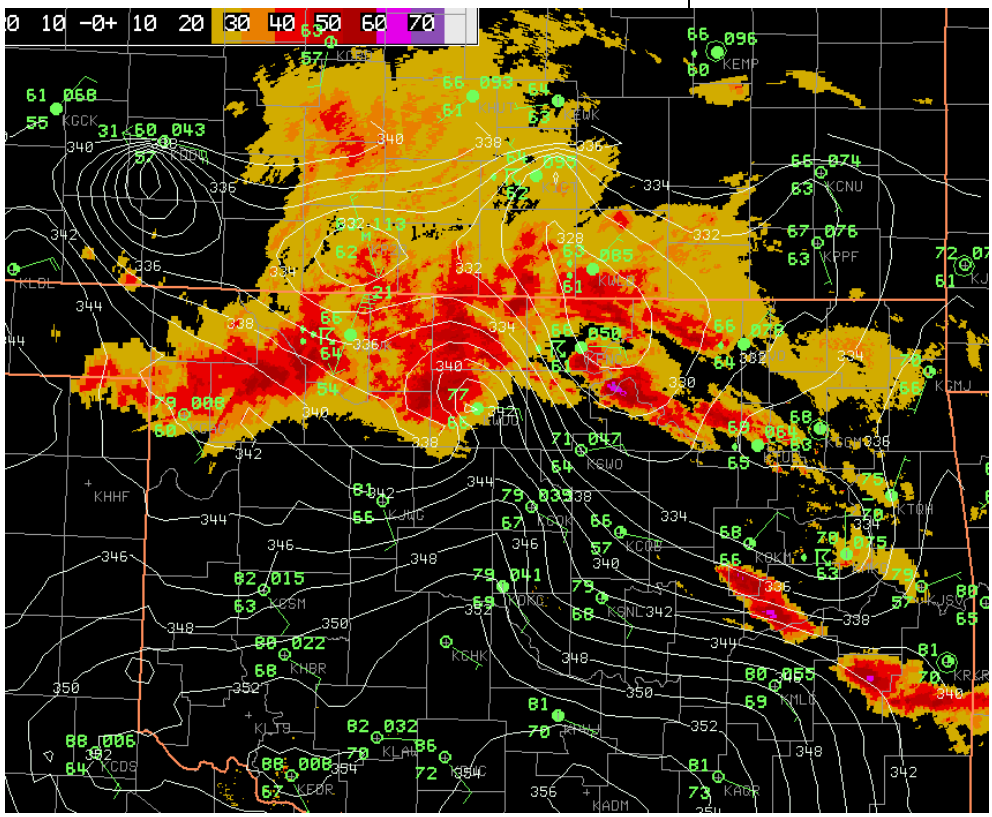

Figure 3-76. A mosaic radar image for 28 May 2001 - 00 UTC showing shaded reflectivities > 25 dBZ. Overlaid are surface theta-E (white contours), surface METARS (green).

sidering cloud bearing winds and propagation effects from the 850 mb jet.

This case also illustrates the problems associated with picking the proper depth in which to calculate a convective steering current, or mean cloud bearing layer. The mean wind should be representative of observed cell motions and typically, the best layer to use is the mean wind from the LFC to the EL (note that is the layer used in BUFKIT). Any analyzed mean wind that doesn't account for upper levels (due to deep CAPE and high ELs) may underestimate advection effects.

Also, the original MBE technique (listed in AWIPS Volume Browser as Corfidi Vectors) assumes the low-level jet is at 850 mb. **Observations at WDTB has found that invariably selecting this layer may not be representative of the maximum inflow to the storm system.** In BUFKIT, the user

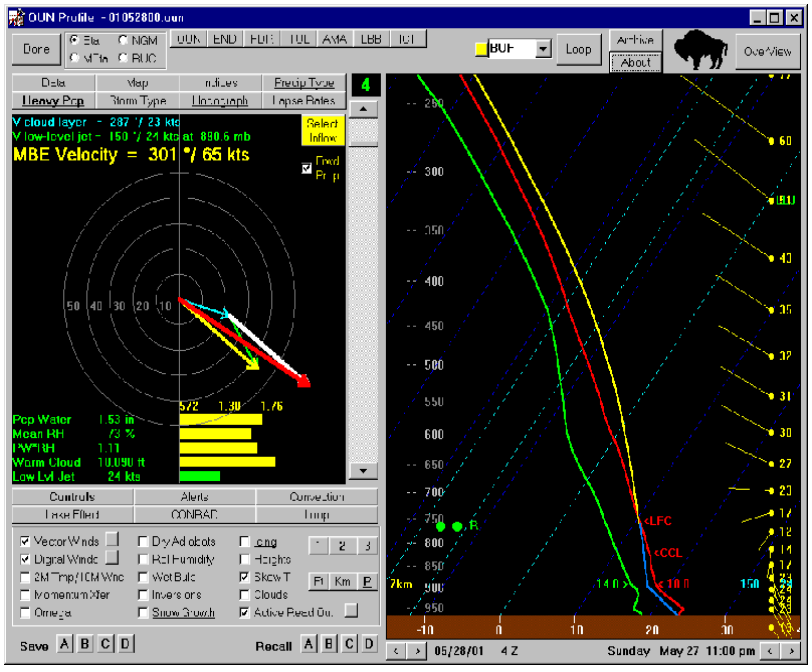

Figure 3-77. A BUFKIT ETA model sounding taken at Norman for 28 May 2001 - 04 UTC. The red vector in the hodograph display represents the forward propagating MBE vector.

can manually select the inflow layer at any level below cloud base if 850 mb winds are not representative. Use surface observations or profiler data to help determine the wind direction that approximates the low-level inflow to multicell systems.

With many multicell systems, there are backward propagation and forward propagation going on simultaneously. Thus, it is often difficult to apply one particular technique for an entire system during its evolution. Often, forecasters observe backward propagation during initial stages of multicell development. Then, with time as the cold pool strengthens, the system transitions to a fully mature forward propagating system.

For elevated convection, multicell motion is more complicated. Observations at WDTB suggest that both MBE vector techniques can work, but modifications must be made to estimate both the cloud layer motion and propagation due to inflow above the surface stable layer.

Boundary Interactions With Other Boundaries or Topography

Interactions with topography (Petersen et al., 1999) and other boundaries (Purdom, 1976; Wilson and Schreiber, 1986; Mahoney, 1988; Fankhauser et al., 1995; Hane et al., 1997; Koch and Ray, 1997) affect the propagation component of multicell storms by focusing new convection at these interaction points. In fact, Mahoney (1988) derived vertical motions up to 16 m/s (32 knots) as high as 2 km (6500 feet) above ground level during boundary collisions. In his study, convective initiation was likely after boundary collisions. According to Koch and Ray (1997), convection initiated on more than 50% of all boundary interactions in Colorado and North Carolina for typical

summertime environments in both states (Fig. 3-78). It follows that a cold pool interacting with other boundaries may initiate new convection and become part of the original multicell complex and, therefore, lead to a propagation vector in the direction of the boundary interaction. Intersecting boundaries frequently 'anchor' multicell convection resulting in heavy rainfall and flash flooding. Weaver (1979) documented multicell motions in the presence of boundary triple points. Multicell storm motions tended to match the motions of the triple point rather than the convective steering-layer flow (Fig. 3-79).

More Than One Propagation Mechanism at Once

Any combination of these mechanisms may affect multicell propagation, even on the same multicell storm. For example, shear/cold pool interactions may result in a downshear propagation component on one side of a multicell storm while boundary interactions on a different side may result in another propagation component. The effect can be

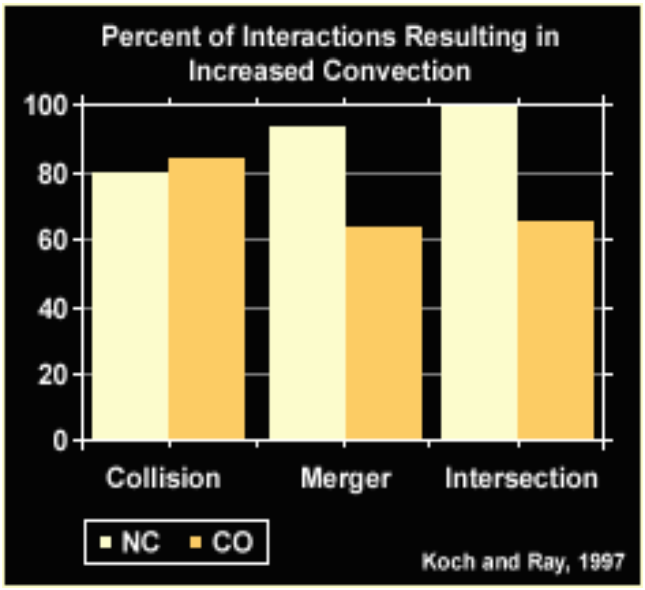

Figure 3-78. Probabilities of convective initiation directly resulting from the interaction of surface boundaries for a typical summertime environment based on field studies in Colorado and North Carolina. Adapted from Koch and Ray (1997).

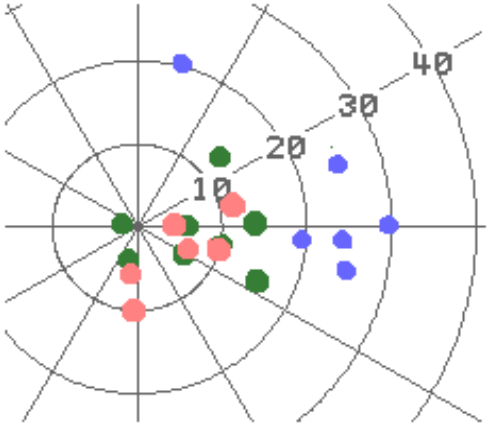

Figure 3-79. A plot of steering-layer flow (blue dots), boundary triple point motions (green dots) and multicell motions (red dots) for several events documented by Weaver (1979).

a splitting of the multicell complex with a downshear and upshear propagation component.

Multicell Longevity

The latter half of this lesson will discuss environmental and storm-induced factors modulating the lifetime and severity of multicell clusters such as squall lines and bow echoes. Rotunno et al. (1988) asserted that a balance between the horizontal vorticity along the cold pool boundary and the vorticity inherent in a 0-2 km environmental shear layer is optimal for enhancing strong updrafts needed to maintain a long-lived squall line. Conversely, Evans and Doswell (2001) did not find the cold pool/shear balance theory to be a factor in observed derecho environments. In their study of derechos, Coniglio and Stensrud (2001) found that deep tropospheric shear was more important than low-level shear in maintaining squall lines. Needless to say, the factors governing the longevity of squall lines are still a controversial subject. There are, however, common environmental parameters including strong convective steering-layer winds, adequate convective instability, and moderate-to-strong deep 0-6 km shear that accompany long-lived severe squall lines (Evans and Doswell, 2001).

RIJs

Rear-Inflow Jets (RIJs) are common with large, linear multicell storms (squall lines). However, numerical simulations suggest the RIJs do not descend in the most severe squall lines (Weisman, 1992). According to Weisman (1992), most squall lines become upshear-tilted as the cold pool dominates environmental shear. A non-descending RIJ restores the balance, allowing the squall line updraft to remain vertically erect for longer periods of time. Non-descending RIJs are found in environments where shear and CAPE are high. The evolution and dynamics of RIJs will be discussed later.

Bow Echoes

Squall line segments exhibiting line-end vortices and a localized RIJ in between the vortices and directed toward the leading edge are often called bow echoes. A series of bow echoes are called Line Echo Wave Patterns (LEWPs). Bow echoes intensify the RIJ between the vortices often leading to localized areas of maximum wind damage. **Small tornadoes may occur just to the left of the maximum wind in an RIJ given enough low-level helicity and instability in the environment. The line-end vortices in bow echoes develop by either tilting negative storm-induced vorticity at the top end of the cold pool from the storm updraft, and/or by tilting positive environmental vorticity downward by the downdraft in the back end of a bow echo**. More will be shown later on specific radar characteristics of bow echoes.

Role of Instability and Shear on Multicells

The influence of convective instability (in terms of CAPE) on the strength of a single thunderstorm has been discussed previously (See Objective 2). For larger convective systems (like squall lines and bow echoes), the buoyancy of the environment plays a similarly important role. As individual

cells begin to organize into multicell structures, a steady source of potentially unstable air in the inflow is necessary (in addition to the other factors) for the convective system to sustain itself. Johns et al. (1990) examined 14 very intense derechos during the months of June and July and found that CAPE values were generally greater than 2400 J/kg near the genesis region, but increased to an average CAPE maximum of 4500 J/kg as the convective system moved eastward.

Weisman (1993) studied the effects of CAPE and shear on numerically simulated squall lines and bow echoes and established a minimum CAPE threshold of 2000 J/kg for long-lived systems.

Evans and Doswell (2001) also studied CAPE distributions in squall lines (via proximity soundings) and found a much greater range of values for derecho events. They found that in most of the cases that were weakly-forced (WF), the instability (and CAPE) were generally larger than in those cases where the forcing was “strong” (SF) (Fig. 3-80 on page 136). The degree of forcing in their study was subjectively related to the strength of the approaching 500 mb vorticity maximum. **For strongly forced events (SF), there were a number of derecho systems that developed and persisted in environments with low values of CAPE.** A few derechos even developed and persisted within regions of conditionally stable surface air.

Thus, squall lines have been observed over a wide range of environmental CAPE (and vertical wind shear). For any given CAPE, the intensity and longevity of linear convective systems seem to increase with increasing synoptic

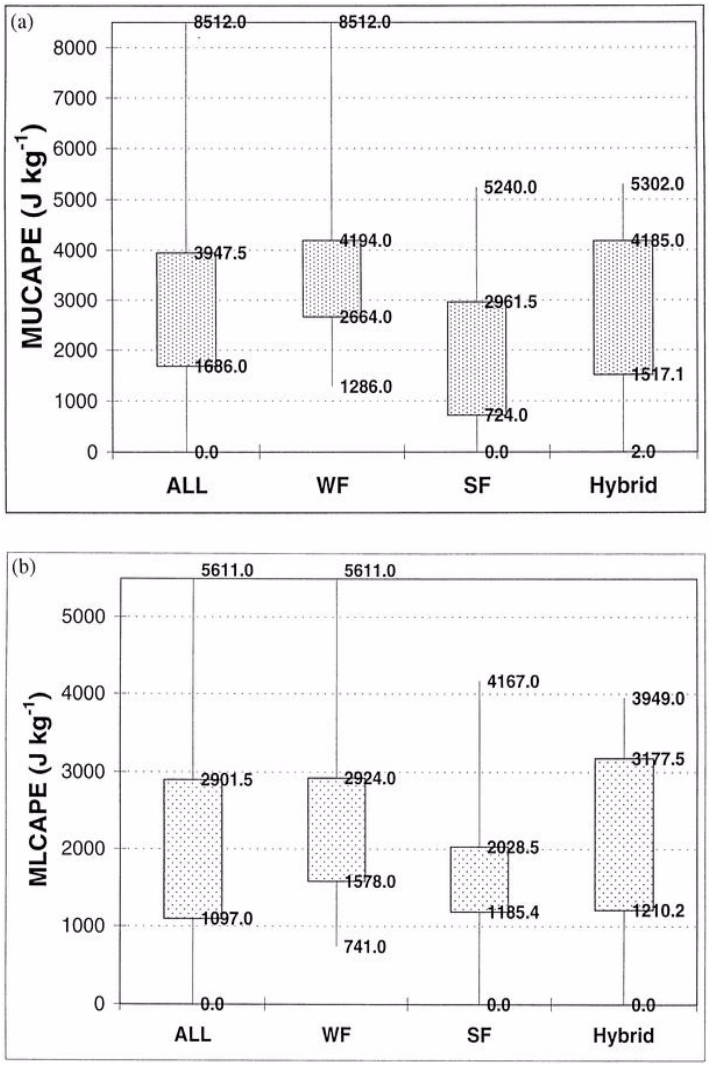

Figure 3-80. A box and whiskers plot of a) Most Unstable CAPE, and b) Mixed Layer CAPE versus the type of derecho observed by Evans and Doswell (2001). The label SF on the x-axis indicates parameters count for only strong synoptic forcing, WF indicates weak synoptic forcing, Hybrid indicates those derechos with aspects of both strong and weak synoptic forcing. The label ALL represents parameters for all derechos.

scale forcing, which includes depth and strength of the vertical wind shear.

Vertical Wind Shear: Effects of and Relationship with CAPE in Squall Lines

Bluestein and Jain (1985) studied squall lines in Oklahoma and found that the magnitude of the **vertical wind shear on average was slightly stronger for severe lines than for the non-severe lines.** In their study, the average CAPE for severe lines was significantly larger than for the

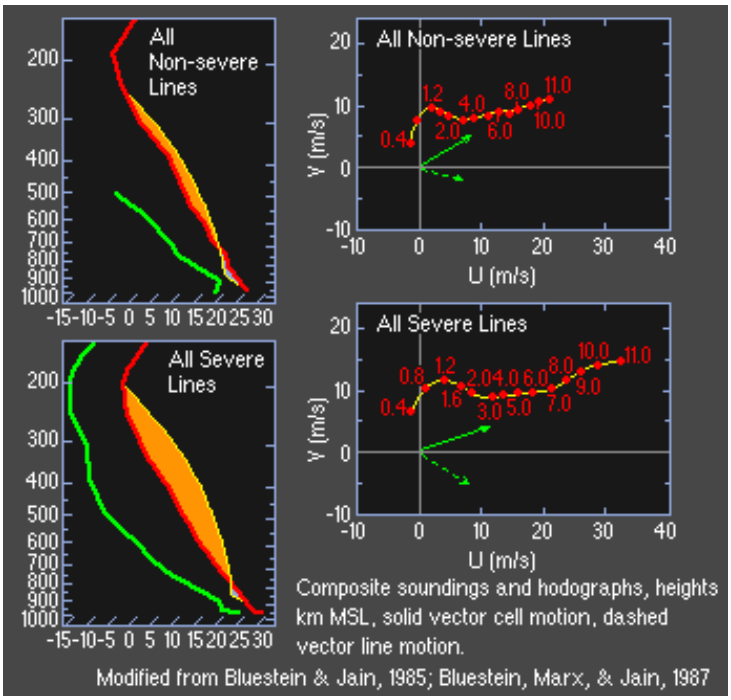

Figure 3-81. Comparison of mean vertical thermodynamic and wind profiles for severe and non-severe squall lines.

non-severe lines (2260 J/kg versus 1372 J/kg), which agrees with other studies (Fig. 3-81).

Numerical cloud modeling simulations of long-lived severe squall lines in *An MCS Matrix* (COMET, 1999) explored the storm-scale evolution in the development and maintenance of long-lived multicellular systems (such as bow echoes). The effects of environmental shear (in the lowest 2.5 to 5 km AGL) in balance with the surface cold-pool circulation were determined to have great influence on squall line/bow echo longevity. Vertical wind shear values of 20 ms^{-1} (40 kts) or greater were determined to be “optimum”. Weisman (1993) indicated that significant, long-lived bow echoes evolved when the cold-pool circulation overwhelmed the low-level shear in the simulations, allowing the system to develop an **upshear-tilted structure** (Fig. 3-82). This setup, which developed after several hours in the simulations, showed a **sloped, warm, front-to-rear**

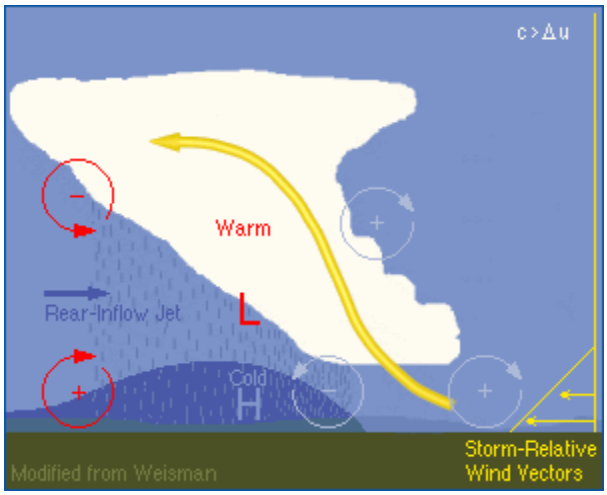

Figure 3-82. Convection developing along a leading edge of a cold pool with an upshear tilted structure (COMET, 1999).

ascending current developing above the cold pool The development of constructively interfering vorticity regions causes the development of a strong **Rear-Inflow Jet (RIJ),** which, if elevated and approaches the leading edge of the system, can contribute to strengthened and upright low-level updrafts. This situation also deepens the surface cold pool. Thus, a feedback mechanism is in place that intensifies the entire system even further (Fig. 3-83). Objective 17 explains the RIJ in more detail.

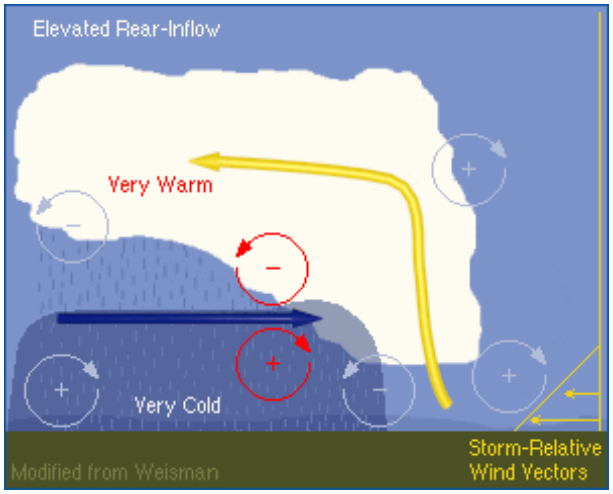

Figure 3-83. Development of an elevated rear-inflow jet in squall line simulations (COMET, 1999).

Shear, CAPE and the Development of Bow Echoes

Earlier modeling simulations suggested that strong low-level vertical wind shear (roughly in the 0-2 km layer) and correspondingly high values of CAPE were needed to support the development of 3-D mesoscale features such as elevated RIJs and bookend vortices within the convective system. **However, Evans and Doswell (2001) did not find a clear relationship between cold pool strength and low-level shear.** Their data showed that DCAPE (used as a proxy for cold pool strength) and shear were not positively correlated (Figure 3-84). However, they were unable to test with their observations the assertion that the elevated RIJ was necessary to re-balance the cold pool/shear circulation (Weisman, 1993).

Role of Deep-layer Shear

Two additional factors likely contributing to squall line strength are deep layer shear and low-level system-relative flow. Evans and Doswell (2001) results showed that the mean winds in the 0-6 km layer and the 0-2 km system-relative inflow were stronger because system speeds were faster for derecho events in Mesoscale Convective Systems (MCSs) as compared to MCSs that did not produce derechos (Figure 3-85 and Figure 3-86). The 0-2 km system-relative flow was enhanced in the strongest derechos likely due to faster forward speed and resultant increased low-level convergence. The midlevel system-relative winds did not show much difference between derecho and non-derecho events.

In a MM5 simulation of 12 progressive derechos, Coniglio and Stensrud (2001) showed that middle to upper-level shear above the surface cold pool was critical in sustaining squall line structure for longer periods of time.

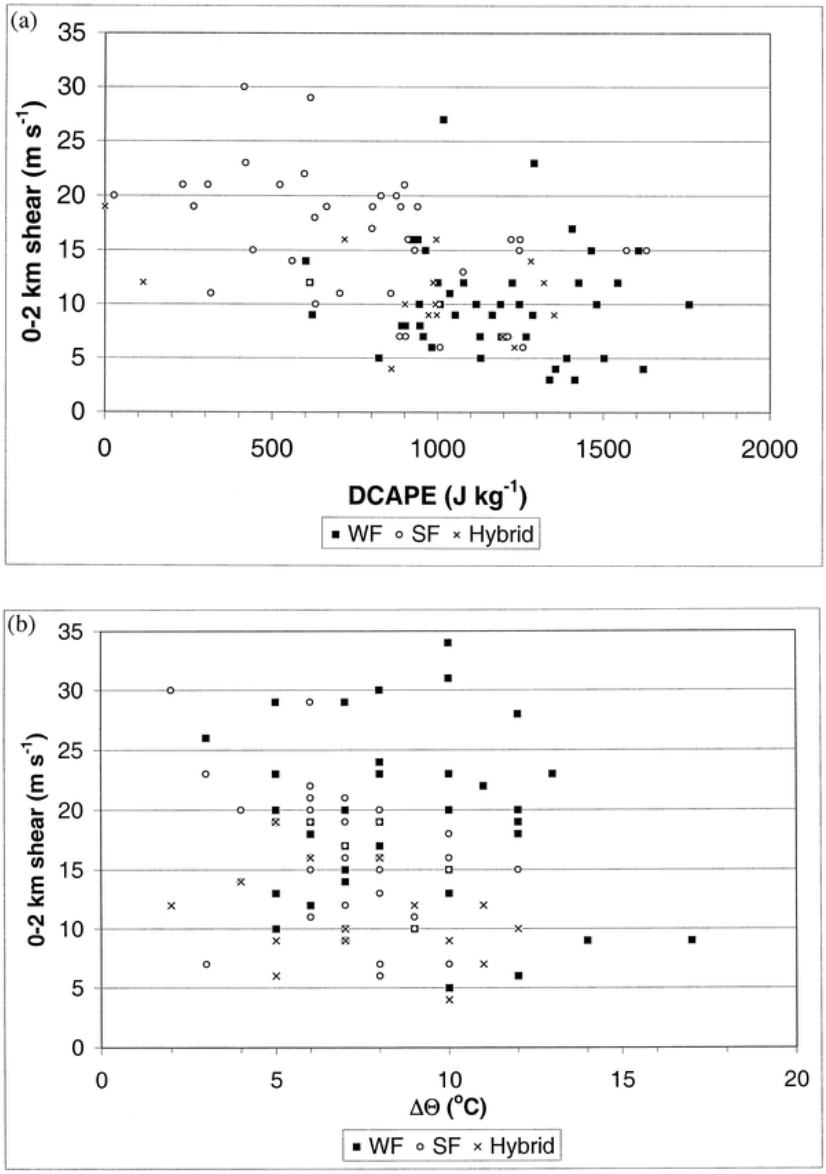

Figure 3-84. Scatter plot of a) DCAPE vs. 0-2 km shear vector magnitude and b) surface $\Delta\theta$ across the cold pool vs. 0-2 km shear. Adapted from Evans and Doswell (2001).

Thus, the results of Coniglio and Stensrud (2001) and the operational data sets in Evans and Doswell (2001) suggested that, in similar thermodynamic environments and weak forcing, it is the strength of the mean wind which appears to distinguish between derecho and non-derecho MCS environments. The mean wind and low-level convergence modulates low-level system-relative flow, which also depends on the forward speed of the surface cold pool.

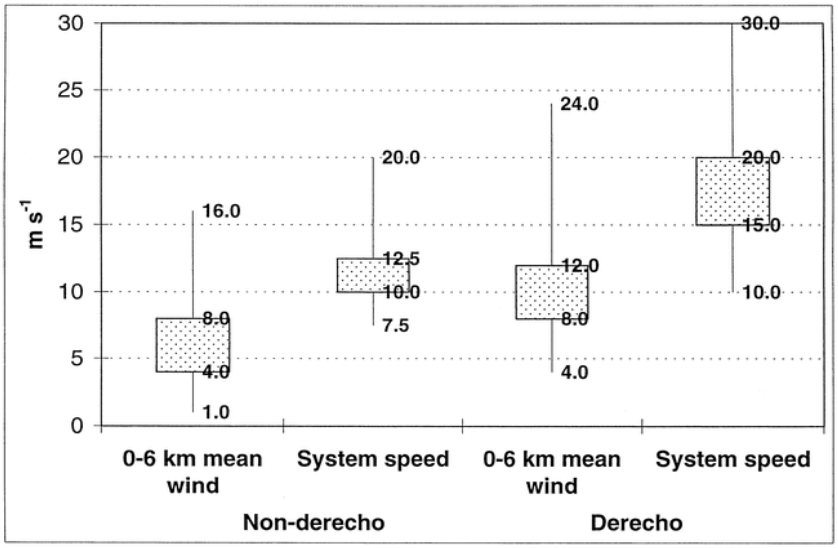

Figure 3-85. Box and whiskers plot of mean wind and system speed for severe and non-severe derechos. The shaded areas represent the 25th and 75th percent quartiles while the endpoints are the maxima and minima. Taken from Evans and Doswell (2001).

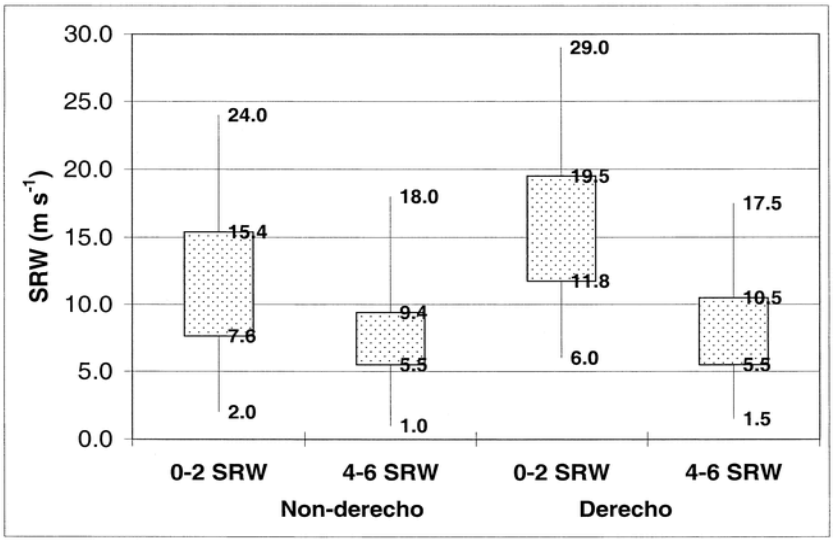

Figure 3-86. Similar to Figure 3-85, except for storm-relative winds.

MCS Longevity

MCSs can be long-lasting depending on the environment and resulting propagation. The COMET MCS module states that squall line lifetimes generally range from as little as 3 to 5 hours for weak shear cases, to as much as 4 to 8 hours for moderate shear cases. The full lifetime of the system, however, can often be much longer if a new round of convection is triggered at the leading edge by the weakening cold pool, a more favor-

able environment, or an external forcing mechanism (e.g., boundary or cold front) helps to continually re-trigger convection. In strongly sheared environments overall system lifetime often extends beyond 12 h, especially if the environment ahead of the system continues to be thermodynamically favorable for convection. External forcing features, such as cold fronts, may extend system lifetime even further.

Derecho events, which are the fastest moving multicell systems, can last from 2 to over 20 hours and can travel across multiple County Warning Areas if downstream instability remains sufficient (see progressive derecho description). An example of this was the 15 July 1995 derecho which started in Michigan, moved into southern Canada overnight and then eventually southeast across New York state from 0700 UTC to 1500 UTC causing 5 deaths, 11 injuries, and widespread damage (close to a million forest acres destroyed). Figure 3-87 shows a broad swath of wind damage from 60-70 mph winds and greater (see case from COMET MCS case exer-

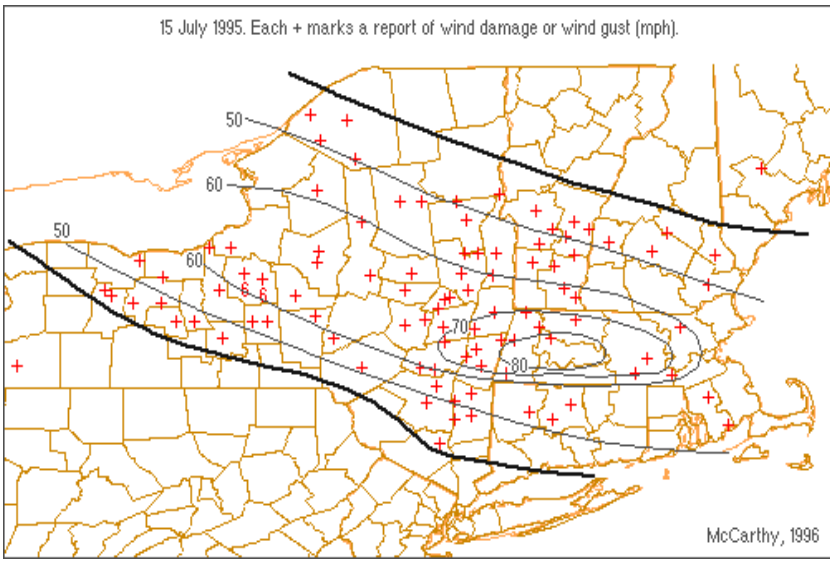

Figure 3-87. Damage reports from the 15 July 1995 progressive Derecho.

cises). These kinds of long-lasting multicell events produce large swaths of extreme winds because typically, there is an abundance of downstream surface-based instability, and system-relative flow remains strong throughout its lifetime.

Inverse Relationship Between CAPE and Shear

To summarize, **the intensity and longevity of squall lines and bow echoes occur within a wide range of environmental conditions and shear/buoyancy parameters. As in supercell environments, for stronger synoptic forcing, deep layer shear is usually stronger and CAPE is smaller.** The converse holds true as well; **in weaker synoptic forcing, higher CAPE and DCAPE are necessary to maintain the strong winds at the surface.**

Objective 17

Describe the morphology and the influence of the Rear- Inflow Jet (RIJ) on multicells.

Definition of a Rear-Inflow Jet (RIJ)

Another factor which influences multicell intensity and longevity is the Rear-Inflow Jet (RIJ). The RIJ is a region of strong winds that originate in the trailing stratiform rainfall region of a squall line near the top of the cold pool and are directed toward the leading edge**. The RIJ can either descend or remain elevated during its transit to the leading edge.** It represents the mature stage of an MCS and may also signify the beginning of its demise. However, a significant number of squall lines continue to show significant longevity and severity after the RIJ forms.

A Brief Background

Observational studies such as Smull and Houze (1987) suggested that the RIJ may be forced by a hydrostatically generated low under the trailing anvil region just behind the leading edge. They observed numerous examples of long-lived squall

lines with persistent RIJs. Fovell and Ogura (1988) noted that the strongest squall lines in their simulations tended to have the strongest cold pools, which would have lead to the greatest imbalance between the cold pool and environmental circulations. Apparently, the theory proposed by Rotunno et al. (1988) needed modification to account for this contradiction. Further 3-D numerical simulations suggested to Weisman (1992) that an elevated RIJ toward the leading edge can restore cold pool circulation balance with the environmental shear, maintaining the longevity of a squall line. Elevated RIJs, according to Weisman (1992), arise when the circulation of the overturning anvil is well matched to that of the rear of the cold pool. Starting around 4 km AGL, the jet horizontally extends to the front of the squall line and just above the cold pool. Since the bottom edge of the RIJ resides above the cold pool, the circulations tend to destructively interfere with each other. This process diminishes the strength of the cold pool in terms of circulation and therefore reduces the dominance of the cold pool over the environmental shear. Owing to the difficult nature of observing this interaction, there have been no statistical studies that can either support or refute this theory.

While some uncertainty exists as to the relationship between an elevated RIJ and a long-lived severe squall line, we present further details of the Weisman (1992) theory to explain the dynamics and forecasting implications of the RIJ. Be sure and review the COMET module on *Mesoscale Convective Systems: Squall Lines and Bow Echoes* (COMET, 1999) for further details on RIJs.

The Dynamics of a RIJ

To explain the dynamics of the RIJ, we will start with a mature squall line schematic (Figure 3-88).

As a squall line matures, high-level anvil material begins to stream from the leading edge into the rear side of the squall line (represented by the yellow trajectory in Fig. 3-88). Loaded with small- and medium-sized hydrometeors that had not fallen out of the leading edge, the anvil begins to precipitate, resulting in the region of trailing stratiform precipitation. The anvil material is also warming the upper-troposphere through latent heat released in the updraft along the leading edge. This heat acts to hydrostatically lower the pressure beneath the anvil but above the cold pool (marked by a 'L' in Figure 3-88). A hydrostatic high still exists near ground-level in the cold pool, dominating any pressure drop caused by anvil material aloft. In terms of pressure dynamics, the anvil-induced low induces air to laterally flow in from both the front and rear sides of the squall line (arrows to the right and left of 'L' in Fig. 3-88). Although the updraft tends to limit the amount of air coming in from the front, there is no obstruction from the rear side and air begins to flow rear to front, initiating the RIJ. Presumably, the strongest midlevel low resides underneath the thickest part

Figure 3-88. A cross-sectional diagram of a squall line taken from the COMET MCS module (1998). The relevant labels include the updraft trajectory (yellow arrow), the midlevel low (red L), the inflow into the low (red arrows) and the cold pool high (blue H).

of the anvil just behind the deep updraft forced along the leading edge of the squall line. Therefore, the RIJ accelerates until it is just behind the updraft. We next discuss the strength of the acceleration and the factors that govern the slope of the RIJ.

Buoyancy Effects on the RIJ

The strength of the low underneath the anvil depends on the intensity of the net warming in the anvil. Looking at Figure 3-89, the squall line updraft with the greatest positive temperature excess is the one utilizing the greatest CAPE. Note the hypothetical sounding profile and the temperature excess of the updraft parcel to the environment. The result of higher CAPE is usually

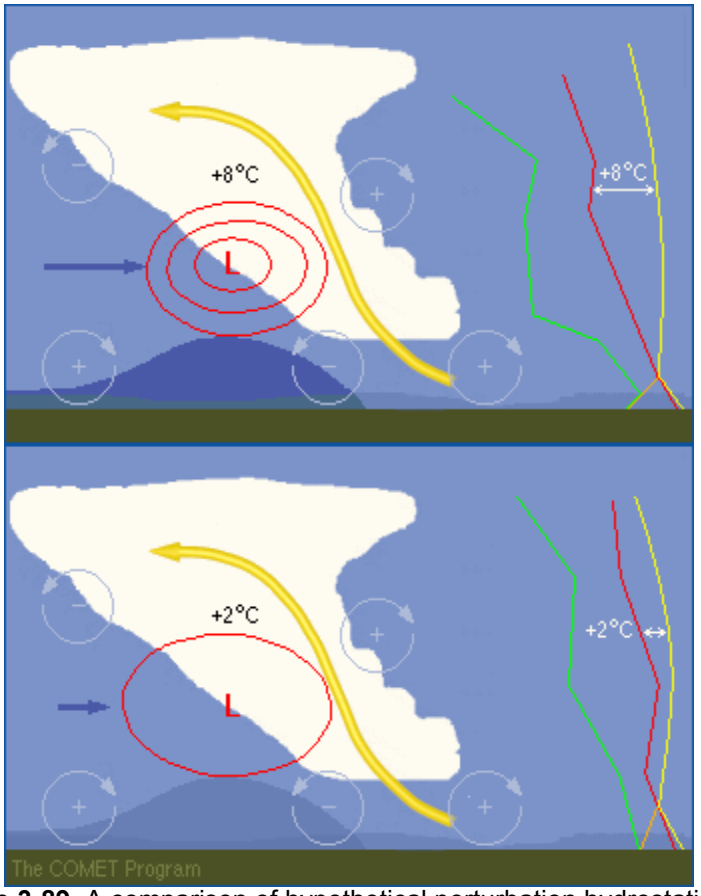

Figure 3-89. A comparison of hypothetical perturbation hydrostatic isobars (red contours) is presented for a high CAPE (top panel) and a low CAPE case (bottom panel). The blue arrow left of the isobars is intended to illustrate the relative magnitude of the rear inflow jet. From the COMET MCS module (COMET, 1999).

a stronger RIJ. Typically in large CAPE environments, lapse rates from the surface to midlevels tend to be larger, promoting stronger cold pools. **From a vorticity argument, a stronger cold pool circulation to the rear of the squall line works with a more buoyant anvil aloft to generate strong midlevel horizontal inflow that forces the RIJ from the rear of the squall line.**

Shear Effects on the RIJ

Given the same buoyancy for updrafts and cold pools, shear can modulate the intensity of the RIJ. According to numerical simulations, as shear increases, the updraft along the leading edge becomes more erect and stronger. More heat is pumped into the anvil just behind the leading edge causing a stronger hydrostatic low in the midlevels. The more intense precipitation from the stronger updraft is hypothesized to create a stronger cold pool as well.

Descending vs. Non-descending RIJs

According to simulations proposed by Weisman (1992), the longevity of the squall line may depend on the rear-to-front slope of the RIJ. Although there may be multiple slopes to the RIJs, there are two extremes:

1. **A descending RIJ and**
2. **A non-descending RIJ.**

A Descending RIJ

A descending RIJ occurs when the vorticity generated just underneath the ascending front-to-rear updraft is weaker than the vorticity generated of the opposite sign on the rear edge of the cold dome. In Figure 3-90, the imbalance between the two circulations can be seen to help force the RIJ downward towards the ground prior to reaching the leading edge of the gust front. The RIJ then reinforces the vorticity along the leading edge

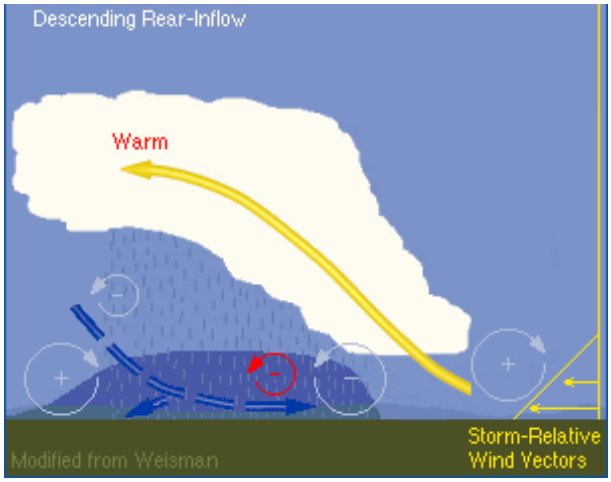

Figure 3-90. A schematic of a descending RIJ. From the COMET MCS module (COMET, 1999).

increasing the imbalance between the cold pool and environmental vorticity. The squall line is theorized to become increasingly sloped rearward and thus weakening. According to simulations by Weisman (1992), this situation occurs with weakening shear (less than 15 m/s over the lowest several km) or if the environmental CAPE is less than 1000 J/kg.

Non-descending RIJ

As CAPE and/or shear increases, the vorticity underneath the rearward expanding anvil becomes much larger due to increased buoyancy. The counter-rotating vorticity along the back edge of the cold dome does not increase as much. This situation results in the increased buoyancy-induced vorticity under the anvil matching the cold dome vorticity to invoke a more horizontally oriented RIJ (Fig. 3-91). This non-descending RIJ progresses towards the leading edge of the cold pool with a horizontal vorticity structure that interferes with the spreading cold pool vorticity near the gust front. Thus the strength of the gust front vorticity decreases, becoming more balanced with the environment, and the updraft retains an upright nature. **Squall lines with a non-descending RIJ**

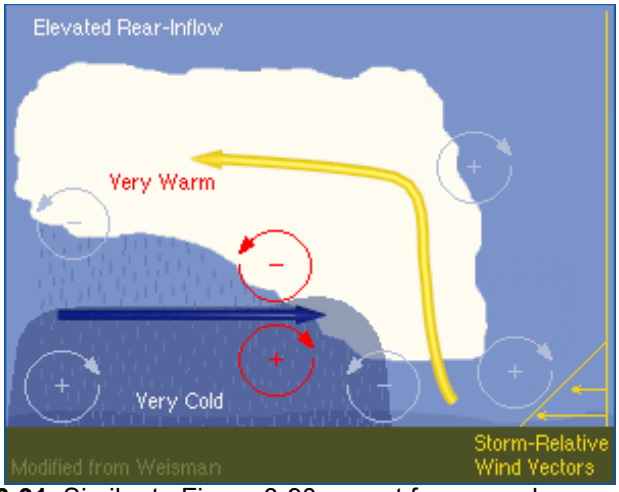

Figure 3-91. Similar to Figure 3-90 except for a non-descending RIJ example. Adapted from Weisman (1992).

tended to live longer than their descending RIJ counterparts (Weisman 1992).

Other Mechanisms that Affect the Intensity of the RIJ in Squall Lines

The role of a non-descending RIJ in squall line longevity put forth by Weisman (1992) may not adequately explain the longevity of some severe squall lines in environments exhibiting low values of 0-3 km shear. Other numerical experiments (Xue, 2000; Shapiro, 1992; and Coniglio and Stensrud, 2001) provide evidence that adding shear in a layer above the lowest few km in such a way to yield low gust front-relative storm motion may allow squall lines to persist longer than predicted by shear/cold pool balance theory. In addition, strong synoptic-scale midlevel winds may boost the initiation time and strength of the RIJ. An example would be a cold-season, pre-frontal squall line in the warm sector of a surface extratropical cyclone (Johns, 1993).

Impact of Synoptic-scale Midlevel Flow

As mentioned earlier, Evans and Doswell (2001) observed numerous cases of derechos without high values of either shear or buoyancy. They did notice a relationship between longevity, mean steering-layer winds, and low-level storm-relative inflow. The latter relationship is likely due to the

fact that derechos move quickly. In addition, strong RIJs may be the result of dynamics beyond that of balancing anvil-level buoyancy with cold pool strength. For example, small amounts of CAPE are sufficient to vertically mix strong, synoptic-scale midlevel winds down to the surface yielding a strong RIJ-like structure.

Therefore, it is important not only to look for high values of low-level shear, but also for the existence of strong deep-layer shear and strong convective steering-layer flow. As is often the case, the parameter space in which long-lived multicell squall lines are observed is often much larger than simulations suggest.

Objective 18

Identify the characteristics of bow echoes and the mechanisms involved in their formation.

Line-end Vortices

In the mature phase of a well-organized squall line system, it is not uncommon to observe three-dimensional features such as elevated RIJs, line-end vortices, and even supercells. **Line-end vortices (often called bookend vortices) typically, by definition, evolve at the end of the line or at breaks within the line.** The development of these features can alter the subsequent evolution of the system.

In numerical simulations presented in the *MCS module* (COMET, 1999), line-end vortices typically developed between 2-4 h into the lifetime of the convective system, just behind the zone of most active convection. **The vortex at the northern end of the system had cyclonic rotation, while the vortex at the southern end of the system rotated anticyclonically** (for a north-south ori-

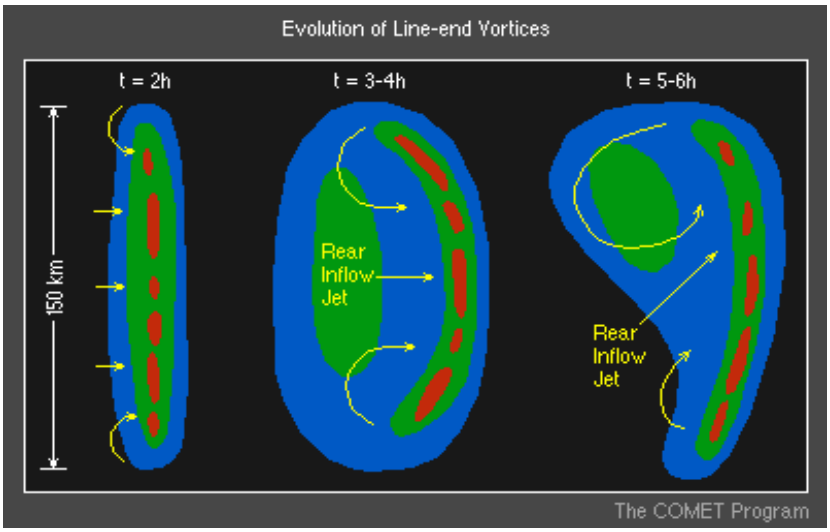

Figure 3-92. Development of a cyclonic "bookend" vortex in a squall line simulation. From the COMET *MCS module* (COMET, 1999).

ented squall line propagating toward the east in the Northern Hemisphere; Figure 3-92).

Cyclonic vs. Anticyclonic Line-end Vortex

The cyclonic vortex at the northern end of line tends to become stronger and larger than the southern, anticyclonic vortex (according to the simulations). As this occurs, the convective system becomes asymmetric, with most of the stratiform precipitation region found behind the northern end of the system and the strongest leading-line convective cells found near the southern end. **In weak-to-moderate shear environments, the dominant northern line-end vortex was typically observed to move rearward with time.** When the ambient shear was strongest and the system updraft remained erect longest, the line end vortices tended to remain closer to the leading line convection.

In the simulations, the impact of midlevel convergence in the presence of Coriolis forcing acted to strengthen the northern cyclonic bookend vortex, but weaken the anticyclonic bookend vortex with time. The strengthening of

the cyclonic bookend vortex is thought to produce the symmetric-to-asymmetric evolution that characterizes most long-lived MCSs.

Mesoscale Convective Vortex (MCV)

The dominant cyclonic vortex can last well beyond the lifetime of the originating convective system and is often referred to as a Mesoscale Convective Vortex (MCV). In some cases, MCVs have been documented to last for several days, helping to trigger subsequent convective outbreaks.

Line-end Vortices are Downdrafts

Since line-end vortices typically develop within the downdraft portion of the squall line, they are not usually associated with significant tornadoes. However, because they can enhance the strength of the RIJ between the vortices, line-end vortices are a source of increased downdraft and stronger surface winds. In this way, they can contribute to the spin-up of tornadoes at the leading edge of the system outflow.

Distance Between Line-end Vortices

According to the *MCS module* (COMET, 1999), **the smaller the distance between the line-end vortices, the more enhancement to the midlevel flow between vortices, which strengthens the RIJ.** The descent of this enhanced RIJ to the surface is hypothesized to produce the extreme surface winds associated with bow echoes. (Figure 3-93).

Characteristics of Severe Bow Echoes

Fujita (1978) coined the term “bow echo” to describe the radar presentation of long (20-120 km) bow-shaped systems of convective cells noted for producing long swaths of strong surface winds. **Bow echoes are typically observed on radar as an accelerating portion of a squall line and are usually concave-shaped.**

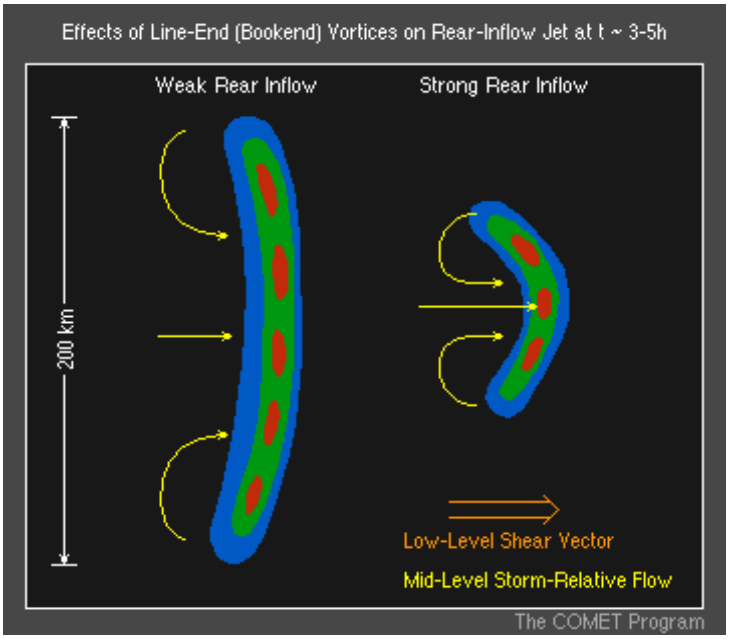

Figure 3-93. Effect of bookend vortices on the strength of an RIJ. From COMET (1999).

Bow echoes often occur from either isolated storms or within much larger convective systems (such as squall lines). **When multiple bow echoes are observed within a squall line, the radar signature is referred to as a Line Echo Wave Pattern (LEWP)**.

LEWPs

Many features of bow echo evolution which cause a typical LEWP structure (such as the rotating comma head and the cyclonic/anticyclonic rotating vortices) are based on the conceptual model from Fujita (1978; Figure 3-94). Fujita found that the initial echo started as a strong isolated cell or a small line of cells. The initial cells then evolved into a symmetric bow-shaped segment of cells over a period of a couple of hours, and eventually into a comma-shaped echo over several hours.

Rear-inflow Notch on Radar

Another radar characteristic of bow echoes noted in the simulations and observed in WSR-88D imagery is the development of the weak echo notch, sometimes referred to as a **Rear-Inflow**

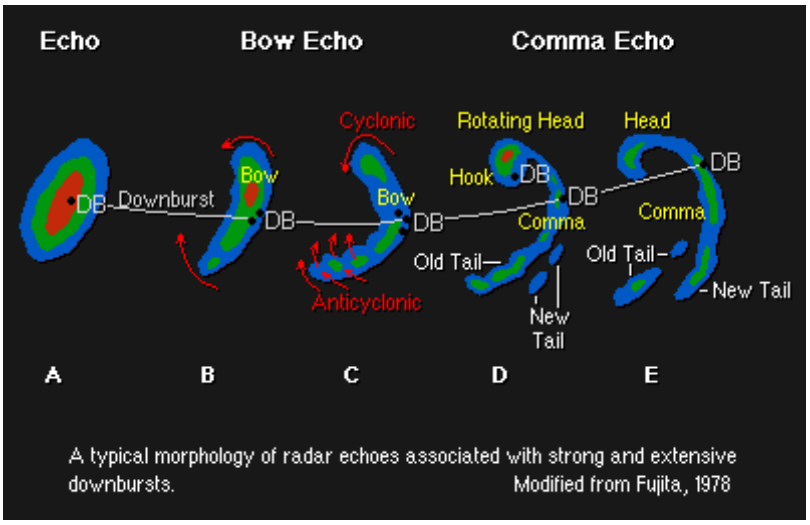

Figure 3-94. Conceptual model of a bow echo evolution. Adapted from Fujita (1978) and COMET (1999).

Notch (RIN). The RIN is located well behind the core of the bow (Figure 3-95), and it often signifies the location of a strong RIJ. **RINs were frequently observed along the trailing edge of each individual bowing segment, signifying a region of evaporatively-cooled lower theta-E air being channeled toward the leading edge of the bow** (Przybylinski and Schmocker 1993). In large, distinctive bow echoes, multiple RINs, or weak echo channels, can be observed on radar imagery

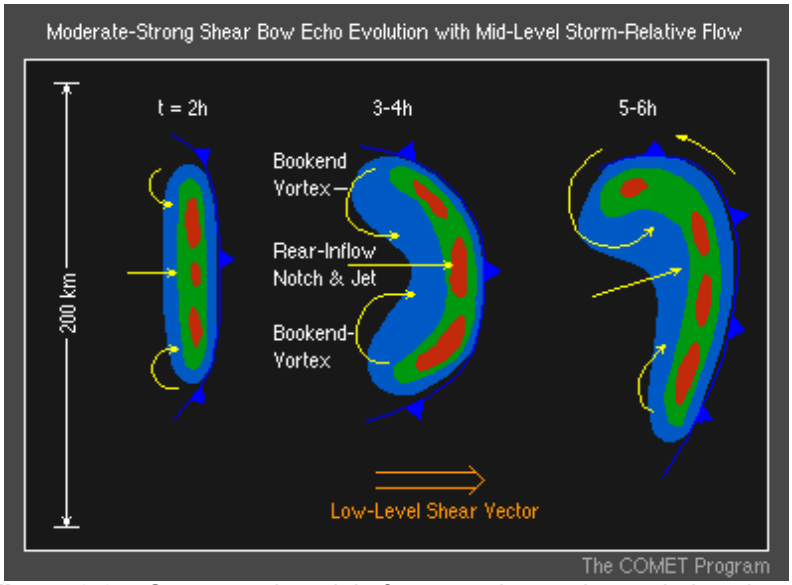

Figure 3-95. Conceptual model of a strong bow echo evolution showing bookend vortices and development of a Rear-Inflow Notch (RIN). From COMET (1999).

(Przybylinski, 1995). These RINs may be locations where the RIJ is descending to the ground. When the RIJ descends to the ground near the leading edge of the bow, it can create a swath of damaging surface winds. Weak tornadoes are often observed just north of this surface jet core.

Cross-section of Bow Echoes

Vertical cross-sections in the core of mature bow echo simulations (Figure 3-96) revealed a strong, vertically erect updraft at the leading edge of the system; a strong, elevated RIJ impinging just behind the updraft region before descending rapidly to the surface; and a system-scale updraft that turned rapidly rearward aloft, feeding into the stratiform precipitation region.

Supercell Transition to Bow Echo

Supercells are also observed occasionally within the larger bow echo structure. **In some cases, an isolated supercell is observed to evolve directly into a bow echo as the supercell decays. This type of evolution is typically seen with HP supercells** (Finley et al. 2001) (Figure 3-97).

Radar Morphologies of Bow Echoes

Przybylinski and DeCaire (1986) identified four types of radar reflectivity signatures associated with derechos (23 cases examined). These signa-

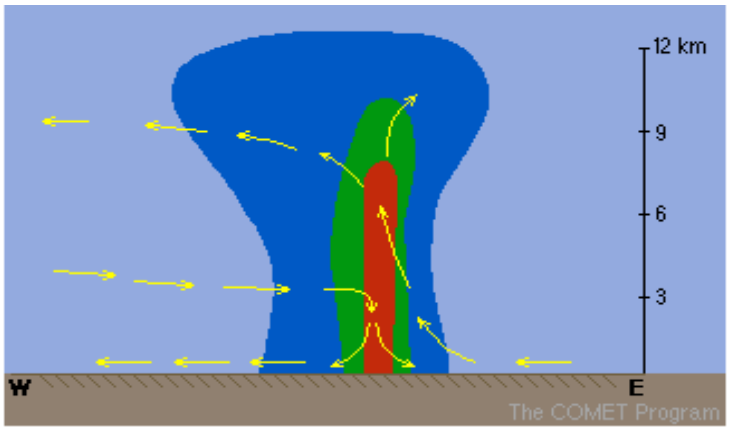

Figure 3-96. Schematic of a vertical cross-section through a mature bow echo. From COMET (1999).

tures are depicted nicely on Page 8 of the Bow Echoes section under *Conceptual Models on the MCS web site* (COMET, 1999). **All of these types of signatures indicate intense, low-level reflectivity gradients along the leading edge of the bow with pronounced RINs and/or weak echo channels on the trailing end of the bow**.

Bow Echo Propagation

Numerical simulations (Weisman, 1993) found that bow echoes tended to propagate in the direction of the mean low-level vertical wind shear vector at a speed influenced by the cold pool propagation. Since the cold pools in bow echoes were often exceptionally strong, their propagation speed was often much faster than nearby convective cells or systems.

Bow Echo Environments

As was discussed in Lesson 1, severe bow echoes (such as derechos) are observed to occur over a wide range of CAPE and shear environments. Bow echo patterns have been studied by many researchers including Johns and Hirt (1987), Johns (1993), and Przybylinski (1995), Kennedy and Rutledge (1995), Davis et al. (2004), Atkins et al. (2004). During the warm season, development

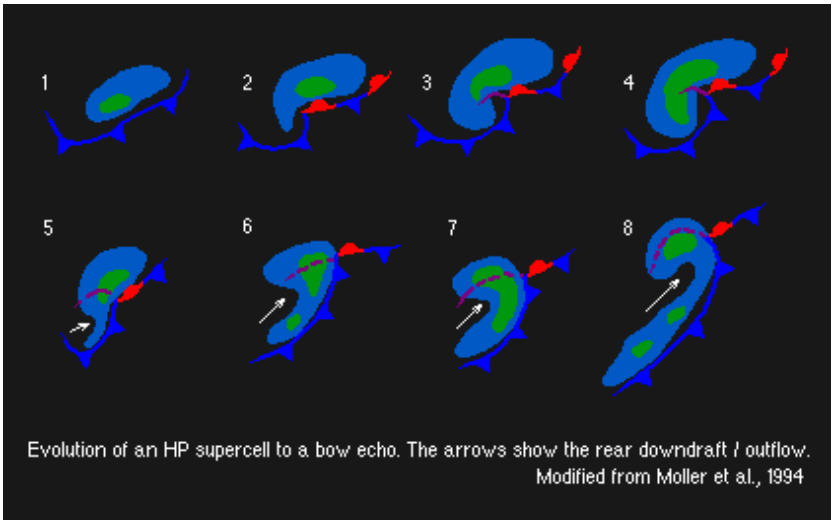

Figure 3-97. Depiction of an evolution of an HP supercell to a bow echo (COMET, 1999).

of progressive derechos are common across portions of the central and eastern United States. These derechos were defined as short bow echo segments that move parallel to a quasi-stationary front in the general direction of the mean flow (Figure 3-98). **Progressive derecho environments consist of a strong warm air advection pattern somewhere near the initiation region of the system, a thermodynamic environment characterized by relatively strong midlevel winds, a large amount of low-level moisture, a steep low- to midlevel lapse rate, and correspondingly high CAPE.** Some sort of east-west oriented boundary is also usually present.

The Influence of the Coriolis Force on Bow Echoes.

Over the first half of a bow echo life span (<3 hours), the Coriolis force is too weak to influence internal flow fields. **If the bow echo flow fields persist for more than a few hours, the integrated effects of the Coriolis force begin to noticeably alter its shape.** Pure divergence at anvil-level begins to acquire an anticyclonic component to it. The same process also creates anticyclonic curvature in the flow within the cold pool, while cyclonic curvature increases in the midlevel hydrostatic low above the cold pool. Eventually, the northern (southern) line-end vortex strengthens (weakens).

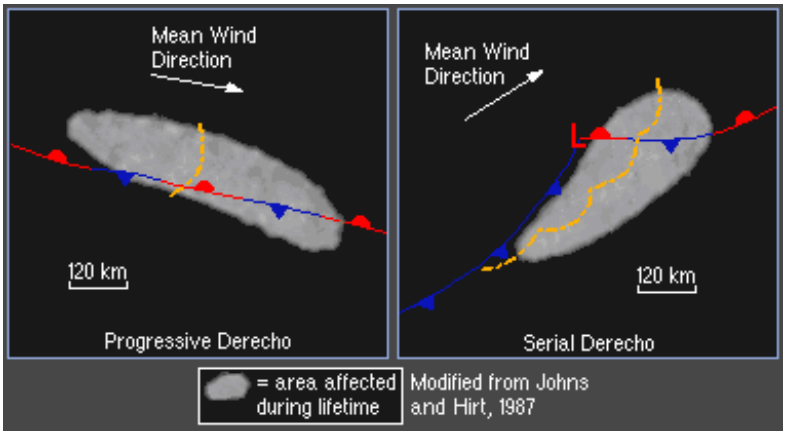

Figure 3-98. Two types of Derecho patterns (COMET, 1999).

Due to the orientation of the leading edge of the surface cold pool (or gust front) normal to the mean wind direction, **system-relative flow is maximized in the downshear direction of progressive derechos.** The cold pools (once generated by the stratiform region) for these types of bow echoes will thus discretely propagate and move rapidly in the direction of the mean wind as a result of momentum transfer and because boundary layer convergence is maximized on the downshear side of the cold pool. The entire convective system associated with progressive derechos typically moves faster than the mean wind (Johns and Hirt, 1987).

Serial Derechos

The serial derecho pattern (Fig. 3-98) consists of an extensive squall line where the angle between the mean wind and squall line axis is relatively small (Johns and Hirt, 1987). The squall line typically moves normal to **the mean wind at speeds of 30 kts or less, while the individual LEWPs and bow echoes move rapidly in the direction of the mean wind and tend to be most frequent near the northern end of the line.** Serial derechos may contain supercells because the patterns which produce these types of derechos, the so-called “dynamic pattern” (Johns, 1993), is typically associated with a strong, migrating low pressure system and has many characteristics of the classic Great Plains tornado outbreak pattern. One slight difference in the dynamic bow-echo synoptic pattern, which actually occurs more frequently in the fall/winter season, is that the low-level jet is usually more parallel to the middle and upper-level jets (Duke and Rogash, 1992). Because both supercells and severe bow echoes require strong vertical wind shear, both storm types often occur in close proximity to one another, or evolve from one structure to the other during their lifetime.

Objective 19

Recognize multicell storm signatures for monitoring and anticipating: 1) damaging winds, 2) large hail, 3) tornadoes, and 4) heavy (potentially flooding) rain.

Storm Signatures for Multicells

The range of storm signatures associated with multicell storms is quite large and complex due to evolutions so we will try to summarize these into four sections based on associated severe weather threat. This tactic is intended to provide a better indication of what a forecaster can expect based on a given storm structure.

High Winds

High winds, defined as 50 kts or greater at the surface or some reported damage associated with a thunderstorm, are common with multicell storms. In fact, severe convective winds comprise the great majority of severe weather "days" east of the Rockies in the course of a "typical severe weather season" (Fig. 3-99).

Storm signatures associated with damaging winds from multicells are typically associated with squall lines containing supercells and/or bow echoes. Squall lines can form a variety of ways (Fig.

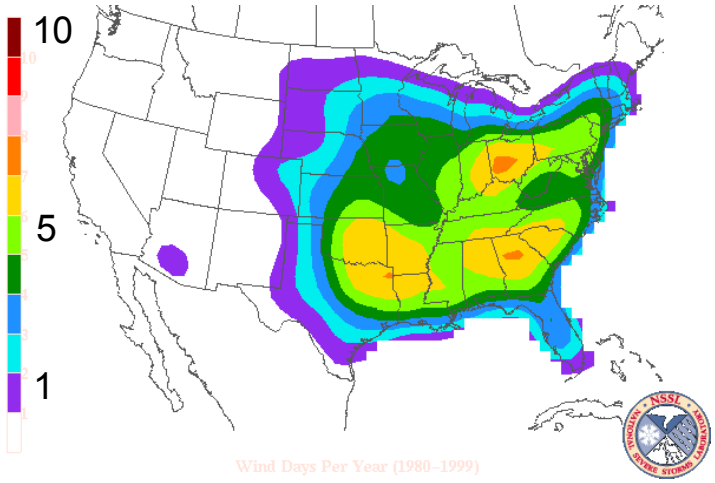

Figure 3-99. Number of days with thunderstorm winds > 50 kts occurring within 60 km of a point in a year. Adapted from Brooks (2000).

3-100). The structure depends largely on the shear profile. With weak to moderate shear, structure of the multicell complex is typically 2-dimensional (no bowing, no bookend vortex). **These squall line types may have the following characteristics:**

a. leading edge higher reflectivity "convective" cores

b. trailing stratiform (low reflectivity) precipitation region

c. movement of line with mean winds (advection dominates)

d. most points along the line do not extend beyond the leading edge

e. gust front often pushes well out from location of leading edge convection

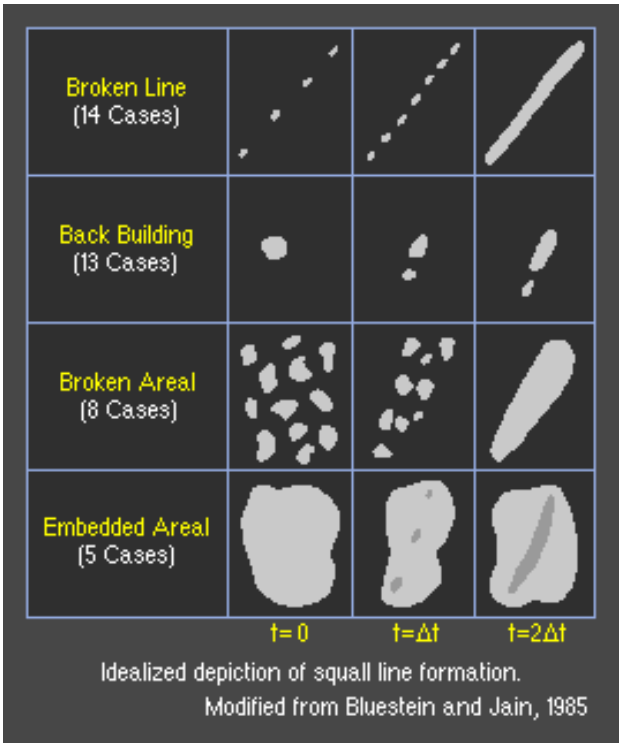

Figure 3-100. Common modes of squall line initiation. Adapted from Bluestein and Jain (1985).

A conceptual plan view graphic of the structure of this type of squall line, which can occasionally produce damaging winds, is shown in Figure 3-101. Two real examples are shown in Figures 3-102 and 3-103.

In the absence of moderate to strong shear, the most probable location of severe weather in this type of multicell structure is along **the gust front** (depicted visually by a shelf cloud in many instances) or in one of the **strongest reflectivity cores near the leading edge**. Flow is typically front to rear in weak forcing events (Evans and Doswell, 2002) such as these. This type of structure is often found in the **early stages of squall line development**. As the system transitions and intensifies, the convective line becomes a near solid echo (Figure 3-103).

The warning forecaster will most likely need to examine the lowest slices of Base Reflectivity and Velocity to evaluate the threat of high

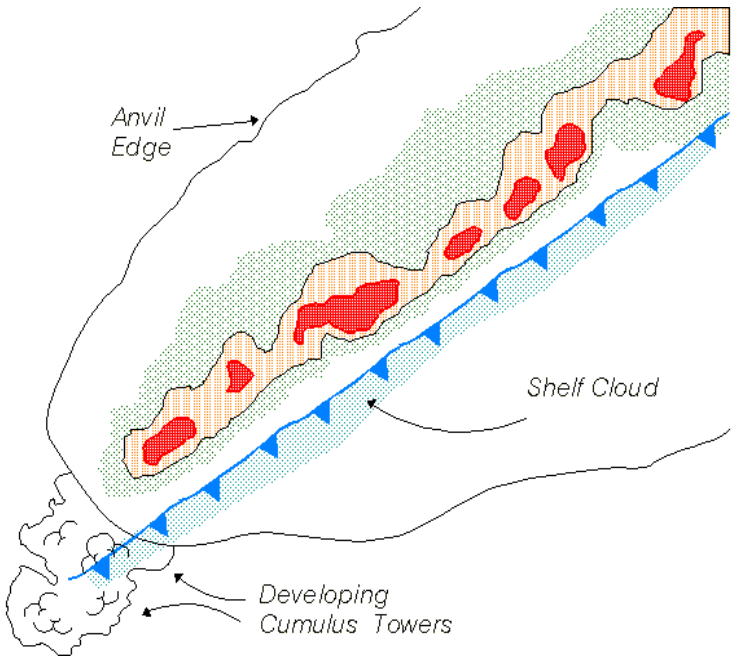

Figure 3-101. A schematic reflectivity structure of a narrow squall line.

winds associated with squall lines and bow echoes. The stronger the reflectivity gradient along the leading edge, the stronger the updraft and associated convergence along the gust front. This structure increases the threat of damaging winds. Also, if the gust front trav-

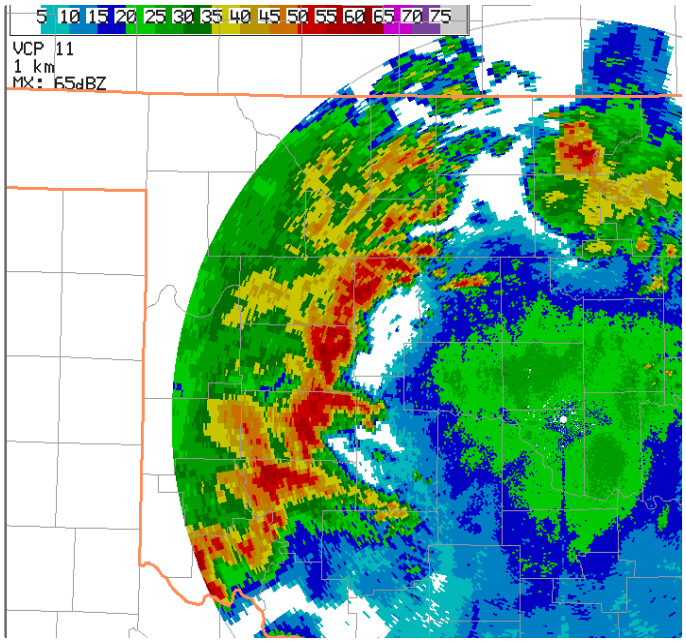

Figure 3-102. A 0.5^{O} reflectivity image from KTLX of a low to moderate shear squall line.

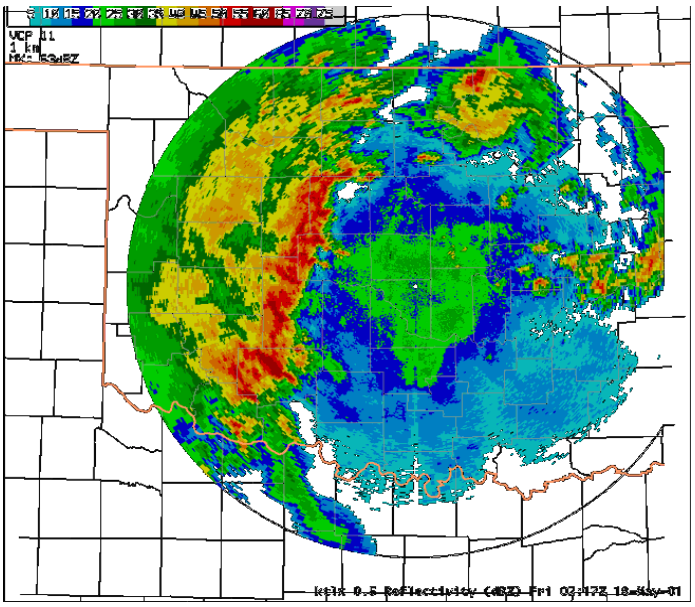

Figure 3-103. A 0.5^{O} reflectivity image from KTLX of a low to moderate shear squall line with the emergence of a stratiform precipitation shield.

els at the same speed as the multicell cluster, the boundary-relative flow maximizes potential for new cell growth along the leading edge.

WER

The existence of a **WER (or BWER)** in the multicell structure may also indicate an enhanced potential for damaging surface winds. Fig. 3-104 shows an example of a WER structure in a multicell. This case illustrates the kind of multicell structures which may result when low-level shear is very strong.

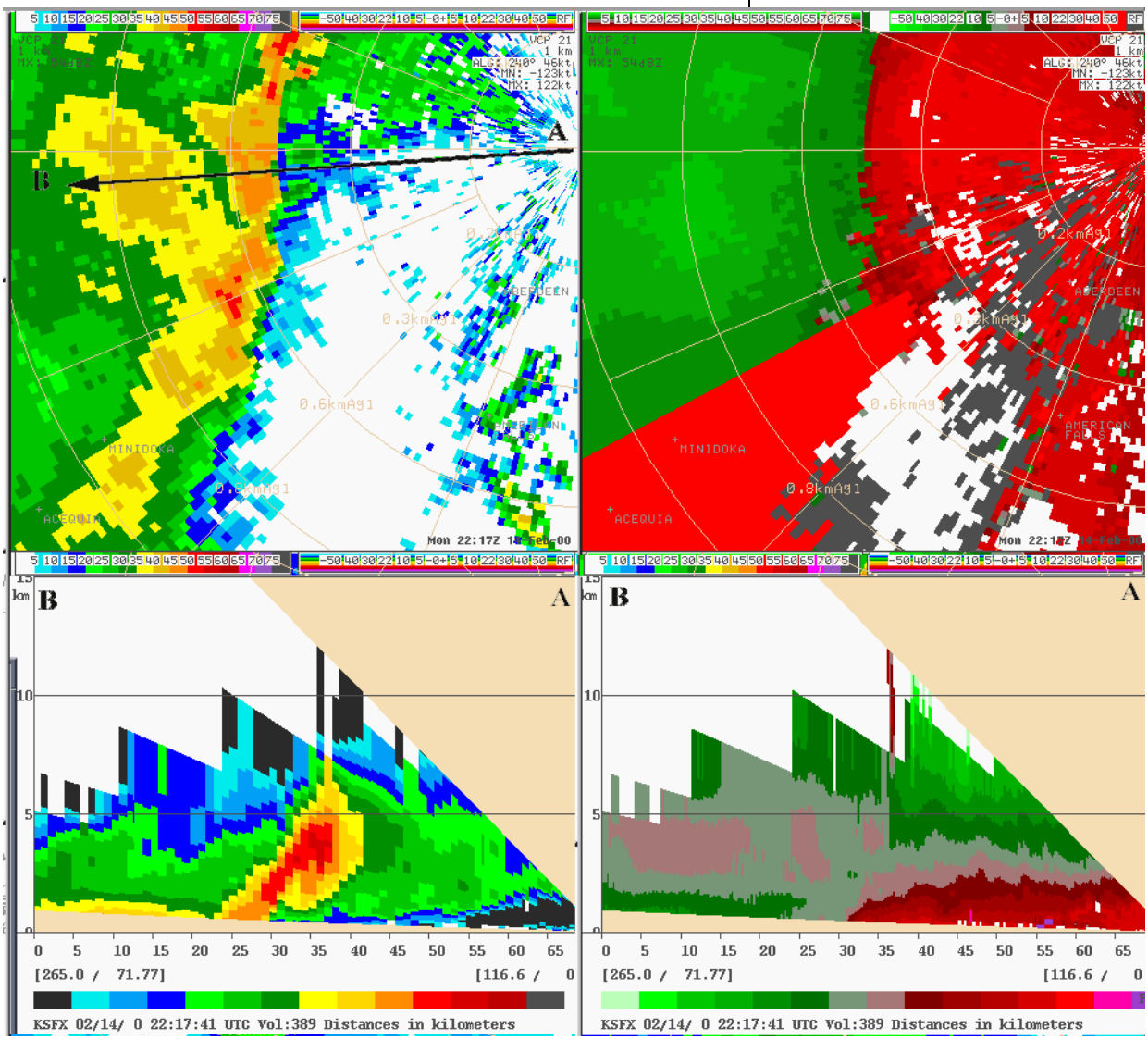

Figure 3-104. 4-panel radar image (Ref - 0.5 deg., SRM 0.5 deg., Ref. cross-section, SRM cross-section) from KPIH 14 Feb 2000 2217 UTC. Labels A-B represent cross-section endpoints.

Bow Echoes

As was previously mentioned, bow echoes are fast-moving, concave-shaped echoes that are common inducers of strong macrobursts and microbursts. **The damaging downburst winds can occur in a larger family (e.g., derecho) or can result from an isolated storm along the line. Downburst winds typically develop along and immediately to the rear of the accelerating portion of the squall line.** The strongest winds are typically at the apex of the bow (see Fig. 3-105).

MARC Signature

Another radar signature which is often associated with high winds and tornadoes is the Mid-Altitude Radial Convergence Signature (MARC).

Observations of a MARC have been noted by Przybylinski (1998) as a precursor to the descent of the elevated RIJ. Enhanced velocity differentials (areas of strong convergence) are often located just downwind of high reflectivity

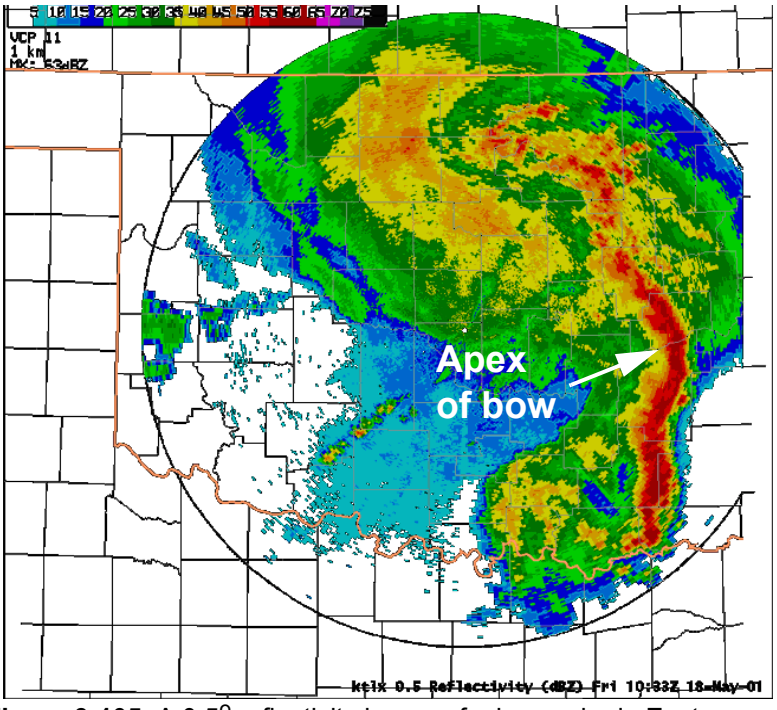

Figure 3-105. A 0.5° reflectivity image of a bow echo in Eastern Oklahoma.

cores along the leading edge of the convective line (Fig. 3-106). Persistent areas of MARC greater than 25 m/s at 3-5 km AGL can sometimes provide lead time for the first report of wind damage (often before a well-defined bow echo with bookend vortex develops).

Large Hail

The production of large hail (0.75 inches in diameter) in supercells is documented in the Anticipating Storm Structure and Evolution CD-ROM (COMET, 1996). **Hail-producing multicell storms are more likely in the early stages of squall line development when reflectivity convective cores are separated and mesocyclone strength in individual storms is strongest**.

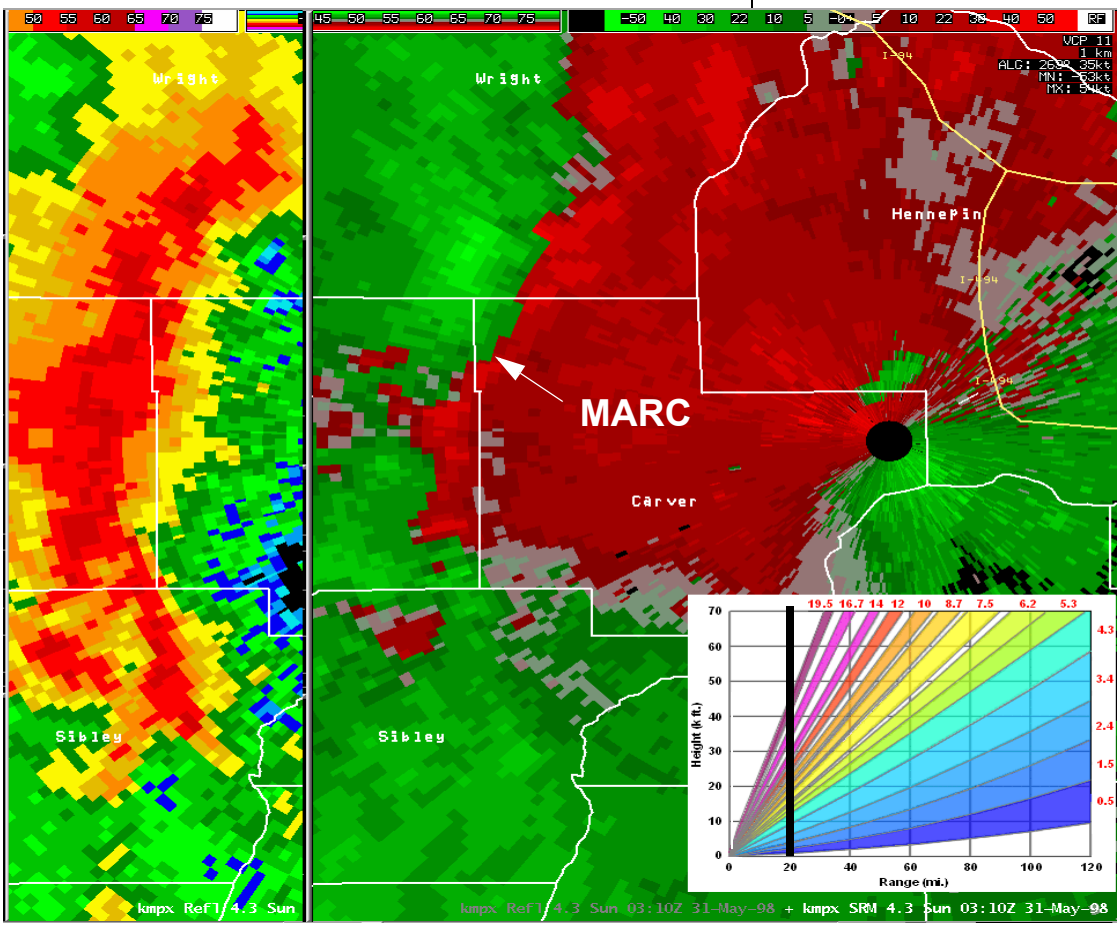

Figure 3-106. A 4.3° storm-relative velocity image of a MidAltitude Radial Convergence (MARC) zone from KMPX on 31 May 1998 - 0310 UTC. The corresponding reflectivity image is on the left. The VCP chart inset shows the approximate distance to the MARC as a vertical black line.

Look for the strongest cells in the line in terms of high reflectivity and areas where deep (7-10 kft) mesocyclones are present. In addition, a strong WER or BWER signature in cells embedded within the multicell system indicates deep lifting and potentially large hail.

In Figure 3-107, the western-most storm along the line is a supercell, and has produced severe hail (0.75 inch) and damaging winds. In 15 minutes, the storm produced a F2 tornado in Crawford County, Iowa. Isolated storms, tail-end storms, or storms which are slightly set apart from the rest of the storms in a multicell system are often hail-producers.

Hail Threats in Multicells

Houze et al. (1990) documented severe weather locations for various mesoscale precipitation systems and found that tornado and hail reports were biased toward the early stages of multicell system

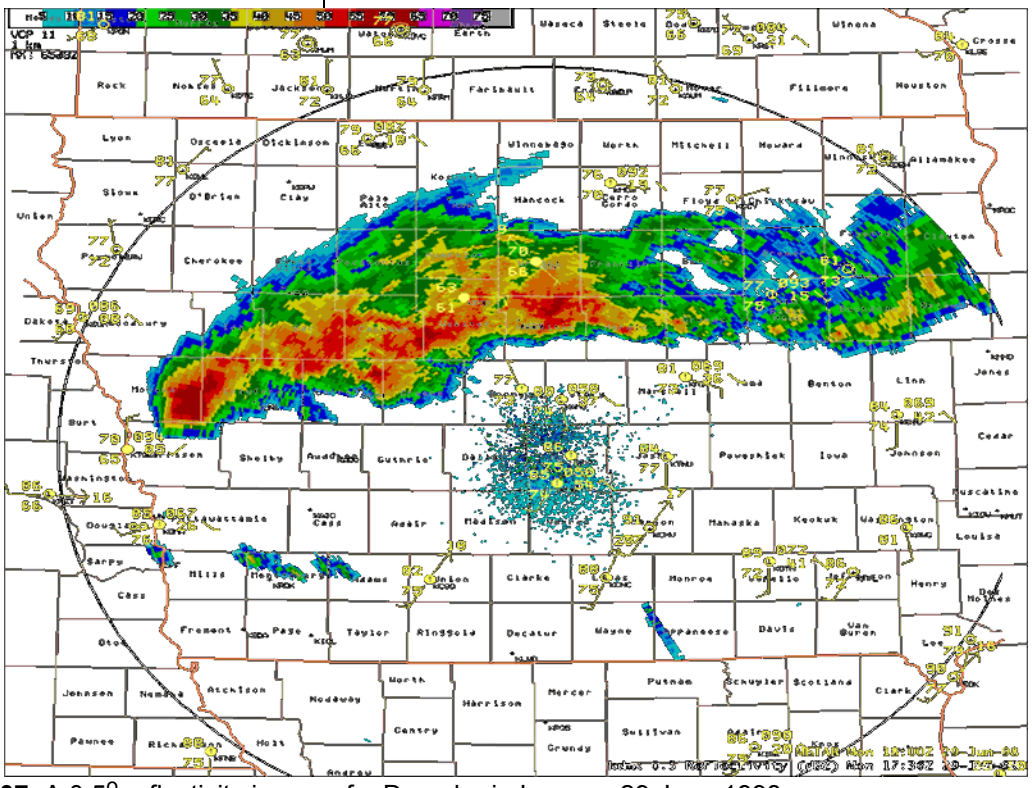

Figure 3-107. A 0.5^{O} reflectivity image of a Derecho in Iowa on 29 June 1998.

development and were most frequently associated with **1) cells located along the southern end of squall lines and 2) isolated strong cells ahead of the squall lines.** This contrasts with high wind reports which are sometimes reported with isolated cells but are more numerous along well-developed convective lines. As multicell systems intensify, the effects of the cold pool and resulting increasing rear-to-front flow in the system tend to force an upright updraft along the leading edge. Any significant hail fall will likely occur in this region, not in the downdraft region or wake of the multicell system, which becomes dominated by cooler, saturated air.

Large hail can occasionally form with quasi-stationary strong cells in a multicell complex, such as cells which form in the vicinity of a surface boundary where strong low-level convergence is focused near the updraft region of the complex.

Thus, for hail detection in multicells, **forecasters should examine the four-dimensional structure of the updraft/downdraft including overhang, and any midlevel rotation. Useful radar products for multicell storm analysis will be similar to supercell storm analysis (SRM, 4-panels, cross-sections, and animations).**

Squall Line Tornadoes

There is a variety of storm structures associated with tornadic multicell systems. Some are associated with processes as a result of line-end vortex formation in bow echoes, while others are due to supercell processes (tilting of horizontal vorticity into the vertical(see Fig. 3-107)). **As was previously stated, supercells are common in the early stages of squall line development, espe-**

cially when the cells are still discrete. The formation process in bow echoes is well documented in the COMET training module, *Mesoscale Convective Systems: Squall Lines and Bow Echoes*.

Supercell storms immediately ahead of a squall line are often notorious tornado-producers.

Because both bow echoes and supercells require strong vertical wind shear, supercells and severe bow echoes often occur in close proximity to one another, or evolve from one of these structures to the other during their lifetime. **Environments of bow echo tornadoes and supercell tornadoes are hard to distinguish.** Thus, it is important to examine storm structure of each individual cell within multicell structures, as supercell tendencies are frequently observed with well-organized multicell systems (i.e., those which develop in either sufficient deep shear and/or large CAPEs).

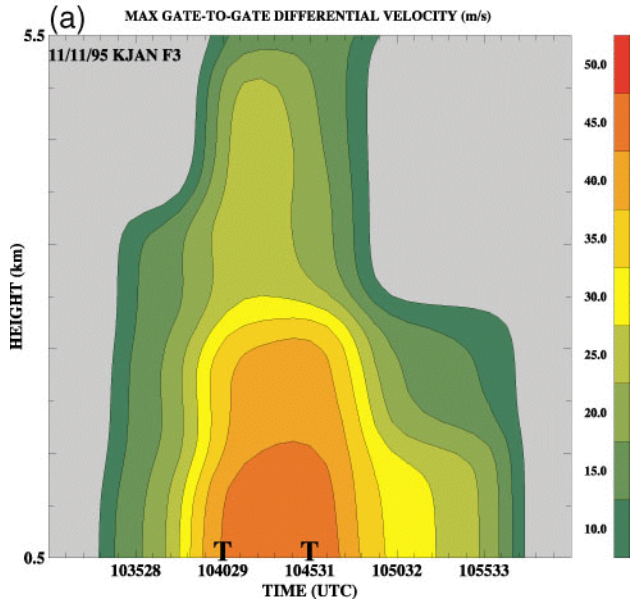

Figure 3-108. A time-height section of gate-to-gate radial velocity differences with a non-descending TVS.

Typical TVS Evolution

Tornadoes within quasi-linear convective systems tend to be associated with tornadic vortex signatures (TVS) that form from low-levels upward as opposed to some classic supercells which have midlevel circulations first and then build downward with time (Trapp et al, 1999). This non-descending paradigm for TVS evolution is shown in Figure 3-108.

Common Radar Signatures

Well-defined front inflow notches (Fig. 3-109) often show up in reflectivity data to the north of a surging area of outflow prior to tornadogenesis. **In these cases, the vertical vorticity is enhanced by strong surface convergence and is at a maximum at low-levels. Thus, tornadoes in squall lines typically form much quicker (mean lead**

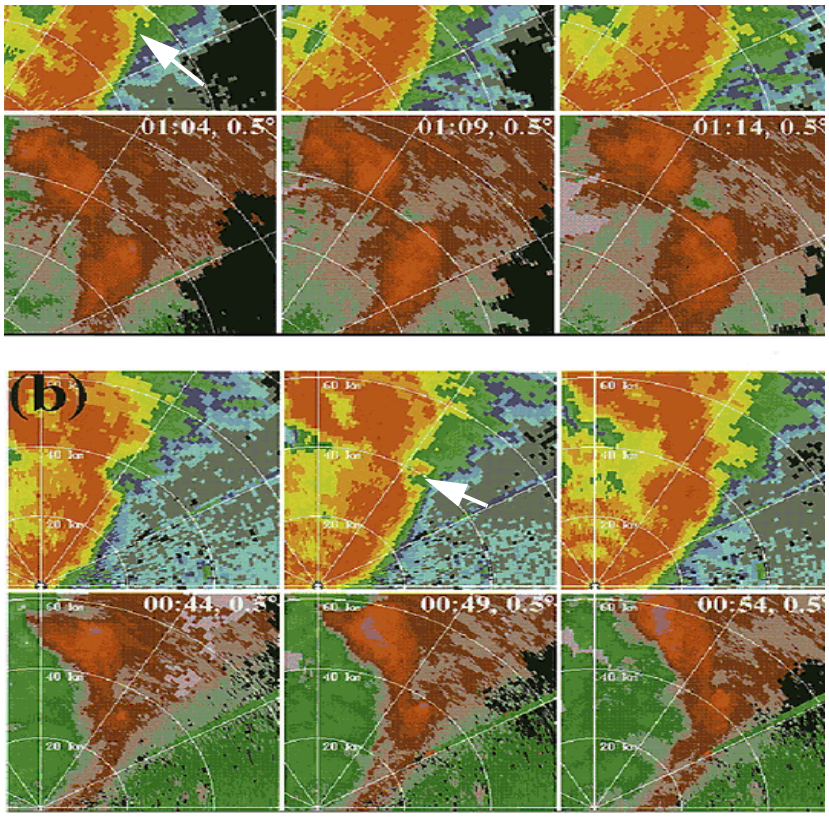

Figure 3-109. Reflectivity and velocity displays of two squall line tornado events. The arrows indicate front inflow notches. Adapted from Trapp et al. (1999).

time of 5 minutes in the Trapp study) than with isolated supercells.

Squall line tornadoes are quite often very difficult to detect at more than 20-40 nm away from the radar, as evidenced by the radar representation of this tornado bearing squall line in Columbia, Missouri in Nov. 1998 (Fig. 3-110).

Flash Flooding

Flash flooding is a result of many factors including some that are not strictly a result of meteorological effects. Flash floods result when favorable meteorological and hydrological conditions coexist (Davis, 2001). The simple meteorological ingredients are high rainfall rates over sufficient duration. Most flash floods are a result of slow moving thunderstorms, or successive storms moving over the same area. **Multicells have a proclivity to produce flash flooding because of their regenerative nature.** The process of new cell growth (and resulting propagation) can act to slow down the

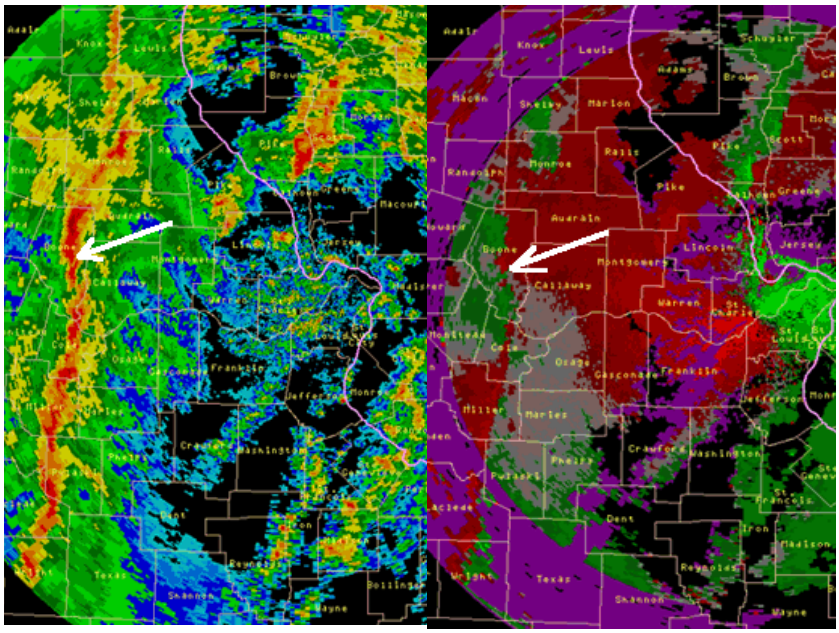

Figure 3-110. A 0.5° reflectivity and Storm-Relative Velocity product of a distant squall line tornado from KLSX 10 Nov 1998 - 0810 UTC. The arrow points to the location of the storm which produced an F3 tornado in Columbia, MO.

net movement of a multicell complex by restricting the effects of advection. **Back Building, or "training" of echoes, typically occurs when the component of a system's motion arising from cell regeneration nearly cancels the effects of motion attributed to mean steering-layer flow. Successive cells associated with the multicell complex can reach maximum intensity and produce maximum rainfall over the same geographical area.**

Method of Estimating Heavy Rain Duration

The ability to diagnose multicell storm structure associated with heavy rain and potential flash flooding is related to the anticipation of the movement of multicell systems, especially those associated with back building or quasi-stationary motion. Thus, forecasts of steering-layer winds and flow affecting propagation effects are critical. **An excellent way to visualize back building potential for multicell complexes is to examine the heavy precipitation option from BUFKIT** (Fig. 3-111).

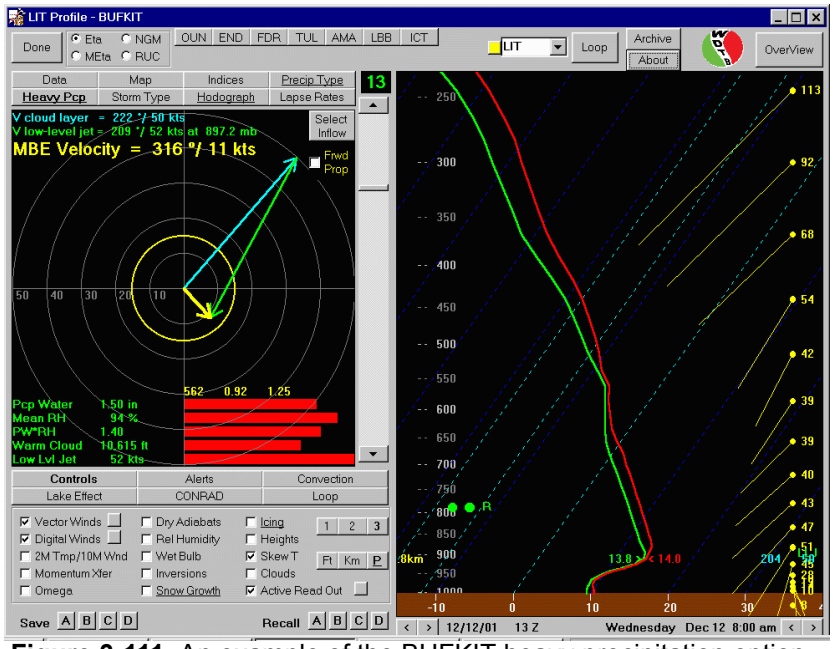

Figure 3-111. An example of the BUFKIT heavy precipitation option showing MBE ("Corfidi") vectors.

From this hodograph depiction, one can visualize the Meso-Beta Element (MBE) velocity vector resulting from propagation (opposite direction and magnitude of low-level jet) and advection (mean cloud layer winds from the LFC to the EL level).

The vectors are representations of Eta model forecasts at various times and can help the forecaster determine the likelihood for heavy rain if multicell structures develop. In the accompanying model sounding example from LIT, a MBE vector of 316 deg/11 knots was forecast to occur over central Arkansas (yellow vector), given a cloud-layer vector of 222 deg/50 kts (blue vector) and a low-level jet vector of 209 deg/52 kts (green vector). The propagation vector is drawn from the tip of the cloud layer vector in the opposite direction of the low-level jet as was mentioned previously in the section on movement of multicells. Note that given the low-level thermodynamic and kinematic structure of the sounding profile, the level "chosen" for the low-level jet was around 900 mb, or the top of the inversion layer.

The ability to select an inflow layer on a thermodynamic sounding is important not only for assessing buoyancy calculations, but also for analyzing the potential source region for multicell inflow and resulting propagation effects.

Heavy rain signatures

Movement affects duration of heavy rain in multicells, but, as was previously discussed in supercells, rainfall rates in multicells are related to precipitation efficiencies and associated upward fluxes of moisture. **In terms of convective storm structure and associated environments, multicell storms with deep moisture profiles, low-level flow parallel to upper-level flow, moderate**

updrafts (due to moderate CAPE), weak to moderate shear (0 to 6 km), and low LCL heights, favor heavy rain potential.

Lower LCL heights diminish the effects of evaporation and cooling in the downdraft portions of individual storms in the multicell cluster. Weak to moderate shear allows hydrometeors to remain in the updraft region longer. High Precipitable Water (PW) content is more important than big CAPEs in heavy rain soundings. Interstorm seeding also increases precipitation efficiencies so storms that are packed together in a line with deep (> 30 dBZ) **sustained** reflectivity cores will favor heavy rain production.

Warm Rain Process-Dominated Convection

Warm-rain processes maximize precipitation efficiencies so look for high Wet Buld Zero (WBZ) heights (>10,500 kft) on associated soundings. Warm rain process-dominated convection is represented on radar by a low echo centroid (LEC) signature. Figure 3-112 is a reflectivity cross section through the core of the persistant rainfall core over I-35 in eastern Kansas, which led to significant flash flooding in the late evening hours of 30 August 2003. **The maximum reflectivity is located at the bottom portion of the storm, and well below the freezing level.** Typically warm rain process dominated storms have very little if any returns higher than the -10 or -20^{o}C level. The LEC is a region with very high quantities of raindrops colliding and coalescing, producing very high rain-rates.

In addition, system-relative flow, as was discussed previously, plays a big role in whether a multicell complex is a slow-mover. If a multicell complex **appears to be tilting downshear** in the lowest

levels, then the system may be a slow-mover and flash-flooding potential should be monitored closely.

Radar Products to Monitor

The Flash Flood Monitoring and Prediction (FFMP) system in AWIPS can be used effectively to help assess flash flood potential. It is the best tool available to assess flash flood threat because it has basins small enough to resolve flash flood producing convective elements, and compares flash flood guidance values (FFG) to quality controlled radar rainfall estimation. FFMP products to be closely monitored are the **Rate**, and **Difference** columns. Most flash floods are rate driven, and thus closely monitoring heavy rates that last for at least 3 volume scans is vital to assessing the flash flood threat. The Difference column represents a

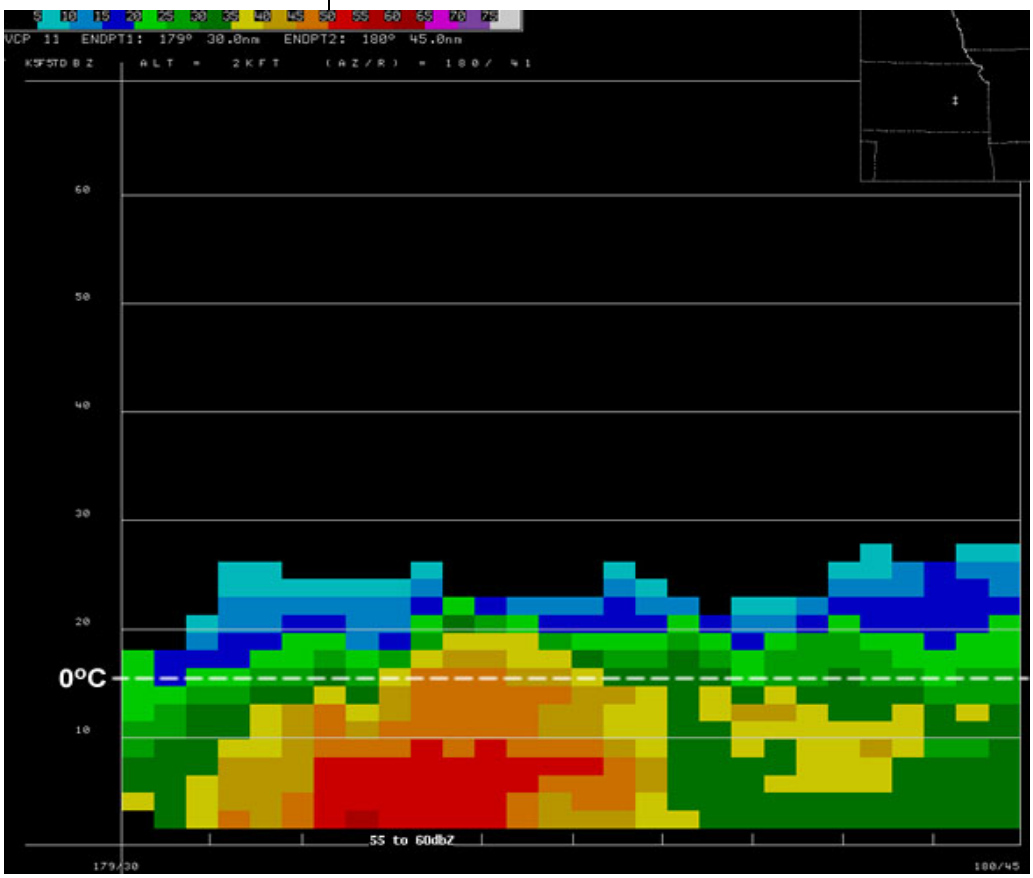

Figure 3-112. Reflectivity Cross-section from KTWX 30 August 2003 0100 UTC. Distances along axis in kft. The max reflectivity is at the lowest available data height.

direct measurement of the magnitude of the flash flooding, as well as the amount of additional rainfall needed to exceed FFG. When the Diff column shows 1 inch over FFG, minor flash flooding is expected to occur; at 3 inches over FFG severe flash flooding is expected, and with 4 or 5 inches over FFG, catastrophic flash flooding is possible. Using FFMP in conjuction with radar reflectivity is important so that you can watch for trends in the convective element movement and assess the potential for additional heavy rainfall.

FFMP Limitations

FFMP is only as good as the data put into it. Any errors in rainfall estimation (IC 5.3 has shown several potential sources of error) will affect FFMP and should be accounted for when utilizing this tool. Also, FFG values may not be representative of individual basins across your CWA, because one FFG value is applied to each CWA zone, and vast differences in topography, soil type, and individual basin size typically exist across any CWA zone. Being cognizant of these limitations and compensating for them as much as possible are important in any flash flood decision making process.

In addition to FFMP, good radar products to use for assessing flash-flood potential in multicell storms are:

- **Precipitation Estimation Suite - One-Hour Precip. (OHP), Storm-Total Precip. (STP), Digital Hybrid Reflectivity (DHR),**
- **4-panels, All Tilts, and Cross-sections of Reflectivity (to assess vertical structure and precipitation potential), and**
- **Vertically Integrated Liquid (VIL)**.

Animating all of these products enhances the diagnosis of movement and potential back building.

Summary

We have covered in this lesson the following for weakly sheared cells, moderate to strongly sheared cells, and multicell convection:

- Characteristics and morphology.
- An understanding of the currently known physical mechanisms behind ordinary-cell, multicell, and supercell motion.
- Detection of severe weather signatures for:
  - High winds,
  - large hail,
  - tornadoes,
  - and heavy rainfall component to flash flooding.

Weakly Sheared Cells

Evolution and Morphology

Weakly sheared cells undergo a life cycle that begins with an updraft pulse. As the updraft extends, it begins to generate a suspended precipitation core visible on radar.

When the core intensifies, it begins to descend. The mature stage of the cell consists of a downdraft and descending precipitation core reaching the ground.

During the dissipating stage, the downdraft spreads out as outflow. The updraft dissipates as the outflow cuts off its supply of potentially buoyant air, and the precipitation core completes its descent to ground.

Ordinary Cell Motion

Weakly sheared cells move with the mean convective steering layer flow. The standard convective layer encompasses the roots of the convection to about 50% of the way up to the equilibrium level. Typically this is the 0-6 km layer.

High Wind Potential

Ordinary cell downdraft intensity depends on the amount of dry air between the downdraft source and the surface, and the amount of precipitation loading. Precipitation loading is a significant forcing mechanism only for wet and hybrid microburst events.

Look for severe dry microbursts when:

- where the LCL exceeds 4 km AGL,
- nearly dry adiabatic lapse rates exist between LCL and ground,
- if the LCL is colder than freezing,
- and the maximum reflectivity of the cell is at least 35 - 40 dBZ.

The descent of the weak reflectivity core is the best precursor to a dry microburst. Weak radial velocity convergence can be detected near cloud base but the lead time to microburst is usually less.

Wet microbursts are favored when:

- there is high CAPE and dry midlevel air,
- theta-E differences between the ground and the level of minimum theta-E typically exceed 25^{o} K,
- a strong reflectivity core (> 50 dBZ) is located around the level of minimum theta-E,
- and the environment should support surface-based convection in order that the downburst experiences no resistance on its way to the surface.

Note that LCL height is not important in wet microburst environments.

Hybrid microburst environments are similar to wet microburst environments except the high LCL implies more negative buoyancy is available to generate a severe microburst.

For both wet and hybrid microbursts, signatures of an imminent microburst are:

- The descent of a high reflectivity core (>50 dBZ). More specifically, the bottom of a strong descending core marks the leading edge of an imminent microburst.
- Monitoring the height and intensity of the initial elevated reflectivity core during the storm updraft phase provides the best lead time to a microburst.
- While the collapse of VIL and echo tops may signal a downburst, the absence of a collapse does not signal an absence of a downburst.
- Midlevel convergence (at or above cloud base) can be detected as a precursor to wet or dry microbursts but lead time is limited.

Large Hail Potential

Large hail favors environments with steep midlevel lapse rates and large CAPE, and relatively low freezing levels.

Look for these signals:

- The stronger the reflectivity core above the -20^{o}C level, the higher the chance for severe hail.
- VILs can be used in a relative way to determine the strength of one storm's core versus another, but VILs should not be used in any way to diagnose hail threat. Problems with VIL lead to the possibility of poor warning performance.

- VIL density also does not perform very well in estimating hail size above severe thresholds.
- The HDA tends to overestimate POH and POSH in weakly sheared cells, but is a better tool for hail threat diagnosis than any other algorithm.
- A three-body scatter spike is very rare in weakly sheared cells, however it is a direct observation of severe hail at the level it is observed.

Tornadoes in Weakly Sheared Environments

This type of tornado depends on pre-existing vertical vorticity along a boundary to be stretched by an updraft. Without mesocyclones, radar is almost unable to detect these tornadoes. Look for these signals:

- A slow moving, well defined boundary with strong vertical vorticity.
- A strong initiating updraft passing over the boundary. The boundary-relative cell motion should be low.
- An environment with little CIN, large CAPE, and steep boundary-layer lapse rates.

Flash Flooding Heavy Rain Potential

Signals favoring heavy rain depend on precipitation efficiency and heavy rain longevity.

Precipitation efficient storms have these signals:

- A deep warm cloud layer (> 10 kft),
- High midlevel tropospheric humidity,
- Wide updrafts,
- The main updraft seeded by an adjacent storm.

Slow storm motion maximizes rainfall longevity.

Moderate to Strongly Sheared Cells

Evolution and Morphology

Updraft strength is enhanced as shear increases through:

- Increased separation between updraft and downdraft,
- a more constrained gust front,
- stronger storm-relative low-level inflow,
- updraft rotation.

Moderate shear through 0-6 km of 10-20 m/s is still a bit too weak for updraft rotation, but enhances new updraft development on the gust front of the primary cell. Organized multicells become likely.

In strong shear (> 20 m/s from 0-6 km), updraft tilting of horizontal vorticity is enough to create a rotating updraft and, therefore, a supercell.

Supercell motion can be estimated using the ID method. That is, supercell motion is to the right (left) of the shear vector for cyclonically (anticyclonically) rotating supercells. The magnitude of deviant motion is 8 m/s from the mean wind.

Anticyclonic and cyclonic supercells are equally strong when the hodograph is straight. Cyclonic (anticyclonic) supercells are favored with clockwise (counterclockwise) curved hodographs.

Supercell Reflectivity Structures

Supercell reflectivity structures contain at least one or more of these features:

- low-level reflectivity notch or concave area

- sharp reflectivity gradient on the side of the updraft
- hook echo
- WER
- BWER

Supercell Velocity Signatures

A radar signature consisting of a localized area of high azimuthal shear is common with supercells. If the shear signature is strong enough, persists for at least 10 minutes, and has vertical continuity, it is called a mesocyclone.

On each elevation slice, mesocyclone strength can be measured by averaging the maximum and minimum velocity within the rotational feature. This is called rotational velocity (V_r).

The basic two-dimensional mesocyclone structure resembles that of a Rankin-Combined vortex.

Mesocyclones undergo a life cycle where there is an organizing stage, a mature stage, and a decaying stage. During the mature stage, the mesocyclone may experience convergence in its lower levels, pure rotation in midlevels and divergence in upper levels.

Supercells often produce multiple mesocyclones. Succeeding mesocyclones develop more quickly than the primary one because of enhanced convergence along the RFD.

Supercell Types

Supercells vary widely in their precipitation amounts. Low Precipitation (LP) storms produce very little precipitation and are outflow deficient. LP storms produce mostly hail and little rain.

Classic supercells (CL) generate enough precipitation to produce outflows, but only a little precipitation is wrapped around the mesocyclone to form a hook. CL storms are capable of all severe weather threats.

High Precipitation supercells (HP) are highly efficient precipitation producers and produce strong outflow. Significant hook echoes form around mesocyclones. In some cases, the mesocyclone may appear to lead the main core. HP storms are capable of all severe weather threats, although are associated with a lessened tornado threat and an enhanced flash flood threat compared to CL storms.

Mini and/or low-topped supercells are structurally similar to large ones, except their dimensions are reduced. This leads to sampling problems for radars.

Left-moving supercells rotate anticyclonically and mostly generate large hail and severe winds.

High Wind Threat

Both cyclonic and anticyclonic supercells generate strong downdraft induced surface winds, including RFDs, given:

- the same environmental considerations that force hybrid or wet microbursts in ordinary cells,
- strong low- to midlevel mesocyclogenesis occurs,
- and the presence of a deep wall of convergence along the right side of the mesocyclone.

Hail Threat

Large hail threat increases when:

- storm-relative flow increases in midlevels

- significant midlevel mesocyclone forms
- large WER, or especially a BWER forms
- the updraft is large
- the environment consists of significant mid- to upper-level buoyancy
- A large amount of very high reflectivities lies above the -20^{o}C level
- three-body scatter spike occurs

Tornado Threat

A velocity structure with very high azimuthal gate-to-gate shear, called a Tornado Vortex Signature (TVS), often accompanies mesocyclone-induced tornadoes.

A tornado threat is high when:

- the environment consists of strong low-level shear, relatively low LCLs, and surface-based CAPE,
- significant vertical vorticity exists before the arrival of the supercell,
- the midlevel mesocyclone descends, contracts and strengthens,
- a TVS forms at low-levels,
- and signatures of a strong low-level updraft are present (e.g., WER, BWER, inflow notch).

While a 30% of solitary TVSs may be associated with tornadoes, when combined with the presence of a BWER and a mesocyclone, the probability jumps to 39%.

Half of all tornadic supercells exhibit a descending TVS with time which helps in warning lead time. However, the other half exhibit non-descending TVSs.

Be careful not to terminate a tornado warning too early with a supercell that has a history of severe weather, even if the supercell temporarily appears to weaken.

In addition, some TVSs may disappear as the scale of rotation contracts during the later stages of a tornado life cycle. The parent updraft may also appear to weaken as well. Allow for about 15 minutes after the disappearance of a TVS just in case there is a rope tornado persisting.

Be sure to monitor the motion of a TVS, it can often differ from the parent supercell motion.

Heavy Rain, Potential Flash Flooding Threat

As with ordinary cells, flash flooding threats from supercells depend on precipitation rate, but efficiency isn't as important. Flash flooding potential can increase when:

- storm motion is small,
- mixing ratio of the inflow is high,
- there is small middle-to-upper storm-relative flow,
- a supercell is seeded by adjacent storms,
- and/or there is a deep, warm cloud layer.

Most CL and HP supercells have intense updrafts and can generate flash flooding rains, even if inefficient at producing precipitation. Small storm motion is the primary factor for increasing flash flooding threats.

Multicells

Multicell storms, consisting of more than one individual ordinary or supercell updraft, also have a propagation vector off the mean wind. Multiple mechanisms may influence the propagation vector including these factors:

- Shear/cold pool interactions
- Horizontal convective stability variations
- Boundary interactions

We have discussed structure and evolution of multicell convection using conceptual models. We showed that most multicell systems can be classified into 3 basic archetypes:

- trailing stratiform
- leading stratiform
- parallel stratiform

We noted that the primary mechanisms for affecting motion of multicell storms are:

- shear-cold pool interactions
- low-level convergence
- instability gradients
- system-relative flow
- three-dimensional boundary interactions

We discussed the two primary modes of motion for Mesoscale Convective Systems (however they can occur simultaneously), how to recognize these motions based on the instability fields and shear profiles, and the type of severe weather they are typically associated with.

- Backward propagation - often leads to flash flooding
- Forward propagation - often leads to high winds

We also discussed variations in using both MBE Vector (Corfidi) techniques, and factors affecting multicell severity and longevity including:

- Rear-Inflow Jets (RIJs)
- Bow echoes
- Deep-layer shear
- Shear and CAPE relationship in terms of synoptic forcing

Since RIJs have been shown in numerical modeling simulations to be a key factor in modulating multicell longevity, we elaborated on the morphology and influence of the RIJ on multicell storm evolution. Note that there are 2 types of RIJs:

- descending
- non-descending

We identified characteristics of bow echoes and mechanisms involved in their formation:

- Coriolis forcing
- System-relative Flow

According to research, there are 2 recognizable types of derechos, which are a special class of multicell systems:

- Serial
- Progressive

We next showed ways to recognize multicell storm signatures based on the associated severe weather threat. Starting with damaging winds,

these are the radar characteristics of linear squall lines (those depicting primarily 2-D features):

- leading edge has high reflectivity cores
- a trailing stratiform precipitation region
- the movement of the line is with the mean wind (advection dominates)
- No bowing of individual cells
- the gust-front location is well in front of the leading edge reflectivity gradient (speed of front not well-matched to squall line speed)

The following are radar characteristics of squall lines that have developed additional 3-D features: (note these also are associated with highest damaging wind potential)

- strong gradient indicating strong updraft and/or convergence
- bookend vortex pair
- WER/BWER
- Bow echo
- MARC

The following are radar characteristics of multicells with large hail potential:

- occurs most often during early stages of development
- deep convergence zone
- cells along the southern end of squall line/isolated cells out ahead of squall line
- similar supercell signatures (BWER, WER, deep mesocyclone)

The following are radar characteristics of multicells with tornado potential:

- storms that develop out ahead of squall line
- TVSs that form from low-levels
- MARC
- similar supercell signatures

The following are characteristics of multicells with heavy rain (potential flash flooding):

- Low echo centroid
- those that exhibit slow movement, back building and/or training of echoes
- those with high precipitation efficiency (warm rain processes)

Useful products to assess flash flooding potential in multicells are model forecast soundings, especially BUFKIT hodographs (which display propagation vectors and resultant multicell motion vectors), and of course, after the storms have developed, FFMP and radar estimated precipitation products, including base reflectivity products and associated cross sections (to assess storm structure).

Appendix A: References

Amburn, S., and P. Wolf, 1997: VIL density as a hail indicator. Wea. Forecasting, 12, 473-478.

Atkins, N. T., and R. M. Wakimoto, 1991: Wet microburst activity over the southeastern United States, *Wea. Forecasting*, **6**, 470-482.

Atkins, Nolan T., Arnott, Justin M., Przybylinski, Ron W., Wolf, Ray A., Ketcham, Bradley D. 2004: Vortex Structure and Evolution within Bow Echoes. Part I: Single-Doppler and Damage Analysis of the 29 June 1998 Derecho. *Mon. Wea. Rev.*, **132**, 2224–2242.

Beard, L. V., and H. T. Ochs, 1993: Warm rain initiation: An overview of microphysical mechanisms. *J. Appl. Meteor.*, **32**, 608-625.

Blaes, J. L. C. S. Cerniglia Jr.,M. A. Caropolo., 1998: VIL density as an indicator of hail across Eastern New York and Western New England. Eastern Region Technical Attachment. No. 98-8, 17pp.

Blanchard, D.O., 1998: Assessing the vertical distribution of convective available potential energy. *Wea. and Forecasting*, **13**, 870-877.

Bluestein, H.B., and M.H. Jain, 1985: Formation of mesoscale lines of precipitation: Severe squall lines in Oklahoma during the spring. *J. Atmos. Sci.*, **42**, 1711-1732.

Brooks, H. E., and J. P. Craven, 2002: A database of proximity soundings for significant severe thunderstorms, 1957–1993. Preprints, *21st Conf. on Severe Local Storms*, San Antonio, TX, Amer. Meteor. Soc., 639-642.

Browning, K. A., and F. H. Ludlum, 1962: Airflow in convective storms. *Quart. J. Roy. Meteor. Soc.*, **88**, 117-135.

Bunkers, M. J., B. A. Klimowski, J. W. Zeitler, R. L. Thompson, and M. L. Weisman, 2000: Predicting supercell motion using a new hodograph technique. *Wea. Forecasting*, **15**, 61-79.

Burgess, d. W. V. T. Wood, and R. A. Brown, 1982: Mesocyclone evolution statistics, Preprints, *12th Conf. on Severe Local Storms*, San Antonio, TX, Amer. Meteor. Soc., 422-424.

____, and L. R. Lemon, 1990: Severe thunderstorm detection by radar. *Radar in Meteorology*, D. Atlas, Ed., Amer. Meteor. Soc., 619-627.

Byers, H. R., and R. Braham, 1949: The Thunderstorm. Govt. Printing Office, Washington, DC, 287 pp.

Cerniglia, C. S., and W. R. Snyder, 2002: Development of warning criteria for severe pulse thunderstorms In the northeastern United States using the WSR-88D. Eastern Region Technical Attachment, No. 2002-03, 14pp.

COMET, 1999: Mesoscale Convective Systems: Squall Lines and Bow Echoes. Online training module, http://www.meted.ucar.edu/convectn/mcs/index.htm.

____, 1996: Anticipating convective storm structure and evolution. CD-ROM.

____, 1995: A convective storm matrix: Buoyancy/shear dependencies. CD-ROM.

Coniglio, M. C., and D. J. Stensrud, 2001: Simulation of a Progressive derecho using composite initial conditions. *Monthly Weather Review*, **129**, 1593—1616.

Corfidi, S.F., J.H. Merritt, and J.M. Fritsch, 1996: Predicting the movement of mesoscale convective complexes. *Wea. Forecasting*, **11**, 41-46.

Corfidi, Stephen F. 2003: Cold Pools and MCS Propagation: Forecasting the Motion of Downwind-Developing MCSs. *Wea. Forecasting*, **6**, 997–1017.

Crook, N.A., 1996: Sensitivity of moist convection forced by boundary layer processes to low-level thermodynamic fields. Mon. Wea. Rev., 124, 1767-1785.

Davies, J.M., 1993: Hourly helicity, instability and EHI in forecasting supercell tornadoes. Preprints, 17th Conf. on Severe Local Storms, St. Louis, Amer. Meteor. Soc., 107-111.

Davis, R. S., 2002: Flash flood forecast and detection methods. Severe Convective Storms C. Doswell III, Ed., Amer. Meteor. Soc., 481-525.

——, and R. H. Johns, 1993: Some wind and instability parameters associated with strong and violent tornadoes. *Part I: Wind shear and helicity. The Tornado: Its Structure, Dynamics, Prediction, and Hazards, Geophys. Monogr.*, No. 79, Amer. Geophys. Union, 573–582.

____, 2002: Significant tornadoes in environments with relatively weak shear. Preprints, 21st Conf. on Severe Local Storms, San Antonio, Amer. Meteor. Soc., 651-654.

Davies-Jones, R., 1984: Streamwise vorticity: The origin of updraft rotation in supercell storms. *J. Atmos. Sci.*, **41**, 2991-3006.

___, Burgess and M. Foster, 1990: Test of helicity as a tornado forecast parameter. Preprints, *16th Conf on Severe Local Storms*, Kananaskis Park, Alberta, Amer. Meteor. Soc., 588-592.

Davis, Christopher, Atkins, Nolan, Bartels, Diana, Bosart, Lance, Coniglio, Michael, Bryan, George, Cotton, William, Dowell, David, Jewett, Brian, Johns, Robert, Jorgensen, David, Knievel, Jason, Knupp, Kevin, Lee, Wen-Chau, Mcfarquhar, Gregory, Moore, James, Przybylinski, Ron, Rauber, Robert, Smull, Bradley, Trapp, Robert, Trier, Stanley, Wakimoto, Roger, Weisman, Morris, Ziegler, Conrad. 2004: The Bow Echo and MCV Experiment: Observations and Opportunities. *Bull. Amer. Meteor. Soc.*, **85**, 1075–1093.

Dowell, D. C., H. B. Bluestein, 2002: The 8 June 1995 McLean, Texas, storm. part II: Cyclic tornado formation, maintenance, and dissipation. *Mon. Wea. Rev.*, **130**, 2649–2670.

Duke, J. W., and J.A. Rogash, 1992: Multiscale review of the development and early evolution of the 9 April 1991 derecho. *Wea. Forecasting*, **7**, 623—635.

Edwards, R., R. L. Thompson, 1998: Nationwide comparisons of hail size with WSR-88D Vertically Integrated Liquid water and derived thermodynamic sounding data. *Wea. and Forecasting,* **13**, 277–285.

_____, _____, 2000: RUC2 Supercell proximity soundings, part II: An independent assessment of supercell forecast parameters. Preprints, *20th Conf. on Severe Local Storms*, Orlando, Amer. Meteor. Soc., 435-438.

Emanuel, K. A., 1994: Atmospheric Convection. Oxford University Press, 883 pp.

Evans, J. S. and C. A. Doswell III, 2001: Examination of Derecho environments using proximity soundings. *Wea. Forecasting*, **16**, 329-342.

Fankhauser, J.C., N.A. Crook, J. Tuttle, L.J. Miller, C.G. Wade, 1995: Initiation of deep convection along boundary layer convergence lines in a semitropical environment. *Monthly Weather Review*:, **123**, 291–314.

Fawbush, E. J., and R. C. Miller, 1954: The types of airmasses in which North American tornadoes form. *Bull. Amer. Soc.*, **35**, 154-165.

Finley, Catherine A., Cotton, W. R., Pielke, R. A.. 2001: Numerical Simulation of Tornadogenesis in a High-Precipitation Supercell. Part I: Storm Evolution and Transition into a Bow Echo. *J. Atmos Sci.*, **58**, 597–1629.

Foster, D. S., 1958: Thunderstorm gusts compared with computed downdraft speeds. *Mon. Wea. Rev.*, **86**, 91-94.

Fovell, Robert G., Yoshi Ogura, 1988: Numerical simulation of a midlatitude squall line in two dimensions. *J. Atmos. Sci.*, **45**, 3846–3879.

Fujita, T.T., 1978: Manual of downburst identification for project NIMROD. SMRP Research Paper No. 156, 104 pp.

Gilmore, M. S. , and L. J. Wicker, 1998: The influence of midtropospheric dryness on supercell morphology and evolution, *Mon. Wea. Rev.*, **126**, 943-958.

Grant, B. N., 1995: Elevated Cold-Sector Severe Thunderstorms: A Preliminary Study. *National Weather Digest* , **19:4**, 25-31.

Hane, Carl E., Howard B. Bluestein, Todd M. Crawford, Michael E. Baldwin, Robert M. Rabin, 1997: Severe thunderstorm development in relation to along-dryline variability: A case study. *Mon. Wea. Rev.*, **125**, 231–251.

Hart, J. A., and W. Korotky, 1991: The SHARP workstation v1.50 users guide. National Weather Service, NOAA, 30pp.

Johns R. H., and C.A. Doswell III, 1992: Severe Local Storms Forecasting. *Symposium of Weather Forecasting*, 72nd AMS Annual Meeting, Atlanta.

Johns, R.H. and W.D. Hirt, 1987: Derechos: widespread convectively induced windstorms. *Wea. Forecasting*, **2**, 32-49.

Johns, R.H., 1993: Meteorological conditions associated with bow echo development in convective storms. *Wea. Forecasting*, **8**, 294-300.

Johns, R.H., J.M. Davies, and P.W. Leftwich, 1990: An examination of the relationship of 0-2 km agl "positive" wind shear to potential buoyant energy in strong and violent tornado situations. *16th Conf on Severe Local Storms*, Kananaskis Park, Alberta, 593-598.

Kennedy, Patrick C., Rutledge, Steven A. 1995: Dual-Doppler and Multiparameter Radar Observations of a Bow-Echo Hailstorm. *Mon. Wea. Rev.*, **123**, 921–943.

Kerr, B.W., and G.L. Darkow, 1996: Storm-relative winds and helicity in tornadic thunderstorm environments. *Wea. Forecasting*, **11**, 489-505.

____, C. A. Ray, 1997: Mesoanalysis of summertime convergence zones in central and eastern North Carolina. *Wea. Forecasting*, **12**, 56–77

Maddox, R. A., 1976: An evaluation of tornado proximity wind and stability data. *Mon. Wea. Rev.*, **104**, 133–142.

Mahoney, W.P. III, 1988: Gust front characteristics and the kinematics associated with interacting thunderstorm outflows. *Mon. Wea. Rev.*, **116**, 1474-1491.

Markowski, P. M., J. M. Straka, E. N. Rasmussen, 2002: Direct surface thermodynamic observations within the rear-flank downdrafts of non-tornadic and tornadic supercells. *Mon. Wea. Rev.*, **130**, 1692–1721.

McCaul, E. W., and M. L. Weisman, 1996: The dependence of simulated storm structure on variations in the shapes of environment buoyancy and shear profiles. Preprints, *18th Conf. on Severe Local Storms*, San Francisco, CA, Amer. Meteor. Soc., 718-722.

Moller, A. R., C. A. Doswell, and r. Przybylinski, 1990: High-precipitation supercells: A conceptual model and documentation. Preprints, *16th Conf. on Severe Local Storms*, Kananaskis Park, AB, Canada, Amer. Meteor. Soc., 52-57.

Petersen, W.r A., L. D. Carey, S. A. Rutledge, J. C. Knievel, R. H. Johnson, N. J. Doesken, T. B. McKee, T. Vonder Haar, and J. F. Weaver, 1999: Mesoscale and Radar Observations of the Fort Collins Flash Flood of 28 July 1997. *Bull. Amer. Meteor. Soc.*, **80**, 191–216.

Przybylinski, R.W., 1995: The bow echo: observations, numerical simulations, and severe weather detection methods. *Wea. Forecasting*, **10**, 203-218.

____, 1995: The bow echo: Observations, numerical simulations, and severe weather detection methods. *Wea. Forecasting*, **10**, 203-218.

____, and G.K. Schmocker, 1993: The evolution of a widespread convective wind storm event over central and eastern Missouri. Preprints, *13th Conf. on Weather Analysis and Forecasting*, Vienna, VA, Amer. Meteor. Soc., 461-465.

____, T.J. Shea, D.L. Ferry, E.H. Goetsch, R.R. Czys, and N.E. Wescott, 1993: Doppler radar observations of high-precipitation supercells over the mid-Mississippi Valley region. Preprints, *17th Conf. on Severe Local Storms*, St. Louis, MO, Amer. Meteor. Soc., 158-163.

____., and D. M. DeCaire, 1985: Radar signatures associated with the derecho. One type of mesoscale convective system. Preprints *14th Conf. on Severe Local Storms*, Indianapolis, IN, Amer. Meteor. Soc., 228-231.

Purdom, J. F. W., 1976: Some uses of high resolution GOES imagery in the mesoscale forecasting of convection and its behavior. *Mon. Wea. Rev.*, 104, 1474–1483

RTM-230, 2000: Skew T Log P Diagram and Sounding Analysis, National Weather Service Training Center Remote Training Module.

Rasmussen, E. N., 2001: Refined supercell and tornado forecast parameters from the 1992 baseline climatology. Unpublished web-based paper.

____, and D. Blanchard, 1998: A baseline climatology of sounding-derived supercell and tornado forecast parameters. *Wea and Forecasting*, **13**, 1148-1164.

____, S. Richardson, J. Straka, P. Markowski, and D. Blanchard, 1998: The association of significant tornadoes with a baroclinic boundary on 2 June 1995. *Mon. Wea. Rev.*, **128**, 174-191.

____, J. M. Straka, 1998: Variations in supercell morphology. Part I: Observations of the role of upper-level storm-relative flow. **Mon. Wea. Rev**:, **126**, 2406–2421.

____, and R. B. Wilhelmson 1983: Relationships between storm characteristics and 1200 GMT hodographs, low-level shear, and stability. preprints, *13th conf. on Severe Local Storms,* Tulsa, OK, Amer. Meteor. Soc., J5-J8.

Richardson, Y.P., 1999: The Influence of horizontal variations in vertical shear and low-level moisture on numerically simulated convective storms. Ph.D. Dissertation, School of Meteorology, University of Oklahoma - Norman, 236 pp.

Roberts, R. D., and J. W. Wilson, 1989: A proposed microburst nowcasting procedure using single-Doppler radar. *J. Appl. Meteor.*, **28**, 285-303.

Shapiro, A. 1992. A hydrodynamical model of shear flow over semi-infinite barriers with application to density currents. *J. Atmos. Sci*. **49**, 2293–2305

Smull, Bradley F., R. A. Houze, Jr., 1987: Rear Inflow in Squall Lines with Trailing Stratiform Precipitation. Mon. Wea. Rev., 115, 2869–2889.

Srivastava, R. C., 1985: A simple model of evaporatively driven downdraft: Application to microburst downdraft. *J. Atmos. Sci.*, **42**, 1004-1023.

Stensrud, D.J., J.V. Cortinas, Jr., and H.E. Brooks, 1997: Discriminating between tornadic and non-tornadic thunderstorms using mesoscale model output. *Wea. Forecasting*, **12**, 613-632.

Thompson, R.L., 1996: Supercell tornado forecasts derived from Eta model storm-relative winds. Preprints, *18th Conf. on Severe Local Storms*, San Francisco, CA, AMS, 362-366.

____, 1998: Eta model storm-relative winds associated with tornadic and non-tornadic supercells. *Wea. Forecasting*, **13**, 125-137.

TWG, 2002: Tornado Warning Guidance. Web page, http://www.wdtb.noaa.gov/resources/PAPERS/twg02/index.html

Wakimoto, R. M., 1985: Forecasting dry microburst activity over the high plains. *Mon. Wea. Rev.*, **113**, 1131-1143.

____, and J. W. Wilson, 1989: Non-supercell tornadoes. *Mon Wea. Rev.*, **117**, 1113-1140.

Wakimoto, R. M., N. T. Atkins, 1996: Observations on the origins of rotation: the Newcastle tornado during VORTEX 94. *Mon. Wea. Rev.*, **124**, 384–407.

____, 2002: Convectively driven high wind events. Severe Convective Storms C. Doswell III, Ed., Amer. Meteor. Soc., 255-298

Weaver, J. F., 1979: Storm Motion as Related to Boundary-Layer Convergence. *Mon. Wea. Rev.*, **107**, 612–619.

Weisman, M. L., 1993: The Genesis of Severe, Long-Lived Bow Echoes. *J. Atmos. Sci.*, **50**, 645–645.

____, 1992: The Role of Convectively Generated Rear-Inflow Jets in the Evolution of Long-Lived Mesoconvective Systems. *J. Atmos. Sci.*, **49**, 1826–1847.

_____., and J. B. Klemp, 1984: The structure and classification of numerically simulated convective storms in directionally varying wind shears. *Mon. Wea. Rev.*, **112**, 2479-2498.

_____, and J. B. Klemp, 1982: The dependence of numerically simulated convective storms on vertical wind shear and buoyancy. *Mon. Wea. Rev.*, **110**, 504-520.

Wicker, L. J., and L. Cantrell, 1996: The role of vertical buoyancy distributions in miniature supercells. Preprints, *18th Conf. on Severe Local Storms*, San Francisco, CA, Amer. Met. Soc, 225-229.

Wilson, J.W., 1986: Tornadogenesis by non-precipitation induced wind shear lines. *Mon. Wea. Rev.*, **114**, 270-284.

____, R. E. Carbone, J. D. Tuttle, and T. D. Keenan, 2001: Tropical island Convection in the Absence of Significant topography. Part II: Nowcasting Storm Evolution. *Mon. Wea. Rev.*, **129**, 1507–1525.

____, and D. L. Megenhardt, 1997: Thunderstorm Initiation, Organization, and Lifetime Associated with Florida Boundary Layer Convergence Lines. *Mon. Wea. Rev*. **125**, 1507–1525

____, and W. E. Schreiber, 1986: Initiation of convective storms by radar-observed boundary layer convergent lines. *Mon. Wea. Rev.*, **114**, 2516—2536

Winston H. A., and L. J. Ruthi, 1986: Evaluation of RADAP-II severe-storm detection algorithms. *Bull. Amer. Meteor. Soc.*, **67**, 145-150.

Witt, A., 1996: The relationship between low-elevation WSR-88D reflectivity and hail at the ground using precipitation observations from the VORTEX project. Preprints, *18th Conf. on Severe Local Storms, San Francisco*, CA, Amer. Meteor. Soc., 183-185.

____, and S. P. Nelson, 1991: The use of single-Doppler radar for estimating maximum hailstone size. *J. Appl. Meteor.*, **30**, 425-431.

____, M. D. Eilts, G. J. Stumpf, J. T. Johnson, e. D. Mitchell, and K. W. Thomas, 1998: An enhanced hail detection algorithm for the WSR-88D. *Wea. Forecasting*, **13**, 286-303.

Xue, M. 2000. Density currents in two-layer shear flows. *Quart. J. Roy. Atmos. Sci.*, **126**, 1301—1320.